Air Pollution Scenario over Pakistan: Characterization and Ranking of Extremely Polluted Cities using Long-Term Concentrations of Aerosols and Trace Gases

Muhammad Bilal[1], Alaa Mhawish[1], Janet E. Nichol[2], Zhongfeng Qiu[1, *], Majid Nazeer[3], Md. Arfan Ali[1], Gerrit de Leeuw[4,5,6,7], Robert C. Levy[8], Yu Wang[1], Yang Chen[9], Lunche Wang[10], Yuan Shi[11], Max P. Bleiweiss[12], Usman Mazhar[13], Luqman Atique[14], and Song Ke[15]

[1] Lab of Environmental Remote Sensing (LERS), School of Marine Sciences, Nanjing University of Information Science and Technology, Nanjing, 210044, China.

[2] Department of Geography, School of Global Studies, University of Sussex, Brighton BN19RH, UK.

[3] Key Laboratory of Digital Land and Resources, East China University of Technology, Nanchang 330013, China.

[4] Royal Netherlands Meteorological Institute (KNMI), R & D Satellite Observations, 3730AE De Bilt, The Netherlands.

[5] School of Atmospheric Physics, Nanjing University of Information Science and Technology, Nanjing, 210044, China.

[6] Aerospace Information Research Institute, Chinese Academy of Sciences (AirCAS), No.20 Datun Road, Chaoyang District, Beijing 100101, China

[7] School of Environment Science and Spatial Informatics, University of Mining and Technology, Xuzhou, Jiangsu 221116, China.

[8] Climate and Radiation Laboratory, NASA Goddard Space Flight Center, Greenbelt, MD, USA.

[9] State Key Laboratory of Information Engineering in Surveying, Mapping and Remote Sensing, Wuhan University, Wuhan 430079, China.

[10] Laboratory of Critical Zone Evolution, School of Earth Sciences, China University of Geosciences, Wuhan 430074, China.

[11] Institute of Future Cities, The Chinese University of Hong Kong, Hong Kong SAR, China.

[12] Department of Entomology, Plant Pathology and Weed Science, New Mexico State University, Las Cruces, NM 88003, USA.

[13] School of Earth Sciences, Zhejiang University, Hangzhou 310027, China.

[14] School of Remote Sensing & Geomatics Engineering, Nanjing University of Information Science and Technology, Nanjing 210044, China.

[15] Geological Survey of Jiangsu Province, Nanjing, 210018, China.

*Corresponding author: Zhongfeng Qiu (zhongfeng.qiu@nuist.edu.cn)

Abstract

Pakistan ranks third in the world in terms of mortality attributable to air pollution, with aerosol mass concentrations ($PM_{2.5}$) consistently well above WHO (World Health Organization) air quality guidelines (AQG). However, regulation is dependent on a sparse network of air quality monitoring stations and insufficient ground data. This study utilizes long-term observations of aerosols and trace gases to characterize and rank the air pollution scenarios and pollution characteristics of 80 selected cities in Pakistan. Datasets used include (1) the Aqua and Terra (AquaTerra) MODIS (Moderate Resolution Imaging Spectroradiometer) Level 2 Collection 6.1 merged Dark Target and Deep Blue (DTB) aerosol optical depth (AOD) retrieval products; (2) the CAMS (Copernicus Atmosphere Monitoring Service) reanalysis PM_1, $PM_{2.5}$, and PM_{10} data; (3) the MERRA-2 (Modern-Era Retrospective analysis for Research and Applications, Version 2) reanalysis $PM_{2.5}$ data, (4) the OMI (Ozone Monitoring Instrument) tropospheric vertical column density (TVCD) of nitrogen dioxide (NO_2), and VCD of sulfur dioxide (SO_2) in the Planetary Boundary Layer (PBL), (5) the VIIRS (Visible Infrared Imaging Radiometer Suite) Nighttime Lights data, (6) MODIS Collection 6 Version 2 global monthly fire location data (MCD14ML), (7) population density, (8) MODIS Level 3 Collection 6 land cover types, (9) AERONET (AErosol RObotic NETwork) Version 3 Level 2.0 data, and (10) ground-based $PM_{2.5}$ concentrations from air quality monitoring stations. Potential Source Contribution Function (PSCF) analyses were performed by integrating with ground-based $PM_{2.5}$ concentrations and the NOAA (National Oceanic and Atmospheric Administration) HYSPLIT (Hybrid Single-Particle Lagrangian Integrated Trajectory) air parcel back trajectories to identify potential pollution source areas which are

responsible for extreme air pollution in Pakistan. Results show that the ranking of the top polluted cities depends on the type of pollutant considered and the metric used. For example, Jhang, Multan, and Vehari were characterized as the top three polluted cities in Pakistan when considering AquaTerra DTB AOD products; for PM_1, $PM_{2.5}$, and PM_{10} Lahore, Gujranwala, and Okara were the top three; for tropospheric NO_2 VCD Lahore, Rawalpindi, and Islamabad and for PBL SO_2 VCD Lahore, Mirpur, and Gujranwala. The results demonstrate that Pakistan's entire population has been exposed to high $PM_{2.5}$ concentrations for many years, with a mean annual value of 54.7 μg/m^3, over all Pakistan from 2003 to 2020. This value exceeds Pakistan's National Environmental Quality Standards (Pak-NEQS, i.e., <15 μg/m^3 annual mean) for ambient air defined by the Pakistan Environmental Protection Agency (Pak-EPA) as well as the WHO Interim Target-1 (i.e., mean annual $PM_{2.5}$ <35 μg/m^3). The spatial analyses of the concentrations of aerosols and trace gases in terms of population density, nighttime lights, land cover types, and fire location data, and the PSCF analysis indicate that Pakistan's air quality is strongly affected by anthropogenic sources inside of Pakistan, with contributions from surrounding countries. Statistically significant positive (increasing) trends in PM_1, $PM_{2.5}$, PM_{10}, tropospheric NO_2 VCD, and SO_2 VCD were observed in ~89%, ~67%, ~48%, 91%, and ~88% of the Pakistani cities (80 cities), respectively. This comprehensive analysis of aerosol and trace gas levels, their characteristics in spatio-temporal domains, and their trends over Pakistan, is the first of its kind. Results will be helpful to the Ministry of Climate Change (Government of Pakistan), Pak-EPA, SUPARCO (Pakistan Space and Upper Atmosphere Research Commission), policymakers, and the local research community to mitigate air pollution and its effects on human health.

Keywords: MODIS; AOD; CAMS; MERRA-2; PM_1; $PM_{2.5}$; PM_{10}; OMI; NO_2; SO_2; PSCF; Pakistan

Highlights:

- Lahore, Gujranwala, and Okara are the most polluted city based on $PM_{2.5}$
- Jhang, Multan, and Vehari are the most polluted cities based on AOD
- Aerosols, nighttime lights, population, cropland, and fire show same spatial patterns
- Pakistan's entire population is exposed to long-term PM_x (x = 1, 2.5, & 10)
- Pakistan's air quality is mainly affected by local anthropogenic sources

1. Introduction

With the rapid increase in population and overexploitation of natural resources, air pollution is a serious global environmental concern. According to the World Health Organization (WHO 2018a), air pollution levels are dangerously high worldwide as 9 out of 10 people breathe polluted air, and each year 7 million deaths are caused by outdoor and indoor aerosol pollutants. Outdoor (ambient) air pollution is due to high concentrations of different species including airborne particulate matter (PM), ozone (O_3), nitrogen dioxide (NO_2), volatile organic compounds (VOC), carbon monoxide (CO), and sulfur dioxide (SO_2), which have adverse health effects (Mannucci and Franchini 2017). Although air pollution is a global problem, the latest WHO air quality database reveals that 97% of affected cities are in low- and middle-income countries with more than 100,000 inhabitants (WHO 2018b). Air pollution is endemic to Pakistan, being listed among low- and middle-income countries as well as being the most urbanized of its South Asian counterparts (77.42 million or 36.37 % of the urban population, with 2.52 % annual growth rate) (UNDP 2019). Purohit et al. (2013) predicted that under current emission control standards, air

pollution would decrease life expectancy by more than 100 months by 2030. The Health Effects Institute (2019) reported that since 1990, Pakistan's entire population has been exposed to $PM_{2.5}$ (the integrated dry mass of aerosol particulates with an aerodynamic diameter less than 2.5 μm) annual mean concentrations of 58 $\mu g/m^3$ in 2017, levels exceeding WHO Interim Target-1 (i.e., <35 $\mu g/m^3$). Pakistan ranks third in the world in terms of mortality attributable to air pollution, with an annual loss of 128,000 lives (Government of Pakistan 2019). Recently, on October 30, 2019, the Air Quality Index (AQI) was 484 in Lahore (the second-largest city with the highest urbanization rate of 6.12 percent per annum), well above the threshold of 300 for "hazardous" level (Amnesty International 2019). The winter of 2019-2020 witnessed a spate of smog, which compelled authorities in Punjab to close schools for an extended period. The formation of this smog was fueled by the buildup of anthropogenic aerosols having 65% of sources within Pakistan. The principal cause for smog formation is NOx, which is emitted primarily from Pakistan's 23.6 million transport vehicles (58%), followed by industry and power, which accounts for 34% of emissions (Amnesty International 2019; Government of Pakistan 2019; UNDP 2019). According to the Pakistan Air Quality Initiative (PAQI), Lahore, Peshawar, Islamabad, and Karachi are the most polluted cities where air quality does not meet WHO air quality guidelines during autumn and winter (PAQI 2018). Air pollution monitoring throughout Pakistan is challenging due to sparsely distributed air quality monitoring stations, though several remote sensing studies have been conducted.

Satellite observations provide spatial distributions of column-integrated concentrations which are related to the near-surface concentrations through meteorological and physico-chemical processes, thus complementing local ground-based observations. Gupta et al. (2013)

analyzed MODIS (Moderate Resolution Imaging Spectroradiometer) AOD (Aerosol Optical Depth) retrievals over Lahore and Karachi from 2001 to 2010 and reported higher aerosol loadings near the city center than outside the city. Tariq et al. (2016) analyzed ground-based and satellite-based aerosol optical properties over Lahore during intense haze events in October 2013 and reported crop residue burning and urban-industrial emissions as the main sources of high AOD levels. Bilal et al. (2016) evaluated the performance of the Aqua-MODIS (MYD04) level 2 aerosol products over Lahore and Karachi from 2007 to 2013, and recommended the use of Dark Target (DT) and Deep Blue (DB) algorithms over Karachi and Lahore, respectively, for regional air quality applications, as these cities have different land cover characteristics and aerosol types. Other remote sensing studies have been conducted on atmospheric trace gases, such as ozone (O_3), nitrogen dioxide (NO_2), sulfur dioxide (SO_2), and carbon dioxide CO_2, as well as their trends over time (Khokhar et al. 2016; Khokhar et al. 2015; Tariq and Ali 2015; ul-Haq et al. 2017; ul–Haq et al. 2014; Ul_Haq et al. 2015). Zhang et al. (2020) conducted the first study of the vertical distribution of aerosol optical properties over Pakistan using CALIPSO (Cloud-Aerosol Lidar and Infrared Pathfinder Satellite Observation) data.

Cities are areas of high activity, and every city is a huge source of local anthropogenic aerosols and trace gases from industrial and human activities, which can impact air quality, visibility, and alter the physico-chemical properties of the atmosphere at local, regional, and global scales. Although several studies of AOD and atmospheric trace gases have been conducted over Pakistan, no study has encompassed different particle fractions (PM_x, x = 1, 2.5, and 10) on the national scale, i.e., the dry mass of ultrafine particles with an aerodynamic diameter less than 1 µm (PM_1), 2.5 µm ($PM_{2.5}$) and 10 µm (PM_{10}). PM_1 is part of $PM_{2.5}$, $PM_{2.5}$ is part of PM_{10}. It is of

great importance to identify the cities most affected by different PM_x fractions, as they have different effects on, for instance, health and chemical and physical processes in the atmosphere, and this is the first study to do so. Moreover, very few studies have investigated the long-term trends in pollutant concentrations at city level, which can provide additional insights into the link between concentrations and the changes in emissions. Furthermore, previous studies are not comprehensive enough to answer questions such as: which are the most and least polluted cities of Pakistan, and what are the likely pollution sources? Therefore, this study aims (1) to extensively characterize and rank the extremely polluted cities of Pakistan, considering multiple sources and aerosol mass fractions, for 80 carefully selected cities, representing almost all major urban centers of Pakistan, and (2) to identify the likely pollutant sources by performing PSCF (Potential Source Contribution Function) analysis with the integration of HYSPLIT (Hybrid Single-Particle Lagrangian Integrated Trajectory) back trajectory and ground-based $PM_{2.5}$ concentrations. This study is based on long-term combined Aqua and Terra (AquaTerra) MODIS data from 2003 to 2017, OMI (Ozone Monitoring Instrument) data (NO_2 and SO_2) from 2004 to 2019, CAMS (Copernicus Atmosphere Monitoring Service) reanalysis PM_1, $PM_{2.5}$, and PM_{10} data from 2003 to 2019, MERRA-2 (Modern-Era Retrospective analysis for Research and Applications, Version 2) $PM_{2.5}$ data from 2003 to 2020, VIIRS (Visible Infrared Imaging Radiometer Suite) Nighttime Lights from 2012 to 2019, LandScan global population density for 2019, MODIS land cover type for 2019, MODIS global monthly fire location data from 2003 to 2020, ground-based $PM_{2.5}$ concentrations from 2018 to 2020, and AERONET (AErosol RObotic NETwork) AOD measurements from 2006 to 2017. Detailed information on the data used in this study is provided in Section 3.

2. Study Area

Pakistan, with a population of 212.82 million, is the sixth most populous country in the world. It lies between 23°35′ to 37°05′ North and 60°50′ to 77°50′ East, having a diverse geographical landscape bordered by China, the Himalayas, India, Afghanistan, Iran, and the Arabian Sea. Geographically, Pakistan falls into three major regions: the northern highlands, constituting parts of the Hindu Kush, the Karakoram Range, and the Himalayas; the Indus River basin plain in the center and east (65% of the total area i.e. 796,096 km^2); and the Balochistan Plateau in the south and west (Government of Pakistan 2019). Administratively, Pakistan has six units: Punjab, Sindh, Khyber Pakhtunkhwa, Balochistan, Azad Kashmir, and Gilgit Baltistan. Punjab is the most populous (112.38 million; 53%) administrative unit of Pakistan, followed by Sindh (49.05 million; 23%), Khyber Pakhtunkhwa (36.5 million; 17%), and Balochistan (12.7 million; 6%). Balochistan has the largest area (43.6 %), followed by Punjab (25.8%), Sindh (17.7 %), and Khyber Pakhtunkhwa (12.78%). Sindh is the most urbanized and industrialized administrative unit of Pakistan with 52% urban population. Islamabad (2.1 million; 1%) Capital Territory (ICT), a rather small unit in terms of area (0.1 %), is, in fact, the second most urbanized (50.58%) region of Pakistan, and has an annual urbanization rate of 4.91 %. Currently, 10 cities in Pakistan have a population of over one million, and 7 have higher per-capita incomes than the national average (UNDP 2019). The Pakistan economic survey 2018-19 reports a total cropped area of 22.6 million hectares, and agricultural contributions of 18.5 % to the GDP, compared with 20.3% from the industrial sector (Government of Pakistan 2019).

This study covers almost all prominent cities in Pakistan including all administrative units and their capital cities, and the Capital of the country (Figure 1). In summary, the study area analyzes 23 cities from the most populated administrative unit, Punjab; Khyber Pakhtunkhwa is also well-represented by 19 urban centers; Balochistan is the least populated but the largest administrative unit, and is represented by 19 cities; 14 other cities exemplify the diversity of Sindh in the South-East, and 5 cities represent the attractive hilly land of Azad Kashmir.

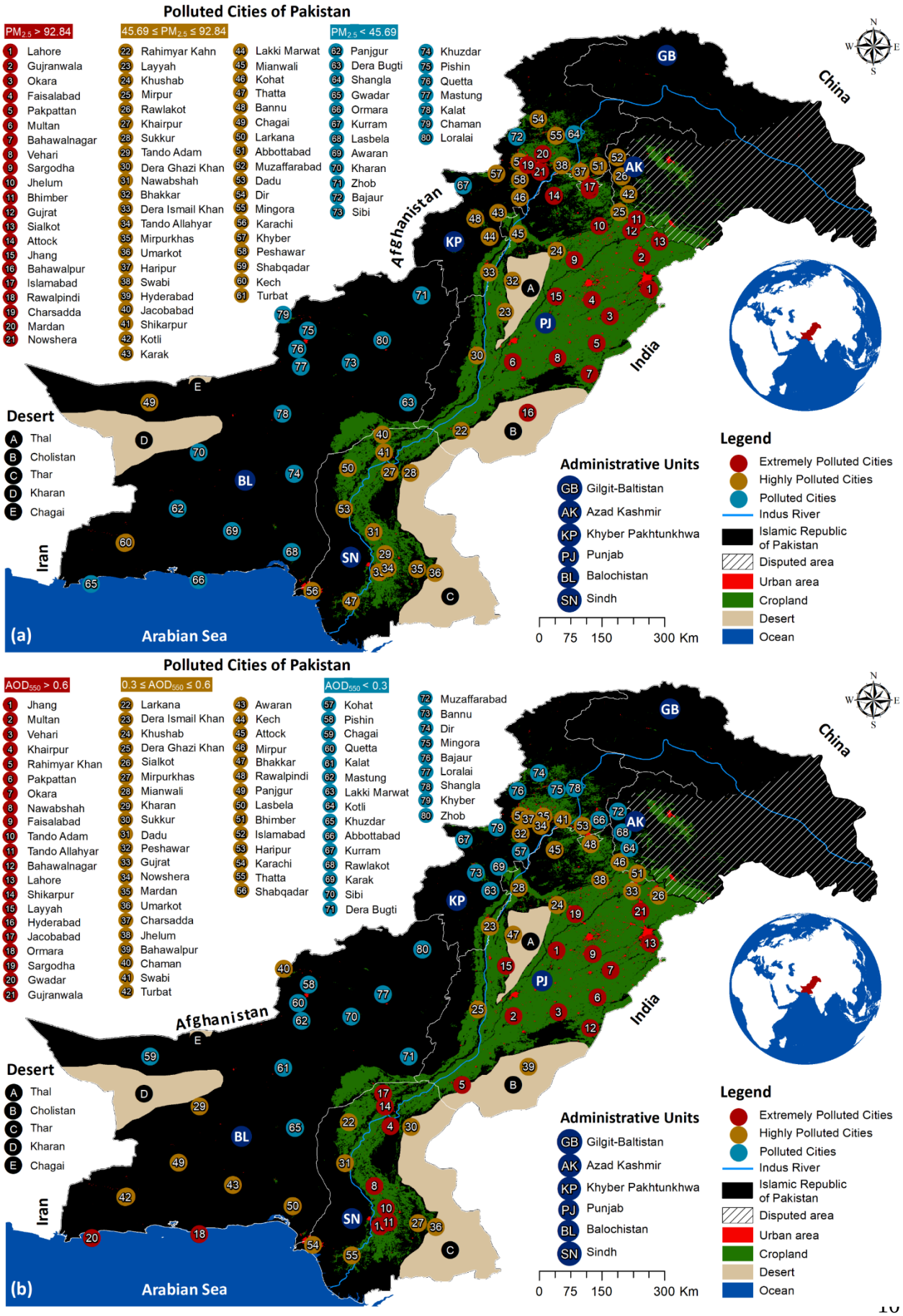
Polluted Cities of Pakistan
PM2.5 > 92.84
1 Lahore
2 Gujranwala
3 Okara
4 Faisalabad
5 Pakpattan
6 Multan
7 Bahawalnagar
8 Vehari
9 Sargodha
10 Jhelum
11 Bhimber
12 Gujrat
13 Sialkot
14 Attock
15 Jhang
16 Bahawalpur
17 Islamabad
18 Rawalpindi
19 Charsadda
20 Mardan
21 Nowshera
45.69 ≤ PM2.5 ≤ 92.84
22 Rahimyar Kahn
23 Layyah
24 Khushab
25 Mirpur
26 Rawlakot
27 Khairpur
28 Sukkur
29 Tando Adam
30 Dera Ghazi Khan
31 Nawabshah
32 Bhakkar
33 Dera Ismail Khan
34 Tando Allahyar
35 Mirpurkhas
36 Umarkot
37 Haripur
38 Swabi
39 Hyderabad
40 Jacobabad
41 Shikarpur
42 Kotli
43 Karak
44 Lakki Marwat
45 Mianwali
46 Kohat
47 Thatta
48 Bannu
49 Chagai
50 Larkana
51 Abbottabad
52 Muzaffarabad
53 Dadu
54 Dir
55 Mingora
56 Karachi
57 Khyber
58 Peshawar
59 Shabqadar
60 Kech
61 Turbat
PM2.5 < 45.69
62 Panjgur
63 Dera Bugti
64 Shangla
65 Gwadar
66 Ormara
67 Kurram
68 Lasbela
69 Awaran
70 Kharan
71 Zhob
72 Bajaur
73 Sibi
74 Khuzdar
75 Pishin
76 Quetta
77 Mastung
78 Kalat
79 Chaman
80 Loralai
Desert
A Thal
B Cholistan
C Thar
D Kharan
E Chagai
Afghanistan
China
India
Iran
Arabian Sea
(a)
Administrative Units
GB Gilgit-Baltistan
AK Azad Kashmir
KP Khyber Pakhtunkhwa
PJ Punjab
BL Balochistan
SN Sindh
0 75 150 300 Km
Legend
Extremely Polluted Cities
Highly Polluted Cities
Polluted Cities
Indus River
Islamic Republic of Pakistan
Disputed area
Urban area
Cropland
Desert
Ocean
Polluted Cities of Pakistan
AOD550 > 0.6
1 Jhang
2 Multan
3 Vehari
4 Khairpur
5 Rahimyar Khan
6 Pakpattan
7 Okara
8 Nawabshah
9 Faisalabad
10 Tando Adam
11 Tando Allahyar
12 Bahawalnagar
13 Lahore
14 Shikarpur
15 Layyah
16 Hyderabad
17 Jacobabad
18 Ormara
19 Sargodha
20 Gwadar
21 Gujranwala
0.3 ≤ AOD550 ≤ 0.6
22 Larkana
23 Dera Ismail Khan
24 Khushab
25 Dera Ghazi Khan
26 Sialkot
27 Mirpurkhas
28 Mianwali
29 Kharan
30 Sukkur
31 Dadu
32 Peshawar
33 Gujrat
34 Nowshera
35 Mardan
36 Umarkot
37 Charsadda
38 Jhelum
39 Bahawalpur
40 Chaman
41 Swabi
42 Turbat
43 Awaran
44 Kech
45 Attock
46 Mirpur
47 Bhakkar
48 Rawalpindi
49 Panjgur
50 Lasbela
51 Bhimber
52 Islamabad
53 Haripur
54 Karachi
55 Thatta
56 Shabqadar
AOD550 < 0.3
57 Kohat
58 Pishin
59 Chagai
60 Quetta
61 Kalat
62 Mastung
63 Lakki Marwat
64 Kotli
65 Khuzdar
66 Abbottabad
67 Kurram
68 Rawlakot
69 Karak
70 Sibi
71 Dera Bugti
72 Muzaffarabad
73 Bannu
74 Dir
75 Mingora
76 Bajaur
77 Loralai
78 Shangla
79 Khyber
80 Zhob
Desert
A Thal
B Cholistan
C Thar
D Kharan
E Chagai
Afghanistan
China
India
Iran
Arabian Sea
(b)
Administrative Units
GB Gilgit-Baltistan
AK Azad Kashmir
KP Khyber Pakhtunkhwa
PJ Punjab
BL Balochistan
SN Sindh
0 75 150 300 Km
Legend
Extremely Polluted Cities
Highly Polluted Cities
Polluted Cities
Indus River
Islamic Republic of Pakistan
Disputed area
Urban area
Cropland
Desert
Ocean

Figure 1: Geographical and administrative map of Pakistan including a list of cities used in the present study. Cities are characterized using (a) yearly mean CAMS (Copernicus Atmosphere Monitoring Service) reanalysis $PM_{2.5}$ concentrations ($\mu g/m^3$) for the years 2003 and 2020, and (b) yearly mean AquaTerra MODIS DTB AOD retrievals at 550 nm from 2003 to 2017. Extremely polluted cities (red color) are defined for $PM_{2.5} > 92.84$ (AOD > 0.6) (3rd quartile), highly polluted cities (brown color) for $45.69 \leq PM_{2.5} \leq 92.84$ (0.3 < AOD < 0.6) (between 3rd and 1st quartiles), and polluted cities (purple color) for $PM_{2.5} < 45.69$ (AOD < 0.3) (1st quartile) using descriptive statistics (Table S1). Cities are not defined as low polluted or clean cities as annual mean $PM_{2.5}$ concentrations for all cities exceed Pakistan's National Environmental Quality Standards (Pak-NEQS) for ambient air (<15 $\mu g/m^3$ annual mean).

3. Dataset

3.1 AERONET Data

The AERONET (AErosol RObotic NETwork) (Holben et al. 1998; Holben et al. 2001) is a global network of calibrated Sunphotometers coordinated by NASA (National Aeronautics and Space Administration) which provides regular measurements of spectral AOD at 340 nm, 380 nm, 440 nm, 500 nm, 675 nm, 870 nm, 1020 nm, and 1640 nm, and AE at 340–440 nm, 380-500 nm, 440–675 nm, and 500–870 nm at three levels, i.e., Level 1.0 (unscreened), Level 1.5 (cloud-screened), and Level 2.0 (cloud-screened and quality-assured), under cloud-free skies (Smirnov et al. 2000) for every 15 minutes with an uncertainty of 0.01–0.02 (Holben et al. 2001). The present study used Version 3 Level 2.0 AOD at 500 nm (AOD_{500}) and AE at 440–675nm ($AE_{440–675}$) (Giles et al. 2019) obtained from the AERONET website (https://aeronet.gsfc.nasa.gov/) for the Lahore

(31.47987° N, 74.26406° E) and Karachi (24.94574° N, 67.13594° E) sites from 2006 to 2017. The Lahore and Karachi AERONET sites are located in an urban area, and approximately 20 km away from the Arabian Sea coast, respectively.

3.2 AquaTerra MODIS Data

In the present study, Aqua and Terra MODIS C6.1 L2 aerosol products at 10 km spatial resolution are obtained from 2003 to 2017 for Pakistan from the LAADS DAAC (https://ladsweb.modaps.eosdis.nasa.gov/). The MODIS aerosol product provides DT AOD retrievals over land and water surfaces (Levy et al. 2013), and DB AOD retrievals only over land (Hsu et al. 2013). The DT and DB AOD retrievals for different collections are extensively validated against Sunphotometer (AERONET) measurements at regional (Bilal et al. 2019b; Bilal et al. 2014; Che et al. 2019; de Leeuw et al. 2018; Fan et al. 2017; Filonchyk et al. 2019; Gupta et al. 2013; He et al. 2018; Islam et al. 2019; Livingston et al. 2014; Mhawish et al. 2017; More et al. 2013; Nichol and Bilal 2016; Shen et al. 2018; Shi et al. 2013; Sogacheva et al. 2018; Wang et al. 2017; Wang et al. 2019; Xiao et al. 2016; Xie et al. 2011) and global scales (Bilal et al. 2018a; Bilal et al. 2017; Levy et al. 2013; Levy et al. 2010; Mehta et al. 2016; Remer et al. 2013; Sayer et al. 2013; Sayer et al. 2014; Sayer et al. 2015; Tong et al. 2020). These studies have reported overestimation and underestimation in DT and DB AOD retrievals respectively, due to error in the estimated surface reflectance and aerosol scheme used in the inversion methods, but overall their performance is satisfactory. Previous studies (Bilal et al. 2018a; Bilal and Nichol 2017; Bilal et al. 2017; Bilal et al. 2018b; Mei et al. 2019; Sayer et al. 2014) have also reported different spatial coverage of DT and DB AOD retrievals over land due to differences in their approaches, i.e., pixel selection criteria,

estimation of surface reflectance, and the cloud mask. Therefore, a new merged Scientific Data Set (SDS: AOD 550 Dark Target Deep Blue Combined) was introduced which contains only the highest quality DT and DB (DTB) AOD retrievals or their average values (Levy et al. 2013). The purpose of this new dataset is to improve spatial coverage over land (Levy et al., 2013; Sayer et al., 2014), i.e., to retrieve AOD in the same image for those regions where either the DT or the DB algorithm does not achieve a successful retrieval (Bilal et al. 2017; Levy et al. 2013). The merged DTB AOD retrievals have been validated at regional and global scales (Ali and Assiri 2019; Bilal et al. 2018a; Bilal and Nichol 2017; Bilal et al. 2017; Sayer et al. 2014; Sogacheva et al. 2018). However, the new customized method-1 (CM1) (Bilal et al. 2017), which is named Simplified Merge Scheme (SMS) in the later publications (Bilal et al. 2018a; Bilal et al. 2018b), provides equally consistent data quality with the combined DTB AOD retrievals available in C6.1, but with significantly improved spatio-temporal coverage.

3.3 CAMS Data

The Copernicus Atmosphere Monitoring Service (CAMS) reanalysis is an atmospheric composition dataset generated by the European Centre for Medium-Range Weather Forecasts (ECMWF). The global CAMS model combines satellite-based observations with chemistry-aerosol modeling using the four-dimensional variational (4D-VAR) data assimilation technique to obtain the mass concentration of aerosols and trace gases. CAMS uses the MACCity inventory at 0.5° × 0.5° spatial resolution for anthropogenic emissions which covers the period 1960–2010 (Granier et al. 2011). Detailed information about the model and the emission inventory can be found in (Flemming et al. 2017; Flemming et al. 2015). In this study, the ground-based mass concentration

of particulate matter, including particles with an aerodynamic diameter of less than 1 μm (PM_1), less than 2.5 μm ($PM_{2.5}$), and less than 10 μm (PM_{10}) was obtained from the CAMS reanalysis data for the years 2003 and 2020. PM_x (x = 1, 2.5, & 10) data were used at two different spatiotemporal resolutions, i.e., (i) CAMS global reanalysis dataset at 0.75° × 0.75° spatial resolution and 3-hourly temporal resolution from 2003 to 2020, and (ii) CAMS near-real time dataset at 0.125° × 0.125° spatial resolution and 12-hourly temporal resolution from 2018 to 2020 (Inness et al. 2019). The PM_x data at 0.75° grid size and 3-hourly temporal resolution were used for long-term climatology and for characterizing extremely polluted cities, whereas, the CAMS near-real time data at 0.125° grid size and 12-hourly temporal resolution were used for validation against ground-based $PM_{2.5}$ concentrations obtained from air quality monitoring stations.

3.4 MERRA-2 Reanalysis Data

The MERRA-2 (Modern-Era Retrospective analysis for Research and Applications, Version 2) atmospheric reanalysis is the latest data released by the NASA GMAO (Global Modeling and Assimilation Office) in 2017 (Buchard et al. 2017; Randles et al. 2017). The MERRA-2 aerosol gridded data, i.e., dust, sea salt, sulfate, black carbon, and organic carbon, are simulated with 72 vertical layers from the surface to higher than 80 km using the GEOS-5 (GMAO Earth system model version 5) model radiatively coupled to the GOCART (Goddard Chemistry Aerosol Radiation and Transport) model (Chin et al. 2002; Colarco et al. 2010). For anthropogenic emissions, MERRA-2 uses the EDGAR-4.2 emission inventory at 0.1° × 0.1° spatial resolution which covers the period 1970–2008 (Janssens-Maenhout et al. 2013). In this study, the MERRA-2 aerosol gridded data (dust, sea salt, sulfate, black carbon, and organic carbon) at 0. 5° × 0.625°

spatial resolution from 2018 to 2020 were used. More details about MERRA-2 reanalysis data can be found in Randles et al. (2017) and Buchard et al. (2017).

3.5 Ground-based $PM_{2.5}$ Measurements

Ground-based $PM_{2.5}$ measurements were obtained from two different air quality monitoring networks. Firstly, $PM_{2.5}$ data were obtained from 4 air quality stations operated by the US Consulates in Islamabad, Karachi, Lahore, and Peshawar, and secondly, 54 air quality monitoring stations operated by PAQI in Lahore (24 stations), Karachi (15), Islamabad (5) Sialkot (3), Peshawar (2), Rawalpindi (2), Faisalabad (1), Gujranwala (1), and Muridke (1). Due to the lack of a well-developed and standard air quality network of ground-based $PM_{2.5}$ measurements, this study is limited to only these cities for the validation of CAMS and MERRA-2 reanalysis $PM_{2.5}$ gridded data. $PM_{2.5}$ concentrations from the US Consulates are measured by beta gauge attenuation monitors (BAM-1020; Met One Instruments), hereafter referred to as BAM $PM_{2.5}$ concentrations. To increase social awareness in Pakistan, PAQI provides $PM_{2.5}$ data using a nationwide network of low-cost air quality monitors (IQAir AirVisual Pro), hereafter referred to as LCM $PM_{2.5}$ concentrations. In this study, LCM and BAM $PM_{2.5}$ measurements were used for January 2018–December 2019 and January 2019–February 2021, respectively. More details about PAQI (LCM) and US Consulates (BAM) $PM_{2.5}$ data can be found in Shi et al. (2020) and Mhawish et al. (2020), respectively.

3.6 OMI Data

The Ozone Monitoring Instrument (OMI) onboard the Aura satellite was launched in July 2004 as a part of the A-Train satellite constellation. OMI is a hyperspectral sensor that measures the radiation reflected from the earth-atmosphere system, in the wavelength range 250–500 nm and provides daily global coverage at a spatial resolution of 13 × 24 km^2 at nadir. The OMI OMAERUV algorithm utilizes the sensitivity of near-UV spectral regions to aerosol absorption, and it retrieves absorbing aerosol optical depth (AAOD) at 388nm (Torres et al. 2013; Torres et al. 2007). Along with the AAOD, the OMAERUV algorithm also provides an ultraviolet Aerosol Index (UVAI), AOD, and Single Scattering Albedo (SSA). OMI also retrieves the atmospheric trace gases O_3, NO_2 and SO_2 (Carn et al. 2017; Krotkov et al. 2017; Krotkov et al. 2016; Li et al. 2017; Li et al. 2013; Veefkind et al. 2006). In this study, OMAERUV version 3 Level 3 daily cloud-screened (cloud fraction < 30 %) NO_2 tropospheric vertical column density (TVCD) (OMNO2e), and SO_2 VCD in the planetary boundary layer (PBL) (OMSO2e) gridded at 0.25° × 0.25° spatial resolution from 2004 to 2019 were used.

3.7 Other Supporting Datasets

Other supporting datasets include (i) annual mean VIIRS nighttime lights data (https://eogdata.mines.edu/products/vnl/) from 2012 to 2019 derived from monthly mean data (Elvidge et al. 2021), (ii) MODIS Collection 6 global monthly Fire Location product (MCD14ML) from 2003 to 2020 (https://firms.modaps.eosdis.nasa.gov/download/), (iv) MODIS Collection 6 Level 3 land cover type product (MCD12Q1) for 2019

(https://ladsweb.modaps.eosdis.nasa.gov/), and (v) the LandScan population density (https://landscan.ornl.gov/) for 2019 (Rose et al. 2020).

4. Research Methodology

To investigate the air pollution scenario over Pakistan and characterize the extremely polluted cities, in this study the following methodology was adopted:

1. MODIS AOD retrievals were obtained from the Scientific Data Set (SDS) "Optical Depth Land and Ocean" and "Deep Blue Aerosol Optical Depth 550 Land Best Estimate". Only the highest quality-assured DT (QA = 3) and DB (QA ≥ 2) retrievals were used, as recommended by previous studies (Bilal et al. 2013; Levy et al. 2013; Mhawish et al. 2019; Sayer et al. 2013). Pakistan has a variety of land cover types, e.g., snow and mountainous land surface in Northern Pakistan, plain and agricultural land surfaces in Central Pakistan, and arid and desert land surfaces in southern Pakistan, where the DT and DB algorithms overestimate and underestimate, respectively. However, the DT algorithm is unable to provide retrievals over the arid and desert land surfaces of Balochistan. Similar results were observed and reported in our previous study over Pakistan (Bilal et al. 2016). Therefore, in the present study, we preferred to generate the combined (merged) DTB AOD_{550} retrievals for both Aqua and Terra MODIS data from 2003 to 2017 using the customized method-1 (CM1) (Bilal et al. 2017), which in later publications is named Simplified Merge Scheme (SMS) (Bilal et al. 2018a; Bilal et al. 2018b), i.e., an average of the DT and DB AOD retrievals or the available one with the highest quality flag (Equation 1), to enhance spatio-temporal coverage.

330

331 $$DTB\ AOD_{550} = \begin{Bmatrix} if\ only\ DT\ AOD\ exists & \rightarrow & DT \\ if\ only\ DB\ AOD\ exists & \rightarrow & DB \\ if\ both\ DT\ and\ DB\ AOD\ exist & \rightarrow & (DT + DB)/2 \end{Bmatrix} \quad (1)$$

332

333 2. Aqua and Terra MODIS may not provide complete spatial coverage due to cloud cover.
334 On days when Aqua provides AOD retrievals, Terra may not, and vice-versa. Therefore,
335 for more complete spatial coverage between Aqua and Terra as well as to represent an
336 average air pollution scenario between morning and afternoon times with a single
337 dataset, the combined AquaTerra DTB AOD retrievals were generated from the Aqua DTB
338 and Terra DTB AOD retrievals using SMS/CM1, i.e., an average of the Aqua and Terra DTB
339 AOD retrievals or the available one (Equation 2).

340 $$AquaTerra\ AOD = \begin{Bmatrix} if\ only\ Aqua\ AOD\ exists & \rightarrow & Aqua \\ if\ only\ Terra\ AOD\ exists & \rightarrow & Terra \\ if\ both\ Aqua\ and\ Terra\ AOD\ exist & \rightarrow & (Aqua + Terra)/2 \end{Bmatrix} (2)$$

341 3. The AquaTerra DTB AOD retrievals are validated against Sunphotometer AOD
342 measurements obtained for Lahore (31.480° N and 74.264° E) and Karachi (24.946° N and
343 67.136° E) AERONET sites. The AERONET Sunphotometer does not provide AOD at 550
344 nm (AOD_{550}), AOD_{550} is interpolated using AOD at 500 nm (AOD_{500}) and Ångström
345 Exponent at 440-675 nm ($AE_{440\text{-}675}$) based on the Ångström Exponent empirical formula
346 (Equation 3) (Eck et al. 1999). Collocated AquaTerra and AERONET AOD retrievals were
347 defined as the average of at least two pixels of DTB within a spatial region of 3 × 3 pixels

(at least 2 out of 9 pixels) centered on the AERONET site and the average of at least two AERONET AOD measurements between 10:00 and 14:30 local solar time.

$$AOD_{550} = AOD_{500}\left(\frac{550}{500}\right)^{-AE_{440-667}} \quad (3)$$

4. Accuracy and errors are reported using the Pearson correlation coefficient (r), the expected error (EE, Equation 4), and relative mean bias (RMB, Equation 5). The slope (β, Equation 6) and intercept (α, Equation 7) between collocated AquaTerra DTB and AERONET AOD data are calculated using the reduced major axis (RMA) regression which incorporates errors in both independent (AERONET) and dependent (MODIS) variables (Bilal et al. 2019a; Harper 2016). The performance of the Terra and Aqua DT, DB, and DTB AOD retrievals is evaluated based on (i) highest correlation coefficient (r), (ii) highest number of collocated retrievals (N), (iii) the highest percentage of retrievals within the EE, and (iv) lowest RMB. To evaluate the performance of the collocated retrievals, the following criteria are utilized (Bilal et al. 2017): the DT, DB, and DTB retrievals are considered to be of equal quality if the relative difference is within (1) 5% for the correlation coefficient (r), (2) 10% for the collocated retrievals, (3) 10% for the percentage of retrievals is within the EE, and (4) RMB < 25%.

$$EE = \pm\,(0.05 + 0.20 \times AERONET_{AOD}) \quad (4)$$

The upper and lower EE envelopes are calculated using Equations 4a and 4b.

$$Upper\ EE\ envelope = AERONET_{AOD} + |EE| \quad (4a)$$

$$Lower\ EE\ envelope = AERONET_{AOD} - |EE| \quad (4b)$$

The percentage of best retrieved MODIS AOD retrievals within the EE is reported using Equation 4c.

$$\%EE = AERONET_{AOD} - |EE| \leq MODIS_{AOD} \leq AERONET_{AOD} + |EE| \quad (4c)$$

Where |EE| is the absolute value of EE.

$$RMB = \frac{(\overline{MODIS_{AOD}} - \overline{AERONET_{AOD}})}{\overline{AERONET_{AOD}}} \times 100 \quad (5)$$

Where, $\overline{MODIS_{AOD}}$and $\overline{AERONET_{AOD}}$ are the mean of MODIS and AERONET AOD retrievals, respectively. RMB > 0 represents overestimation in MODIS AOD compared to AERONET AOD, RMB < 0 represents underestimation, and RMB = 0 represents no over- and under-estimations.

$$\beta = \frac{\sigma_{MODIS_{AOD}}}{\sigma_{AERONET_{AOD}}} \quad (6)$$

$$\alpha = \overline{MODIS_{AOD}} - \left(\frac{\sigma_{MODIS_{AOD}}}{\sigma_{AERONET_{AOD}}}\right) \times \overline{AERONET_{AOD}} \quad (7)$$

Where, $\beta, \alpha, \sigma_{MODIS_{AOD}}$, and $\sigma_{AERONET_{AOD}}$ are the slope, intercept, the standard deviation of MODIS AOD, and standard deviation of AERONET AOD, respectively.

5. To show the long-term variation of the mean spatial distributions of AquaTerra AOD over Pakistan, the AOD retrievals from 2003 to 2017 are used to generate monthly mean

spatial AOD maps, and their corresponding pixel counts are calculated for reporting the retrieval performance of both the DT and DB algorithms.

6. To assure the quality of the $PM_{2.5}$ data, validation of daily average CAMS and MERRA-2 $PM_{2.5}$ data was conducted against in-situ $PM_{2.5}$ measurements obtained from the air quality monitoring stations. The performance was evaluated based on the correlation coefficient (r), RMB (Eq. 5), and slope (Eq. 6). MERRA-2 $PM_{2.5}$ concentrations were calculated based on five aerosol components using Equation 8 (Song et al. 2018), and CAMS $PM_{2.5}$ and PM_{10} concentrations were calculated using Equations 9 and 10 (Rémy et al. 2019).

$$PM_{2.5} = [Dust_{2.5}] + [SS_{2.5}] + 1.375 \times [SO_4] + [BC] + 1.6 \times [OC] \quad (8)$$

Where, $Dust_{2.5}$, $SS_{2.5}$, BC, OC, and SO_4 are the GOCART concentrations of dust, sea salt, black carbon, organic carbon, and sulfate in particles with a diameter smaller than 2.5 μm, respectively.

$$PM_{2.5} = \rho([SS_1]/4.3 + [SS_2]/4.3 + [DD_1] + [DD_2] + 0.7[OM] + [BC] + 0.7[SU] + 0.7[NI_1] + 0.25[NI_2] + 0.7[AM]) \quad (9)$$

$$PM_{10} = \rho([SS_1]/4.3 + [SS_2]/4.3 + [DD_1] + [DD_2] + 0.4[DD_3] + [OM] + [BC] + [SU] + [NI_1] + [NI_2] + [AM]) \quad (10)$$

Where [$SS_{1,2}$] = sea salt aerosol, [$DD_{1,2,3}$] = desert dust, [$NI_{1,2}$] = nitrate, [OM] = organic matter, [BC] = black carbon, [SU] = sulfate, and [AM] = ammonium (concentrations in particles with a diameter smaller than 2.5 μm from the CAMS model).

7. To characterize extremely polluted cities in Pakistan, the DTB AOD retrieved from AquaTerra, the PM_1, $PM_{2.5}$, and PM_{10} from CAMS data, and the SO_2 VCD and NO_2 TVCD from OMI are used. Polluted months as well as years, for the corresponding polluted cities, are also characterized based on each pollutant.
8. To assess recent changes in the concentrations of atmospheric constituents, the non-parametric Mann Kendal test (Kendall and Gibbons 1990; Mann 1945) associated with Theil-Sen's slope (Sen 1968; Theil 1992) was used to estimate and detect trends over the main cities of Pakistan from 2003 to 2020. The non-parametric Mann Kendal test is often used to detect monotonic trends in a time series and is also suitable for non-normally distributed data, or if the data have some missing observations such as environmental data. Further, the bootstrapping technique was used to eliminate serial autocorrelation in the monthly mean aggregated time series data and increase the robustness of the test (Hamed and Ramachandra Rao 1998; Salmi et al. 2002). The significance of the calculated trend was assessed using the two-tailed test method at a 95% confidence interval.
9. The NOAA (National Oceanic and Atmospheric Administration) HYSPLIT (Hybrid Single-Particle Lagrangian Integrated Trajectory Model) (Stein et al. 2015), a complete transport, dispersion, and chemical transformation model, is used for back trajectory analysis to determine the origin of air masses (Fleming et al. 2012) and highlight the possible sources of aerosol pollutants affecting the air quality of Pakistan using the PSCF (Potential Source

Contribution Function) analysis. In this study, 72 hours HYSPLIT backward trajectories at the height of 500 m above the ground level (AGL) were computed for every 6 hours at seasonal scales from March 2020 to February 2021 using the GDAS (Global Data Assimilation System) meteorological data at 1° × 1° spatial resolution (available at ftp://arlftp.arlhq.noaa.gov/pub/archives/gdas1). The PSCF analysis was performed for 4 cities selected because of the availability of ground-based $PM_{2.5}$ measurements from the air quality stations operated by the US Consulates, namely, Peshawar, Islamabad, Lahore, and Karachi. The height of 500 m AGL has been reported very useful as it is the approximate height of the mixing layer (Begum et al. 2005). The backward trajectory clustering and investigation of the origins of the particulate matter at the receptor locations were studied using MeteoInfo TrajStat software (Version 2.0, available at http://meteothink.org/products/trajstat.html) (Wang et al. 2009) in conjunction with HYSPLIT and Geographic Information System (GIS).

The PSCF analysis was performed using 24-hour average ground-based $PM_{2.5}$ concentrations over a grid with a resolution of 0.5°, for the days that exceeded the Pak-NEQS 24-hour air quality standards (35 µg/m^3). The PSCF value for a specific grid cell was calculated on the assumption that the trajectory endpoint is located within a cell (i, j) and the trajectory is assumed to collect pollutants emitted from different pocket emission sources within that cell (i, j). The PSCF value can be interpreted as a conditional probability describing the potential contributions of a grid cell to the high $PM_{2.5}$ loadings at the receptor site. The error associated with the trajectory is proportional to the distance from

445 the receptor location (Begum et al. 2005). The PSCF value for the ijth grid cell can be
446 computed using Equation 11:

447 $$PSCF(i,j) = m_{ij}/n_{ij} \quad (11)$$

448 Where, n_{ij} represents the number of endpoints that fall or pass through the ij^{th} cell
449 and m_{ij} denotes for the number of endpoints in the ij^{th} cell having a higher pollutant
450 concentration than the 24-hour Pak-NEQS. The uncertainty arising due to small n_{ij} is
451 reduced by multiplying an arbitrary weight function $W_{i,j}$, which is multiplied into the
452 PSCF. In this case, the weight function is given in Equation (12):

453 $$W_{i,j} = \begin{cases} if\ n_{ij} > 3\overline{n} \rightarrow 1.00 \\ if\ 1.5\overline{n} < n_{ij} \leq 3\overline{n} \rightarrow 0.70 \\ if\ \overline{n} < n_{ij} \leq 1.5\overline{n} \rightarrow 0.42 \\ if\ n_{ij} \leq \overline{n} \rightarrow 0.15 \end{cases} \quad (12)$$

454 Where $\overline{n}$ denotes the average number of endpoints per cell, which is calculated for each
455 cell that has at least one endpoint. Therefore, the Weighted PSCF is expressed as Equation
456 (13):

457 $$WPSCF = W_{i,j} \times PSCF\ (i,j) \quad (13)$$

458 ## 5. Results and Discussion

459 ### 5.1 Aqua and Terra MODIS AOD data

460 #### 5.1.1 Validation of AOD products against AERONET

461 The MODIS AOD data used in this paper were evaluated by comparison with the AERONET
462 AOD data over Lahore and Karachi. The scatterplots in Figure 2 show that Terra DT (Figure 2a),

DB (Figure 2b), and DTB (Figure 2c) retrieved AOD are equally correlated (r = 0.83) with AERONET-derived AOD, and have the same percentage of retrievals within the EE. However, the number of collocated observations for DTB (N = 2796) is significantly higher than for DT (N = 1437) and DB (N = 2486) i.e., 94.6% and 12.5% more data are available from DTB than from DT and DB, respectively. The AOD retrieved from DT is significantly overestimated (RMB = 17.17%), with 34.38% of the data are above the EE (+EE). DB underestimates the AOD (RMB = -9.87%) with 28.24% of the data below the EE (-EE). These uncertainties appear to be averaged out in the DTB AOD product, as the overestimations and underestimations are fewer than for DT and DB, individually. Furthermore, the RMB (-0.03%) is significantly improved, being 99.9% and 99.8% lower than for DT and DB, respectively. These results indicate the better performance of the Terra DTB AOD product as compared to DT and DB over Pakistan. Similar to Terra, the performance of the Aqua DTB AOD product (Figure 2f) is much better than for DT (Figure 2d) and DB (Figure 2e) products, with a significantly higher number of collocated AOD values and lower RMB. However, Aqua performs equally as Terra in terms of correlation and the percentage of retrievals within the EE. It is important to mention that a larger number of both DT and DB AOD retrieval products was available for Lahore than for Karachi and also that DB provides a greater number of AOD retrievals over Pakistan than DT. Based on the superior performance of the Aqua and Terra DTB AOD retrievals, the merged AquaTerra DTB AOD product was generated for further analysis (see Figure S1 in the supplementary data for the validation of AquaTerra DTB AOD retrievals).

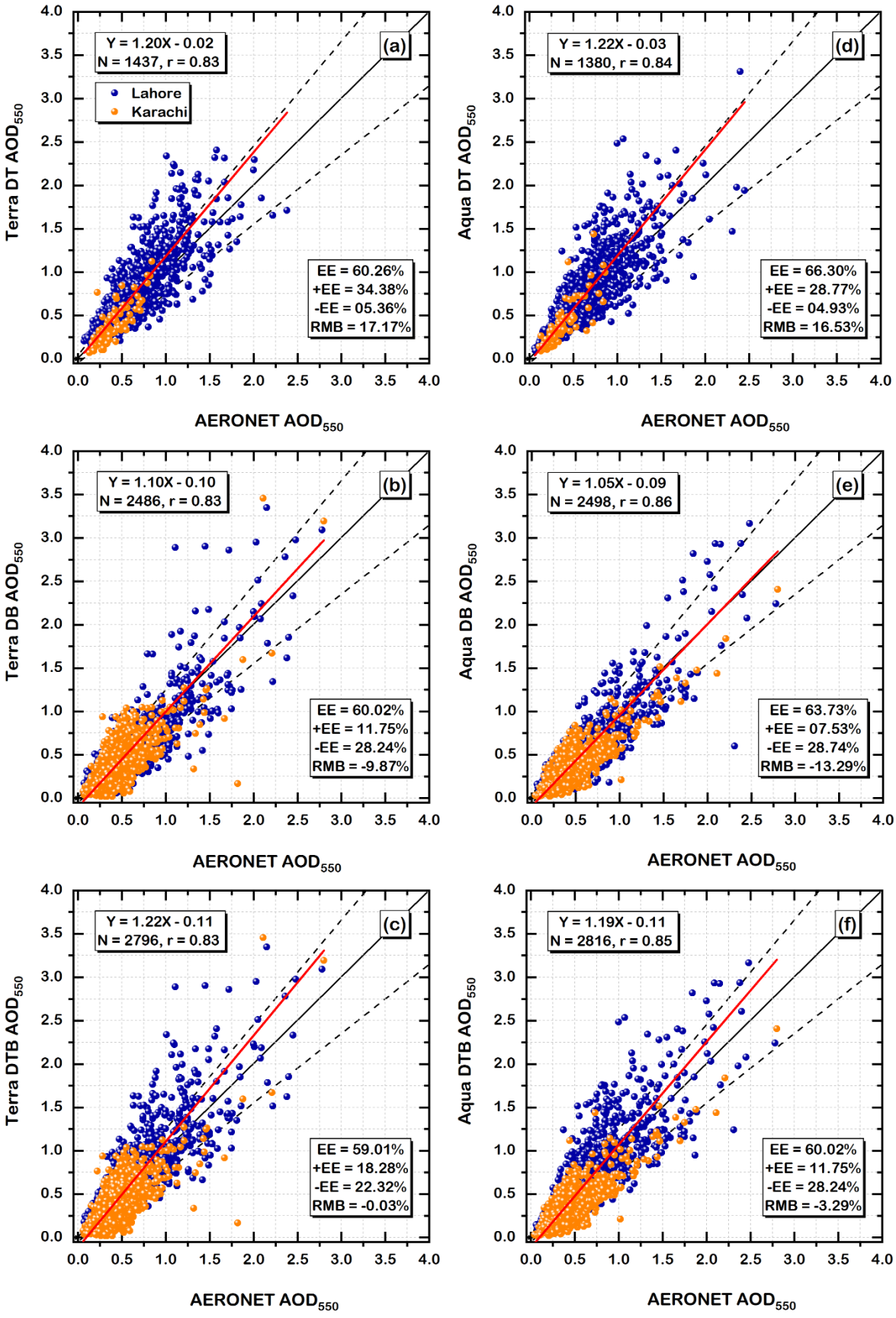
Y = 1.20X - 0.02
N = 1437, r = 0.83
(a)
Lahore
Karachi
EE = 60.26%
+EE = 34.38%
-EE = 05.36%
RMB = 17.17%
Terra DT AOD550
AERONET AOD550
Y = 1.22X - 0.03
N = 1380, r = 0.84
(d)
EE = 66.30%
+EE = 28.77%
-EE = 04.93%
RMB = 16.53%
Aqua DT AOD550
AERONET AOD550
Y = 1.10X - 0.10
N = 2486, r = 0.83
(b)
EE = 60.02%
+EE = 11.75%
-EE = 28.24%
RMB = -9.87%
Terra DB AOD550
AERONET AOD550
Y = 1.05X - 0.09
N = 2498, r = 0.86
(e)
EE = 63.73%
+EE = 07.53%
-EE = 28.74%
RMB = -13.29%
Aqua DB AOD550
AERONET AOD550
Y = 1.22X - 0.11
N = 2796, r = 0.83
(c)
EE = 59.01%
+EE = 18.28%
-EE = 22.32%
RMB = -0.03%
Terra DTB AOD550
AERONET AOD550
Y = 1.19X - 0.11
N = 2816, r = 0.85
(f)
EE = 60.02%
+EE = 11.75%
-EE = 28.24%
RMB = -3.29%
Aqua DTB AOD550
AERONET AOD550

482

Figure 2: Validation of Terra and Aqua DT, DB, and DTB AOD products versus AERONET Version 3 Level 2.0 AOD measured in Lahore (for location, see no. 1 in Fig. 1a) and Karachi (for location, see no. 56 in Fig. 1a) from 2006 to 2017. The red line represents the regression line, the solid black line represents the identity line, and the dashed black lines represent the upper and lower EE envelopes. The orange points represent AOD pairs at Karachi, the blue dots at Lahore.

5.1.2 Spatial distribution of AOD retrievals

Figure 3 shows the spatial distributions of the monthly mean AquaTerra DTB AOD over Pakistan together with the corresponding pixel counts (PC) averaged over the years 2003 - 2017. Significant monthly variations in both AOD and PC are observed. AOD retrievals are missing over the Gilgit-Baltistan and Jammu & Kashmir (disputed territory) throughout the year, except for January, as the DT and DB algorithms do not provide AOD retrievals over high mountain regions and snow-covered surfaces. The presence of AOD retrievals during January is because the DB algorithm does not use the MODIS snow mask product directly, and the internal snow/cloud mask does not work well over these regions. Surprisingly, high AOD values > 1.0 are observed during June and July over the Northwestern region of Khyber Pakhtunkhwa, which is a high mountainous region with permanent snow cover. These high AOD values over snow-covered regions could be due to an error in the internal snow/cloud mask of the DB algorithm which has missed these pixels during preprocessing; DT does discard bright pixels during preprocessing. AOD >1.0 is observed in July followed by June and August over Punjab and Sindh, mainly attributed to hygroscopic growth of the aerosol particles during summer relative humidity is high, similar to other reports using MODIS and MISR aerosol products (Mehta et al. 2016; Mhawish et

al. 2021). Most of the major cities of Punjab and Sindh are surrounded by cropland, and the results show that high AOD over Pakistan follows the same spatial pattern as that of the cropland. The AOD over cropland is significantly higher than over non-agricultural (i.e., mainly desert) regions throughout the year, even during late spring and summer when dust storms are considered a major source of aerosols over Punjab and Sindh. Local production of anthropogenic aerosols from urban and industrial emissions and agricultural pre- and post-harvest burning may be responsible for the high pollution levels over the region. Over Balochistan, especially over the desert areas, the AOD is low compared to that in Punjab and Sindh, but still higher than over other administrative units. Over Punjab, the highest AOD values are observed during the post-harvest seasons, i.e., throughout September to November, peaking in November, probably due to biomass (crop residue) burning activities (Jethva et al. 2019; Mhawish et al. 2021). However, if the high AOD levels would only be due to locally produced aerosols, the spatial patterns during each month should be similar, but they are not. Therefore, the transboundary transport of aerosols may contribute to Pakistan's deteriorating air quality. This is confirmed by the well-known smog episodes, occurring every year over Punjab due to both local production of aerosols from crop residue burning and across the border, during which atmospheric visibility is reduced to a few meters in both urban and rural areas. Overall, much higher AOD levels were observed in Pakistan during June, July, and August (summer), followed by September, October, and November (autumn), March, April, and May (spring), and December, January, and February (winter). The higher AOD in the summer is attributed to several reasons, including (i) hygroscopic growth of aerosol particles, due to high relative humidity, which increases the extinction efficiency of the atmospheric aerosols (Dickerson et al. 1997; Li and Wang 2014), (ii) the

enhancement of secondary aerosol formation rate due to faster photochemical reactions during higher temperatures (Jacob and Winner 2009; Kulmala et al. 2020), and (iii) the larger contribution of natural aerosols (mainly dust) during the summer monsoon (Mhawish et al. 2021).

Figure 3 shows a distinct pattern of PC which suggests that the DT and DB algorithms do not perform equally temporally or spatially. For example, between 2003 to 2017, from late spring to early autumn, a large number of AOD retrievals (> 400) per pixel are available over Balochistan and some parts of Punjab, and from late autumn to early spring, a large number of AOD retrievals (> 400) per pixel are available over Sindh and some parts of Punjab. This could be attributed to the seasonality in the surface albedo due to changes in vegetation cover and/or the presence of cloud cover. Only October provides favorable conditions to both the DT and DB algorithms, when more than 400 AOD retrievals are available over Pakistan from both algorithms, except for Gilgit-Baltistan and disputed areas, due to high surface albedo for snow/ice surfaces.

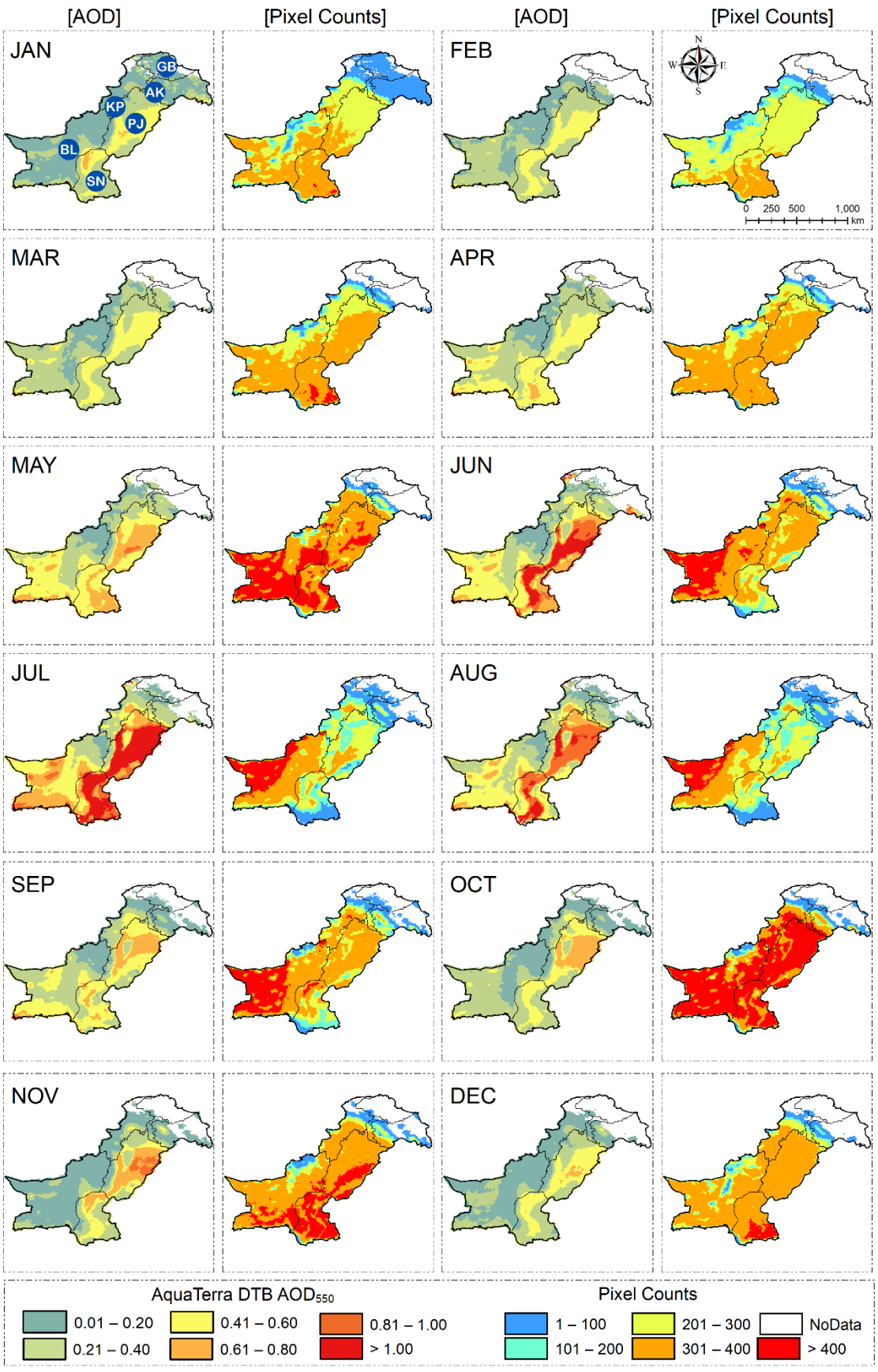
[AOD]
[Pixel Counts]
[AOD]
[Pixel Counts]
JAN
FEB
MAR
APR
MAY
JUN
JUL
AUG
SEP
OCT
NOV
DEC
GB
AK
KP
PJ
BL
SN
N
W
E
S
0 250 500 1,000
km
AquaTerra DTB AOD550
0.01 – 0.20
0.21 – 0.40
0.41 – 0.60
0.61 – 0.80
0.81 – 1.00
> 1.00
Pixel Counts
1 – 100
101 – 200
201 – 300
301 – 400
NoData
> 400

539

Figure 3: Monthly mean spatial distributions of AquaTerra DTB AOD_{550} and the total number of corresponding Pixel Counts (PC) over Pakistan, both averaged over the years from 2003 to 2017. The six units in Pakistan are indicated in the upper-left figure: GB = Gilgit-Baltistan, AK= Azad Kashmir, KP = Khyber Pakhtunkhwa, PJ = Punjab, BL = Balochistan, and SN = Sindh.

5.1.3 Characterization of extremely polluted cities using MODIS data

Figure 4a shows the mean AOD_{550} retrievals for 80 cities (Figure 1) obtained from the annual mean AquaTerra DTB AOD_{550} images and categorizes the extremely polluted to polluted cities. The thresholds for polluted and extremely polluted cities are defined based on the values of first (Q1) and third (Q3) quartiles respectively, and these quartiles are calculated by analyzing descriptive statistics (Table S1) for the AOD values extracted for 80 cities. Highly polluted cities are defined based on the AOD range between the first and third quartiles. For example, AOD < 0.3 (1^{st} quartile) represents polluted cities, 0.3 ≤ AOD ≤ 0.6 (between 1^{st} and 3^{rd} quartiles) represents highly polluted cities and AOD > 0.6 represents extremely polluted cities (3^{rd} quartile). A total of 21 cities fall within the category of extremely polluted cities (Punjab: 12, Sindh: 7, and Balochistan: 2), 35 cities in the category of moderately polluted cities (Punjab: 11, Sindh 7, Balochistan: 7, Khyber Pakhtunkhwa: 8, Azad Kashmir: 2), and 24 cities in the category of low polluted cities (Punjab: 0, Sindh 0, Balochistan: 10, Khyber Pakhtunkhwa: 11, Azad Kashmir: 3). The top 3 polluted cities are Jhang, Multan, and Vehari in Punjab, as Punjab is the most urbanized and populated administrative unit (Figures 1b and 4a), with more vehicles and industries, and also faces severe smog episodes and dust storms, resulting in extremely high AOD levels over the region. Along with anthropogenic aerosols produced locally from cropland, urban and industrial

emissions, regional transport of aerosols may be responsible for Punjab's severe air pollution problems which will be investigated using the PSCF analysis based on the HYSPLIT air parcel back trajectory analysis and BAM $PM_{2.5}$ concentrations (see section 5.7).

Figure 4b shows the pixel counts (PC) of the daily AOD retrievals for each city from 2003 to 2017. Results show a large number of PC for most cities, indicating that the characterization of extremely polluted to polluted cities is based on a large number of PC, which supports the results in Figure 4a and provides confidence in the use of merged AquaTerra DTB AOD products for quantitative research applications over Pakistan. However, it is noted that the lowest number of PC is observed for the coastal (Ormara and Gwadar) and mountainous (Dir) cities, where the inversion scheme of both the DT and DB algorithms needs to be improved.

The monthly mean AOD retrievals are plotted to identify the high and low polluted months in Pakistan (Figure 4c). The months of June, July, and August are by far the most polluted, with AOD > 1.20 for extremely polluted cities. A similar pattern of monthly variation in AOD is observed for all other cities, though at lower pollution levels. As mentioned in section 5.1.2, these months may be affected by aerosol pollutants from local sources such as agricultural land, urban and industrial regions, and deserts. Figure 4d, showing inter-annual variations, indicates very high AOD levels for extremely polluted cities throughout the last two decades, with annual mean AOD > 0.60, and with the most polluted years being 2004, 2006, 2008, 2016, and 2017.

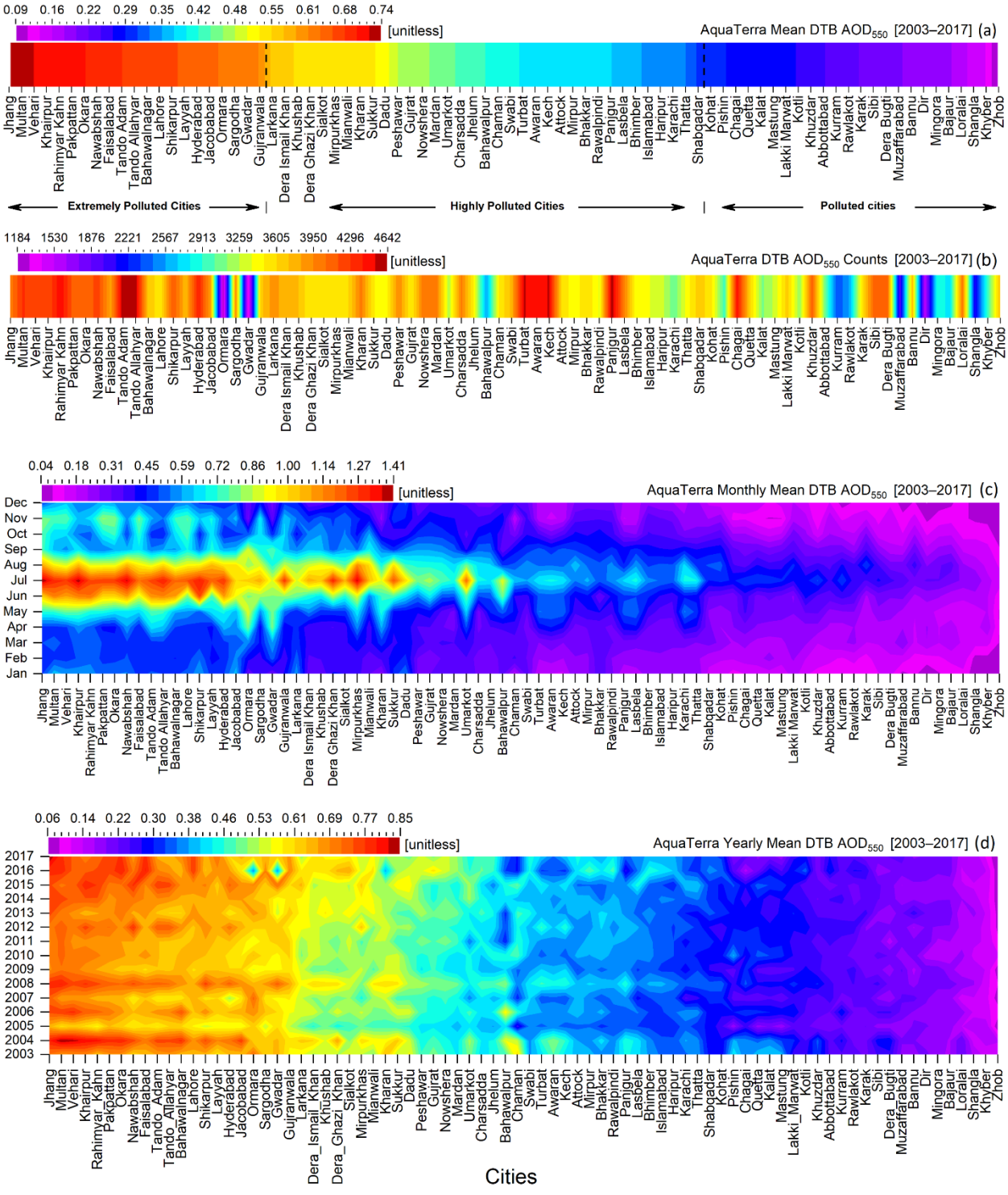
0.09 0.16 0.22 0.29 0.35 0.42 0.48 0.55 0.61 0.68 0.74
[unitless]
AquaTerra Mean DTB AOD550 [2003–2017] (a)
Extremely Polluted Cities
Highly Polluted Cities
Polluted cities
1184 1530 1876 2221 2567 2913 3259 3605 3950 4296 4642
[unitless]
AquaTerra DTB AOD550 Counts [2003–2017] (b)
0.04 0.18 0.31 0.45 0.59 0.72 0.86 1.00 1.14 1.27 1.41
[unitless]
AquaTerra Monthly Mean DTB AOD550 [2003–2017] (c)
Dec
Nov
Oct
Sep
Aug
Jul
Jun
May
Apr
Mar
Feb
Jan
0.06 0.14 0.22 0.30 0.38 0.46 0.53 0.61 0.69 0.77 0.85
[unitless]
AquaTerra Yearly Mean DTB AOD550 [2003–2017] (d)
2017
2016
2015
2014
2013
2012
2011
2010
2009
2008
2007
2006
2005
2004
2003
Jhang Multan Vehari Khairpur Rahimyar Kahn Pakpattan Okara Nawabshah Faisalabad Tando Adam Tando Allahyar Bahawalnagar Lahore Shikarpur Layyah Hyderabad Jacobabad Ormara Sargodha Gwadar Gujranwala Larkana Dera Ismail Khan Khushab Dera Ghazi Khan Sialkot Mirpurkhas Mianwali Kharan Sukkur Dadu Peshawar Gujrat Nowshera Mardan Umarkot Charsadda Jhelum Bahawalpur Chaman Swabi Turbat Awaran Kech Attock Mirpur Bhakkar Rawalpindi Panjgur Lasbela Bhimber Islamabad Haripur Karachi Thatta Shabqadar Kohat Pishin Chagai Quetta Kalat Mastung Lakki Marwat Kotli Khuzdar Abbottabad Kurram Rawlakot Karak Sibi Dera Bugti Muzaffarabad Bannu Dir Mingora Bajaur Loralai Shangla Khyber Zhob
Cities

Figure 4: Characterization of extremely polluted to polluted cities in Pakistan using AquaTerra DTB AOD_{550} products from 2003 to 2017. (a) polluted cities based on mean AOD, (b) pixel counts, (c) polluted months based on mean AOD, and (d) polluted years based on mean AOD.

5.2 CAMS and MERRA-2 reanalysis data

5.2.1 Validation of $PM_{2.5}$ reanalysis data

Previous studies have evaluated the uncertainties in both CAMS and MERRA-2 $PM_{2.5}$ reanalysis data compared to ground-based $PM_{2.5}$ measurements (Cuevas et al. 2015; He et al. 2019; Song et al. 2018; Ukhov et al. 2020). Recently, Ukhov et al. (2020) reported overestimation in CAMS $PM_{2.5}$ over the middle east and west Asia which have been attributed to the deficient size distribution of the emitted dust. Additionally, significant underestimation in MERRA-2 $PM_{2.5}$ was reported over China and India (He et al. 2019; Navinya et al. 2020; Song et al. 2018) which could be due to the lack of nitrate concentrations in the reanalysis data and underestimation of OC emission for urban/suburban areas (Buchard et al. 2016; Provencal et al. 2017).

The MERRA-2 and CAMS $PM_{2.5}$ reanalysis data over Pakistan were evaluated by comparison with BAM (beta gauge attenuation monitor) $PM_{2.5}$ concentrations for 2019-2020 provided by the US Consulates and with LCM (low-cost monitor) $PM_{2.5}$ concentrations for 2018-2019 provided by PAQI. The scatterplots in Figure 5 show a significant underestimation of both daily (Figures 5a and 5b) and monthly (Figures 5e and 5f) MERRA-2 $PM_{2.5}$ concentrations compared to both BAM and LCM $PM_{2.5}$ measurements: for the daily data the slopes are 0.45 and 0.54 and the RMB are -34.2% and -26.8%, respectively, and for the monthly data the slopes are 0.30 and 0.52 with -

35.9% to 25.3%, respectively. The results also show the weak correlation of MERRA-2 $PM_{2.5}$ data with both BAM and LCM daily (r = 0.22 and 0.25, respectively) and monthly (r = 0.10 and 0.27, respectively) $PM_{2.5}$ data. The weak correlation suggests that MERRA-2 $PM_{2.5}$ data based on the GOCART aerosol module is unable to accurately reproduce the temporal variations in $PM_{2.5}$. A significant underestimation of MERRA-2 $PM_{2.5}$ data was also reported over China (He et al. 2019; Song et al. 2018) and India (Navinya et al. 2020), but over Pakistan, the correlation is even weaker. Moreover, the grid size of MERRA2 (0. 5° × 0.625° grid size) could introduce errors due to heterogeneity within the large area that affects the correlation with the in-situ measurements.

In comparison with the MERRA-2 data, the correlation coefficients of the CAMS daily (Figures 5c and 5d) and monthly (Figures 5g and 5h) $PM_{2.5}$ data versus ground-based in situ $PM_{2.5}$ measurements are substantially higher for both BAM and LCM. However, the data in Figure 5 show significant deviations of the CAMS-estimated $PM_{2.5}$ from the ground-based $PM_{2.5}$ values, with over- or under-estimation depending on grid size. For example, CAMS overestimates $PM_{2.5}$ at the 0.75° grid size by 30.4% in comparison with the daily BAM data and by 55.4% in comparison with the daily LCM data. For monthly data, these percentages are 30.4% and 57.4%. In contrast, CAMS underestimates $PM_{2.5}$ at the 0.125° grid size in comparison with BAM data and overestimates in comparison with LCM data. These results suggest that grid size and ground-based $PM_{2.5}$ measurement methods (BAM and LCM) play an important role in the overestimation/underestimation of CAMS $PM_{2.5}$ data. For illustration, in comparison with the BAM $PM_{2.5}$ measurements, CAMS data are overestimated for one grid (0.75°) and underestimated for another grid (0.125°), and CAMS $PM_{2.5}$ data at the same grid size (0.125°) are underestimated when compared with data measured using the BAM method and overestimated

622 when compared with data measured using the LCM method. It is worth mentioning that both
623 MERRA-2 and CAMS simulate 5 types of fine particulate matter components (dust, sea salt,
624 sulfate, organic carbon, and black carbon), but nitrate concentrations are not included. If the lack
625 of nitrate concentrations is the main reason for underestimation in MERRA $PM_{2.5}$ data, as
626 reported by previous studies (Buchard et al. 2016; He et al. 2019; Provencal et al. 2017; Song et
627 al. 2018), then underestimation should be observed in CAMS $PM_{2.5}$ data at 0.75° grid size, but
628 this is not the case. Therefore, the exact reasons for underestimation in both MERRA-2 and CAMS
629 as well as overestimation in CAMS data should be thoroughly investigated in future studies. The
630 results show a higher correlation for CAMS monthly data (Figures 5g and 5h) compared to the
631 daily data (Figures 5c and 5d). Although CAMS monthly data at 0.75° grid size show
632 overestimation, they have a good correlation coefficient (r = 0.72–0.76) with ground-based $PM_{2.5}$
633 measurements and could be useful for characterizing pollution levels in the cities of Pakistan
634 compared to the MERRA-2. The comparisons in Figure 5 do not provide a strong reason for
635 choosing one data set over the other. We have selected the CAMS data at the 0.75° grid taking
636 into account the deviation in the CAMS data observed in this evaluation, in addition to the large
637 scatter in individual data points which adds uncertainty.

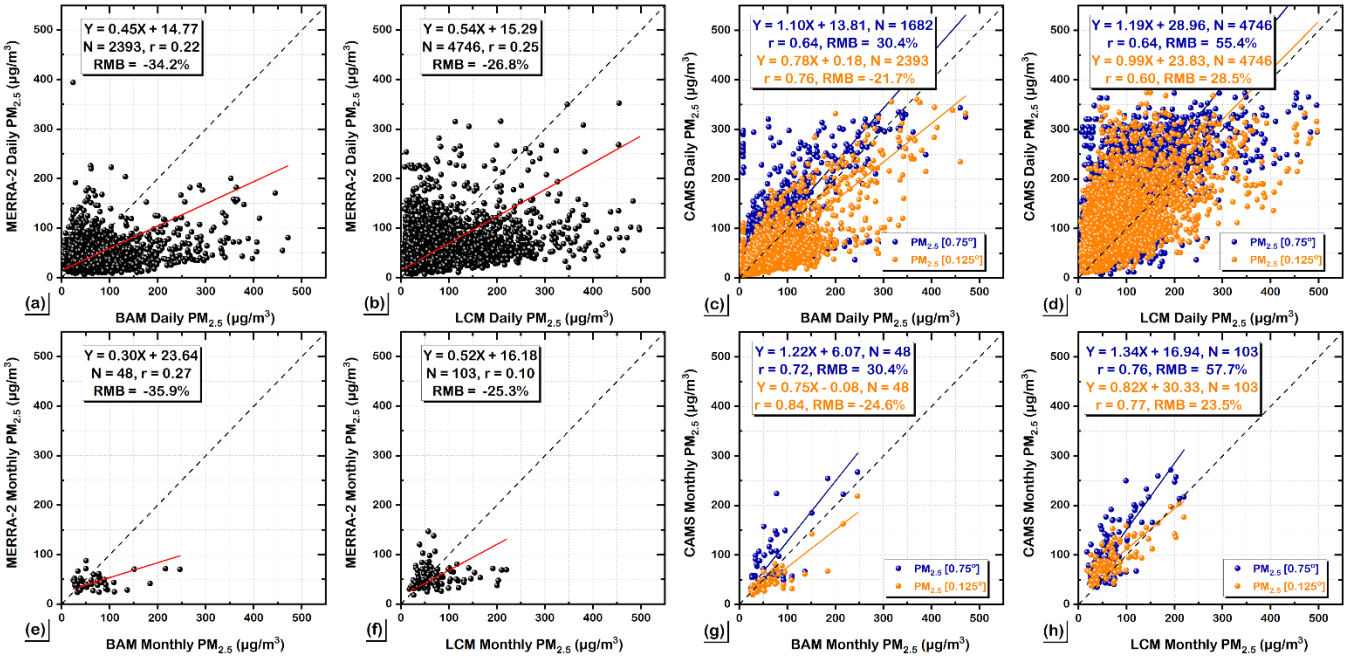

Figure 5: Validation of MERRA-2 and CAMS PM2.5 reanalysis data against BAM (beta gauge attenuation monitor) PM2.5 concentrations for 2019-2020 provided by the US Consulates and LCM (low-cost monitor) PM2.5 concentrations for 2018-2019 provided by PAQI. Where, (a) MERRA-2 daily $PM_{2.5}$ vs. BAM daily $PM_{2.5}$, (b) MERRA-2 daily $PM_{2.5}$ vs. LCM daily $PM_{2.5}$, (c) CAMS daily $PM_{2.5}$ vs. BAM daily $PM_{2.5}$, (d) CAMS daily $PM_{2.5}$ vs. LCM daily $PM_{2.5}$, (e) MERRA-2 monthly $PM_{2.5}$ vs. BAM monthly $PM_{2.5}$, (f) MERRA-2 monthly $PM_{2.5}$ vs. LCM monthly $PM_{2.5}$, (g) CMAS monthly $PM_{2.5}$ vs. BAM monthly $PM_{2.5}$, and (h) CAMS monthly $PM_{2.5}$ vs. LCM monthly $PM_{2.5}$. The dashed line in each figure is the identity line and the blue and orange solid lines are the fit lines with parameters presented in the legends.

5.2.2 Characterization of extremely polluted cities using PM_1 and $PM_{2.5}$ concentrations

PM_1 and $PM_{2.5}$ are fine particulate matter associated with human health issues. PM_1 is more harmful than $PM_{2.5}$ as it can reach deeper into the lungs and affect the respiratory system (Liu et

al. 2013; Meng et al. 2013). A previous study over China reported that most health issues associated with $PM_{2.5}$ were mainly due to greater contributions of PM_1 in $PM_{2.5}$ (Chen et al. 2017). The ranking of extremely polluted to polluted cities in Pakistan according to annual mean CAMS PM_1 concentrations from 2003 to 2020 in Figure 6a indicates that the top 10 extremely polluted cities are Lahore (135.44 μg/m^3), Gujranwala (131.99 μg/m^3), Okara (107.72 μg/m^3), Faisalabad (98.96 μg/m^3), Pakpattan (94.06 μg/m^3), Jhelum (85.51 μg/m^3), Sargodha (84.30 μg/m^3), Bhimber (83.99 μg/m^3), Gujrat (83.99 μg/m^3), and Sialkot (83.99 μg/m^3). Similarly, the top 10 extremely polluted cities (Figure 7a) ranked according to $PM_{2.5}$ concentrations are Lahore (170.53 μg/m^3), Gujranwala (163.63 μg/m^3), Okara (139.43 μg/m^3), Faisalabad (129.85 μg/m^3), Pakpattan (126.97 μg/m^3), Multan (113.09 μg/m^3), Bahawalnagar (110.81 μg/m^3), Vehari (110.81 μg/m^3), Sargodha (109.81 μg/m^3), and Jhelum (107.68 μg/m^3). The WHO air quality guidelines (AQG) are not yet defined for PM_1 as PM_1 is not as widely monitored as $PM_{2.5}$, therefore the WHO recommended AQG for $PM_{2.5}$ (<10 μg/m^3 annual mean) and Pak-NEQS for $PM_{2.5}$ (<15 μg/m^3 annual mean) are used for comparison purposes. Not a single city in Pakistan falls within the $PM_{2.5}$ standards defined by Pak-NEQS and WHO, and the values of PM_1 and $PM_{2.5}$ respectively for the top 10 cities are 5.6 (8.4) to 9.0 (13.5) times and 7.2 (10.8) to 11.4 (17.1) times greater than the Pak-NEQS (WHO AQG). For PM_1 and $PM_{2.5}$, 9 out of 10, and 10 out of 10 cities respectively, are in Punjab. The extremely high pollution level may be due to emissions from local anthropogenic activities, confirming the results of a previous modeling study that suggested local anthropogenic activities as the major cause of high particulate concentrations in Pakistan (Shi et al. 2020). All major cities selected in this study (80 cities) are exposed to $PM_{2.5}$ concentrations during a long period of time (Figures 1a and 7a), which exceed the Pak-NEQS (<15 μg/m^3) and 68, 73, and 80, out of 80 cities

exceeded the WHO Interim Target-1 (<35 µg/m^3), Target-2 (<25 µg/m^3), and Target-3 (<15 µg/m^3), respectively. These exceedances are set in strong perspective against the much lower recommended WHO AQG for $PM_{2.5}$ of 10 µg/m^3. These results suggest that the top polluted cities are extremely hazardous for human health, as an increase of $PM_{2.5}$ by 10 µg/m^3 can increase mortality, lung cancer, and cardiopulmonary diseases by 8%, 6%, and 4%, respectively, due to long-term exposure to fine particulates (Pope et al. 2002).

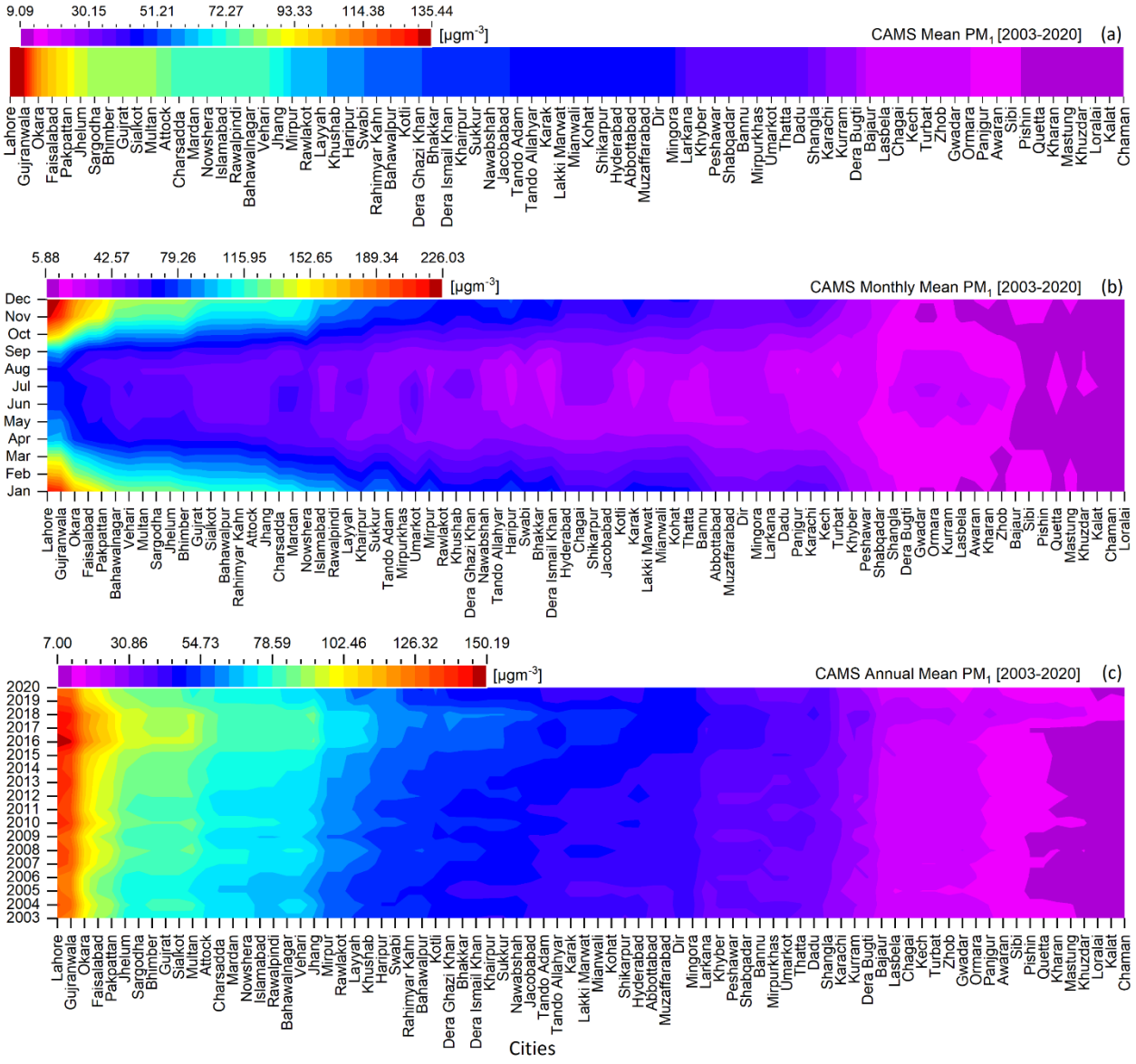

Figure 6: Ranking of extremely polluted to polluted cities in Pakistan according to annual mean CAMS PM_1 concentrations from 2003 to 2020. Where (a) polluted cities based on yearly mean PM_1 averaged over the years 2003-2020, (b) polluted months based on PM_1 averaged over the years 2003-2020, and (c) polluted years based on yearly mean PM_1.

Figures 6b and 7b show months with the highest levels of PM_1 and $PM_{2.5}$, averaged over the years 2003-2020, for the extremely polluted cities. The higher PM_1 and $PM_{2.5}$ concentrations were observed in cold months (October to February) with the maximum concentrations in December and January, while warmer months (March to September) showed lower PM_x concentrations. The high levels of fine particulates in October and November may be attributed to both cross-border transport of aerosol produced from biomass burning activities (from India) as well as locally produced aerosols by anthropogenic activities. As the highest values of fine particulates were observed in December and January which are not the main months of biomass burning activities, these are not likely the main source of the high levels of fine particulates pervasive across these highly polluted cities. At this time of year, less surface heating and less turbulence due to lower intensity of solar irradiation lead to stable and shallow boundary layers. Furthermore, with higher concentrations of light-absorbing aerosols, mainly BC, the atmospheric stability increases due to local heating near the top of the boundary layer, induced by BC, which further lowers the boundary layer height (BLH) (Ding et al. 2016). Stable atmospheric conditions that imply low BLH together with low wind speed, both limiting aerosol transport, lead to the accumulation of aerosols and enhancement of particle concentrations near the surface. As a result, anthropogenic aerosols such as those produced from fossil fuel combustion and other urban and industrial activities may linger for long periods (Mhawish et al. 2020). In October and

November, both local and remote (cross-border) biomass (crop residue) burning activities coupled with stable atmospheric conditions have been recognized to cause severe haze and smog episodes, especially over Punjab (Mhawish et al. 2020; Tariq et al. 2015; Tariq et al. 2016). The formation of secondary inorganic aerosol during haze episodes is also responsible for higher $PM_{2.5}$ concentrations as reported from recent studies over China (Nichol et al. 2020; Zhang et al. 2018). An increase in $PM_{2.5}$ concentrations was observed in June and July, and PM_1 concentrations slightly increased in July. This means that $PM_{2.5}$ exhibited two peaks: the first in winter and the second in summer, whereas a single peak in winter was observed for PM_1. The second $PM_{2.5}$ peak in summer may be attributed to the fine particulates from dust, as dust storm activities are very common in Pakistan during summer, as well as local anthropogenic activities. The lower peak of $PM_{2.5}$ in the summer, compared to winter, may be due to the unstable atmospheric conditions due to the higher surface heating by solar irradiation, leading to the generation of strong turbulence with rising air and thus strong mixing conditions which promote the vertical dispersion of pollutants.

The annual mean concentrations of PM_1 (Figure 6c) and $PM_{2.5}$ (Figure 7c) show strong inter-annual variations with distinct PM_x levels and very poor air quality conditions throughout the last two decades. The annual mean mass concentrations in extremely polluted cities range from 63 $\mu g/m^3$ to 150.19 $\mu g/m^3$ for PM_1 and from 85 $\mu g/m^3$ to 187.35 $\mu g/m^3$ for $PM_{2.5}$, which are 4.2 (6.3)–10 (15) and 5.7 (8.5)–12.5 (18.7) times greater than the Pak-NEQS (WHO AQG), respectively.

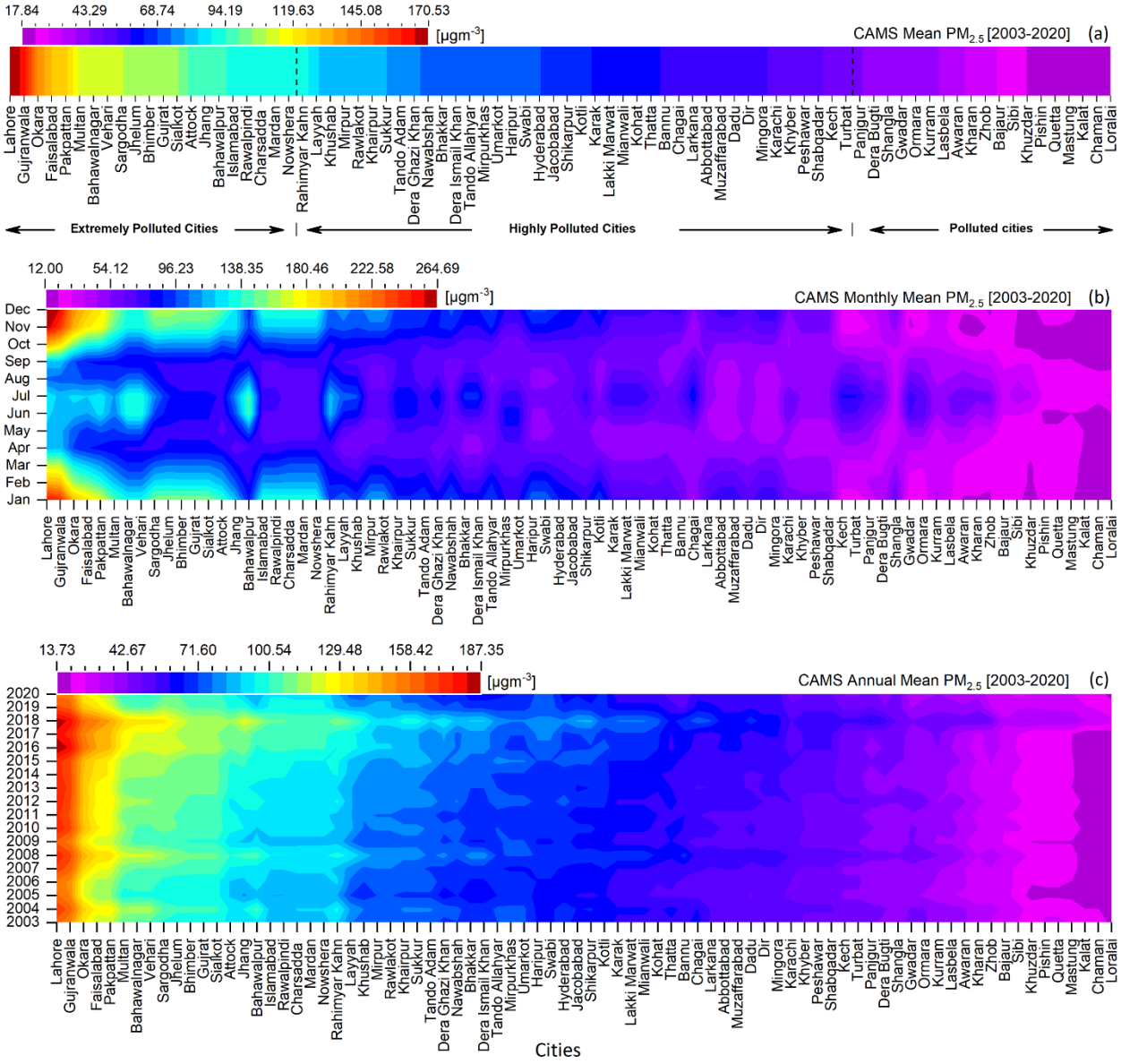

Figure 7: As Figure 6, but for $PM_{2.5}$.

5.2.3 Characterization of extremely polluted cities using PM_{10} concentrations

Figure 8a shows the ranking of polluted cities according to PM_{10} concentrations. The PM_{10} fraction with an aerodynamic diameter larger than $PM_{2.5}$ (PM_{10}-$PM_{2.5}$), i.e. the mass concentration of coarse particles, mainly originates from natural sources such as desert dust and

resuspended soil particles. The top 10 most polluted cities according to the PM_{10} concentrations are Lahore (238.9 μg/m^3), Gujranwala (229.1 μg/m^3), Okara (194.5 μg/m^3), Faisalabad (180.6 μg/m^3), Pakpattan (177.9 μg/m^3), Bahawalnagar (160.6 μg/m^3), Vehari (160.6 μg/m^3), Multan (157.5 μg/m^3), Sargodha (152.3 μg/m^3), and Jhelum (149.7 μg/m^3). PM_{10} concentrations are 1.2 to 11.9 times higher than the WHO AQG for PM_{10} (20 μg/m^3 annual mean) for all the cities shown in Figure 8a, suggesting that very poor air quality conditions, hazardous for human life, prevail in all Pakistani cities. Overall, the PM_{10} temporal trend pattern is very similar to that for $PM_{2.5}$, i.e., December is the month with the highest PM_{10} concentrations, followed by January. In summer, July is the most polluted month followed by June (Figure 8b). Similar to the $PM_{2.5}$ variations, PM_{10} also exhibited peaks in both winter and summer. The higher concentrations during the winter months (i.e. December and January) may be due to increased anthropogenic emission activities along with stable atmospheric conditions (stagnant conditions, and shallower boundary layer). Despite the abundance of coarse particulate matter in spring and summer seasons which are transported from the arid and semiarid regions, the strong convection combined with a deeper boundary layer enhances the dispersion of the near-surface pollutant that decreases the PM_{10} concentrations along with the wet deposition during the rainy summer season. The pre-harvest, harvesting, and post-harvest burning activities along with meteorological conditions such as low wind speed and low boundary layer height may contribute to higher surface PM_{10} levels especially during October and November as these activities produce both fine (PM_1 and $PM_{2.5}$) and coarse (PM_{10}) particles as reported by (Jain et al. 2020; Singh et al. 2017) over South Asia and by Le Blond et al. (2017) over South American countries.

Similar to the annual mean $PM_{2.5}$ variations (Figure 7c), the annual mean PM_{10} concentrations also show distinct interannual variations for all cities (Figure 8c), and severe air pollution levels were observed throughout the last two decades. According to these findings, Pakistani people are not only exposed to long-term $PM_{2.5}$ but also to PM_{10} concentrations exceeding the WHO recommended AQG for PM_{10} (<20 μg/m^3). Overall, these results suggested that Pakistani cities are a severe threat to human life due to extremely poor air quality conditions.

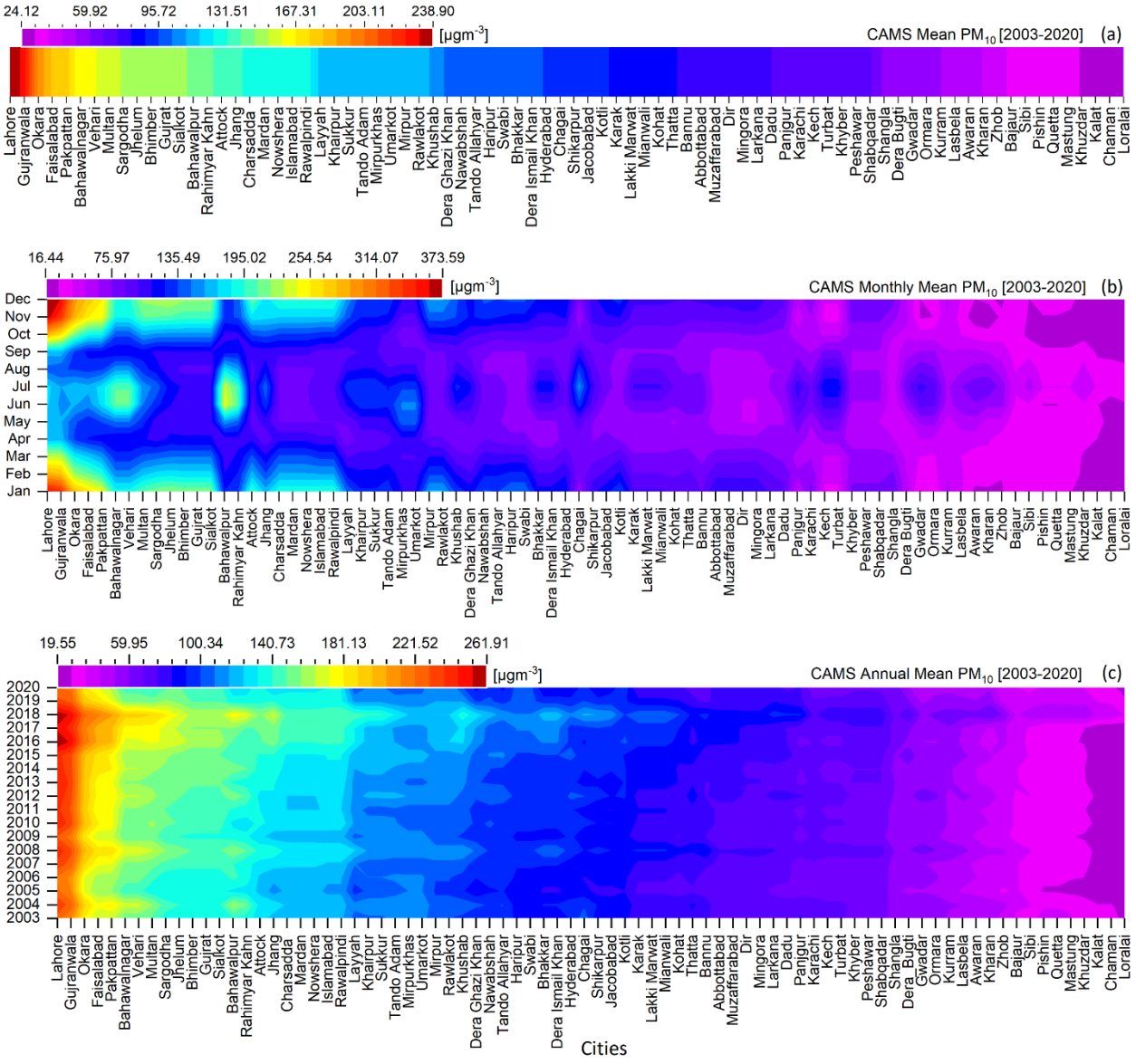

Figure 8: As Figure 6, but for PM_{10}.

5.2.4 $PM_1/PM_{2.5}$ and $PM_{2.5}/PM_{10}$ ratios

The PM_x ratios are very useful for understanding the contributions among particulate size, as revealed by a study in China where PM_1 contributed nearly 80% of $PM_{2.5}$ (Wang et al. 2015), which would have consequences for human health. Over Pakistan, the $PM_1/PM_{2.5}$ (Figure 9a) and $PM_{2.5}/PM_{10}$ (Figure 9b) ratios are lower than those observed over China (Wang et al. 2015), indicating lower contributions of PM_1 to $PM_{2.5}$ and $PM_{2.5}$ to PM_{10}. However, the pattern of ratios is similar to that observed for China, i.e., the $PM_1/PM_{2.5}$ ratios are higher than $PM_{2.5}/PM_{10}$ ratios. Relatively higher $PM_1/PM_{2.5}$ ratios (>75%) are observed from October to March (Figure 9a), indicating a larger fraction of PM_1 in $PM_{2.5}$ due to more anthropogenic activities. The directly emitted PM_1 from the automobile and combustion of fossil fuel, and indirectly by formation from precursor gases, are most likely higher from October to March, leading to the enhanced $PM_1/PM_{2.5}$ ratio. This also suggests that the $PM_{2.5}$ concentrations from October to March are driven by emissions from combustion and secondary aerosols formation (Jain et al. 2020). However, low $PM_1/PM_{2.5}$ ratios are observed from April to September in most of the cities, and low ratios during all months are observed in the cities located in Balochistan, indicating a lower contribution of PM_1 to $PM_{2.5}$, which is mainly dominated by the larger particles especially during summer (June, July, and August) which not contributed to PM_1.

Figure 9b shows large contributions of $PM_{2.5}$ to PM_{10} throughout the year with maximum contributions during summer as indicated by the large $PM_{2.5}/PM_{10}$ ratios. This suggests that the air quality in these cities is mainly (and significantly) influenced by fine particulates, largely from

anthropogenic sources. The large $PM_{2.5}/PM_{10}$ ratios in Gwadar and Ormara (Figure 9b), coastal cities in Balochistan, throughout the year suggest that also in these coastal cities the PM is dominated by $PM_{2.5}$ particles, which indicates that the PM_{10} is driven by $PM_{2.5}$ which is highly influenced by anthropogenic sources. Gwadar has the deepest seaport in the world and the ship-based emissions may be one of the sources of fine anthropogenic particles throughout the year. However, lower $PM_{2.5}/PM_{10}$ ratios are observed for other cities located in Balochistan, indicating the greater influence of coarse particulates (mainly desert dust).

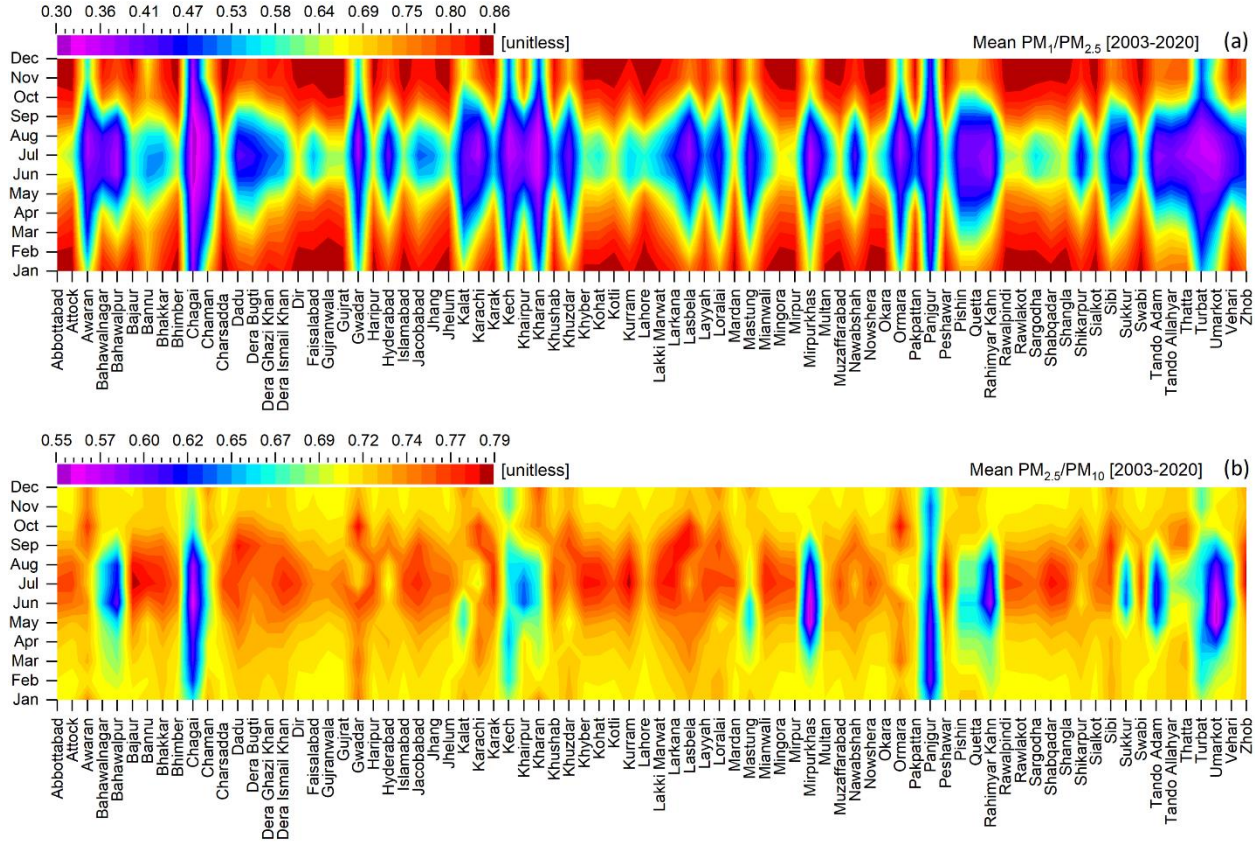

Figure 9: (a) Monthly mean ratios of $PM_1/PM_{2.5}$ and (b) $PM_{2.5}/PM_{10}$.

Scatter plots of PM_1 vs. $PM_{2.5}$ (Figure 10a) and $PM_{2.5}$ vs. PM_{10} (Figure 10b) show that the PM_x fractions over Pakistan are well-correlated, with Pearson's correlation coefficients (r) of 0.95 and 0.99, and slopes of 0.90 and 0.70, respectively. The strong linear relationship between PM_{10} and $PM_{2.5}$ (higher r values) suggests common sources of fine and coarse particulates compared to PM_1 vs $PM_{2.5}$ relationship. While the higher slope values suggest larger contributions of PM_1 to $PM_{2.5}$ than $PM_{2.5}$ to PM_{10}. Overall, both the contribution of PM_1 to $PM_{2.5}$ and that of $PM_{2.5}$ to PM_{10} are smaller over Pakistan than over China (Wang et al. 2015) as indicated by the PM_x ratios (Figure 9) and slope values (Figure 10). This might be due to a higher contribution of anthropogenic emissions to the PM concentrations in China than in Pakistan; however, other processes may also contribute, and unraveling the different contributions requires more detailed research. Figures 10a and 10b show some scattered points, within a red circle or ellipse, which represent the data from May to September and these scattered points suggest lower contributions of PM_1 in $PM_{2.5}$ and $PM_{2.5}$ in PM_{10}, as also indicated by low PM_x ratios (Figure 9).

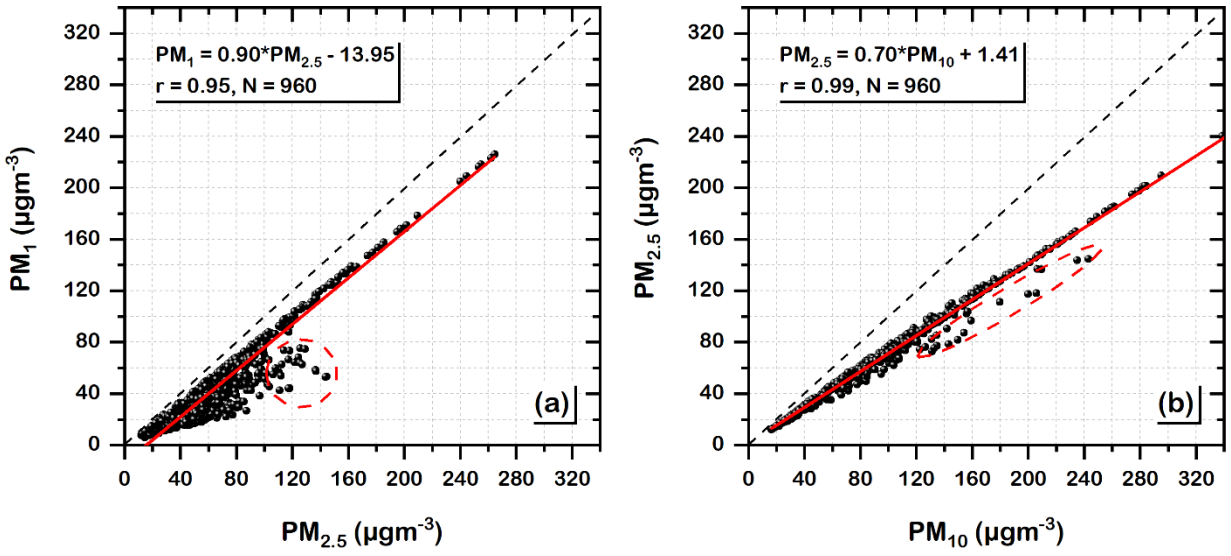

Figure 10: Scatter plots between (a) PM_1 vs. $PM_{2.5}$ and (b) $PM_{2.5}$ vs. PM_{10}. The red solid line represents the regression line and the black dashed line represents the identity line. The data points in the red circle and ellipse are explained in the text.

5.2.5 Monthly mean temporal trend of PM_1, $PM_{2.5}$, and PM_{10}

The month-to-month variations of the multi-year (2003–2020) monthly mean PM_1, $PM_{2.5}$, and PM_{10} concentrations for the top 10 polluted cities are shown in Figure 11. These cities vary according to population growth, the number of automobiles, urbanization, industrialization, city size, land cover types, and climatic conditions, and PM concentrations are expected to behave differently due to these factors. This study follows the hypothesis of our previous study conducted over Hong Kong (Bilal et al. 2019c) i.e., if the PM concentrations have different magnitudes but follow the same temporal pattern at different locations, they are influenced by local as well as regional contributions. Thus for PM_1 concentrations, Figure 11a shows the same pattern for each of the 10 cities, suggesting that both local and regional sources contribute to PM_1 concentrations. For both $PM_{2.5}$ (Figure 11b) and PM_{10} (Figure 11c), similar patterns are only evident from September to April, and dissimilar patterns due to variation in magnitudes are evident from May to August, suggesting more local contributions for the summer months of May to August. This local contribution during summer may be attributed to the frequent dust/sand storms. Similarly, from October to January, the PM_1, $PM_{2.5}$, and PM_{10} concentrations in Lahore and Gujranwala show similar patterns as in other cities, but with higher concentrations, probably because Lahore and Gujranwala are the largest cities, with consequently more transport, fossil fuel, and industrial emissions, and some local and cross-border biomass burning activities in

822 autumn (Ali et al. 2013; Tariq et al. 2015; Tariq et al. 2016), which reinforce the effects of
823 meteorological impacts, such as shallower boundary layer height and lower wind speed, which
824 result in the accumulation of particulate matter near the surface (Miao et al. 2019; Miao and Liu
825 2019; Miao et al. 2018; Qu et al. 2017; Sun et al. 2019; Wang et al. 2018).

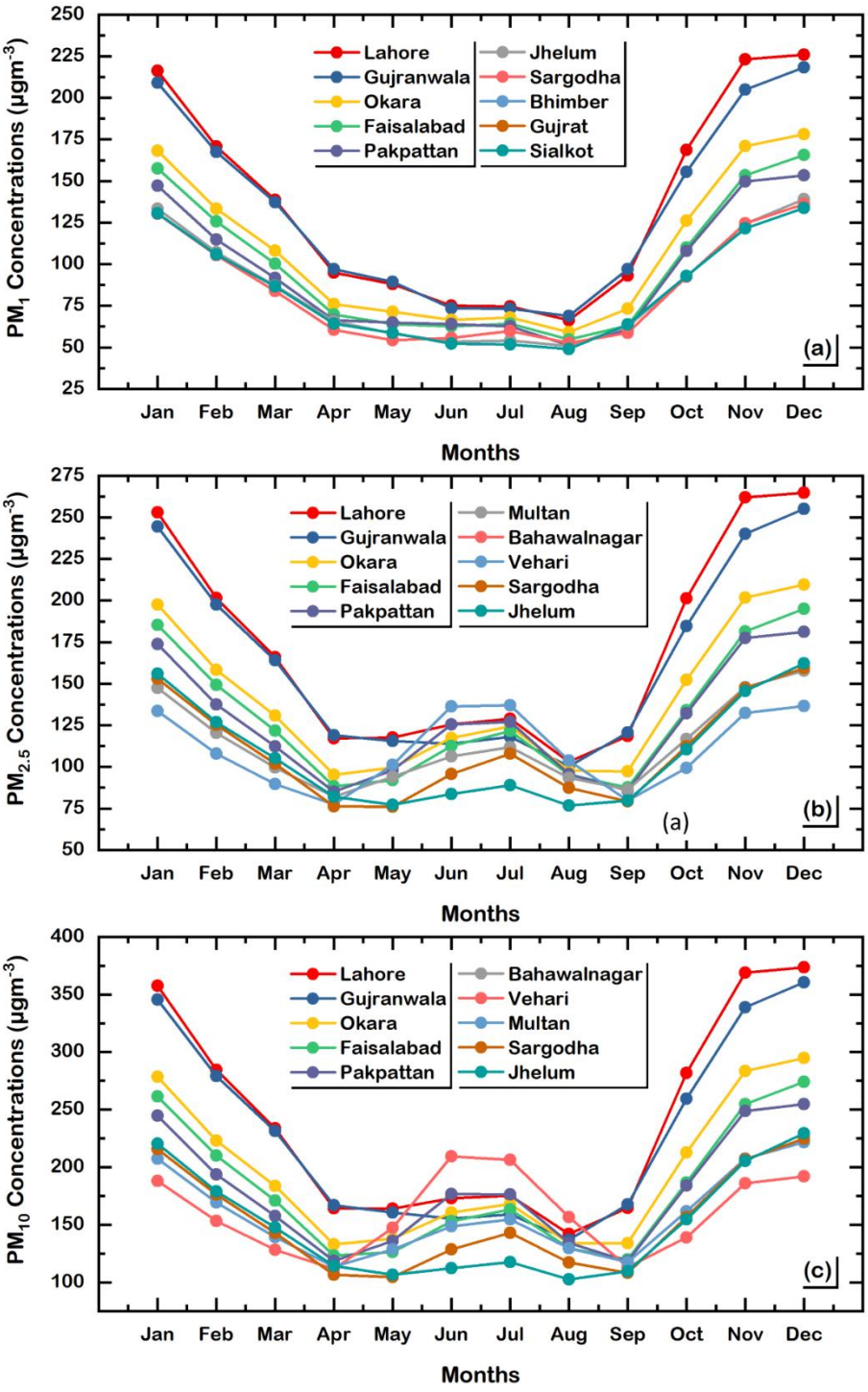

826

827 **Figure 11:** Multiyear (2003 - 2020) monthly average variations of PM_1, $PM_{2.5}$, and PM_{10}

828 concentrations in the corresponding top 10 polluted cities (see legend). Cities are plotted with

829 the rank of high to low polluted.

5.3 OMI vertical column densities of NO_2 and SO_2

5.3.1 Characterization of extremely polluted cities using NO_2 data

NO_2 is mainly produced from fossil fuel combustion, industrial emission, automobile emission, biomass burning, natural lightning, and soil microbe emissions (Cheng et al. 2012; Lee et al. 1997; Olivier et al. 1998; Richter and Burrows 2002). NO_2 has an adverse effect on health and contributes to low atmospheric visibility, and poor air quality conditions (Khokhar et al. 2015; ul–Haq et al. 2014). Pakistan's top ten polluted cities according to NO_2, where we use Tropospheric vertical column densities (TVCDs) as a proxy, are those with the highest levels of urbanization, vehicle emissions, and industrialization, suggesting anthropogenic activities to be the major cause. They are Lahore (5.69×10^{15} molecules/cm^2), Rawalpindi (3.65×10^{15} molecules/cm^2), Islamabad (3.65×10^{15} molecules/cm^2), Karachi (3.60×10^{15} molecules/cm^2), Gujranwala (3.32×10^{15} molecules/cm^2), Sialkot (2.81×10^{15} molecules/cm^2), Haripur (2.73×10^{15} molecules/cm^2), Okara (2.72×10^{15} molecules/cm^2), Faisalabad (2.72×10^{15} molecules/cm^2), and Gujrat (2.47×10^{15} molecules/cm^2) (Figure 12a). Similar results are reported by Tabinda et al. (2019), Ashraf et al. (2013), and Khanum et al. (2017). In terms of data availability from OMI, Figure 12b indicates the largest number of PC available for Lasbela (4168), Awaran (4154), and Panjgur (4140), all located in Balochistan. On a monthly mean basis, NO_2 (Figure 12c) follows the same patterns as observed for PM_1 and $PM_{2.5}$ concentrations; i.e., higher values in winter, especially for the extremely polluted cities (Lahore, Rawalpindi, Islamabad, and Karachi), which are attributed to emissions of automobiles, industries, and fossil fuel combustion, under stable atmospheric conditions. The NO_2 atmospheric lifetime is higher in winter than in summer due to

851 higher mixing ratio and less sunlight that initiates the breakdown reaction of $NO_{2;}$ therefore stays
852 longer in the atmosphere in winter than in summer. A different trend observed for cities located
853 in Balochistan, with higher NO_2 in summer, could be due to natural lightning as reported by
854 Khokhar et al. (2015). Figure 12d shows that Lahore, Rawalpindi, Islamabad, and Karachi are
855 polluted in all years from 2004 to 2019, subjecting citizens to long-term exposure associated with
856 respiratory diseases, otitis media, and mortality (Latza et al. 2009).

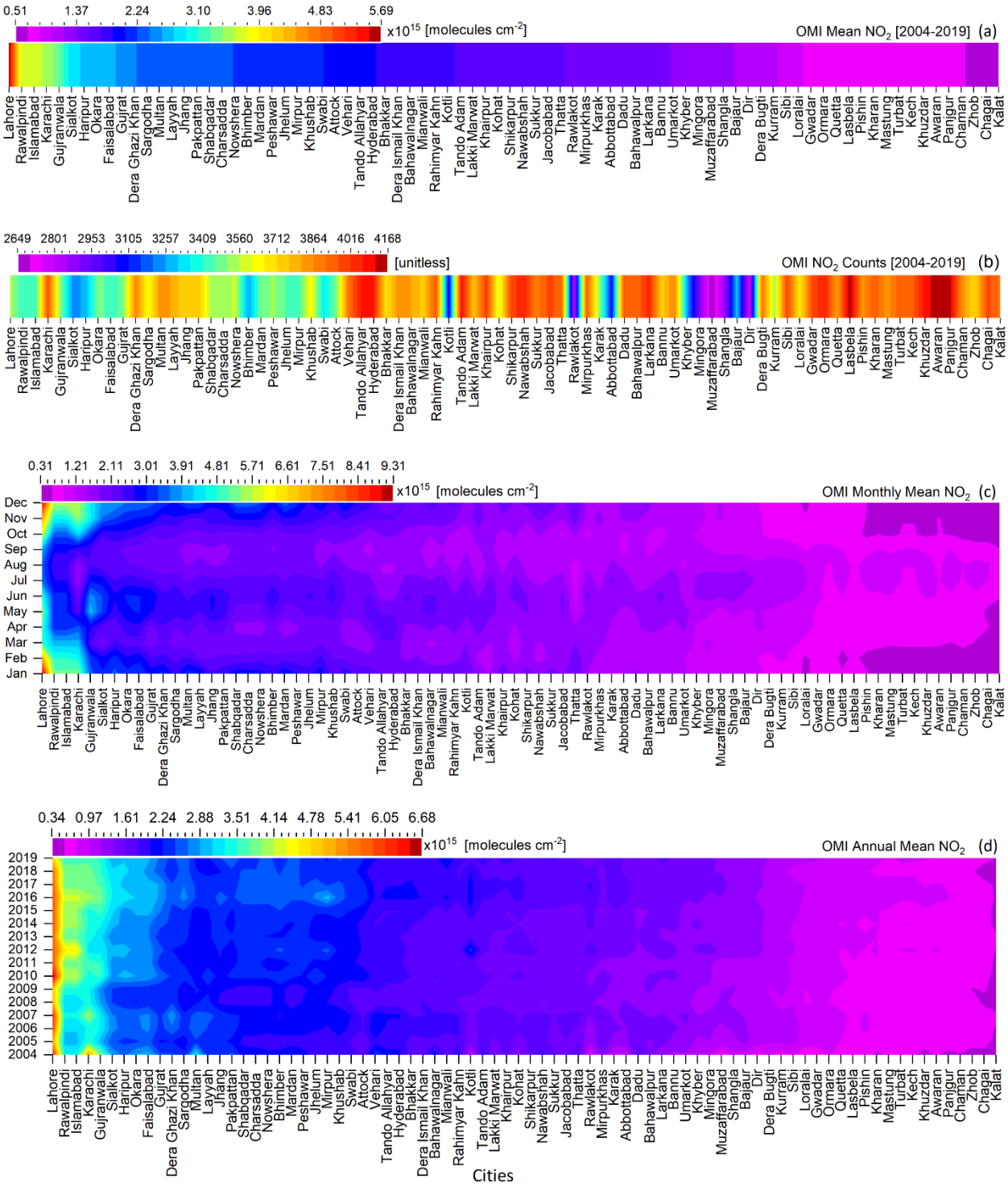
0.51 1.37 2.24 3.10 3.96 4.83 5.69
x10^15 [molecules cm^-2]
OMI Mean NO2 [2004-2019] (a)
2649 2801 2953 3105 3257 3409 3560 3712 3864 4016 4168
[unitless]
OMI NO2 Counts [2004-2019] (b)
0.31 1.21 2.11 3.01 3.91 4.81 5.71 6.61 7.51 8.41 9.31
x10^15 [molecules cm^-2]
OMI Monthly Mean NO2 (c)
Dec
Nov
Oct
Sep
Aug
Jul
Jun
May
Apr
Mar
Feb
Jan
0.34 0.97 1.61 2.24 2.88 3.51 4.14 4.78 5.41 6.05 6.68
x10^15 [molecules cm^-2]
OMI Annual Mean NO2 (d)
2019
2018
2017
2016
2015
2014
2013
2012
2011
2010
2009
2008
2007
2006
2005
2004
Lahore
Rawalpindi
Islamabad
Karachi
Gujranwala
Sialkot
Haripur
Okara
Faisalabad
Gujrat
Dera Ghazi Khan
Sargodha
Multan
Layyah
Jhang
Pakpattan
Shabqadar
Charsadda
Nowshera
Bhimber
Mardan
Peshawar
Jhelum
Mirpur
Khushab
Swabi
Attock
Vehari
Tando Allahyar
Hyderabad
Bhakkar
Dera Ismail Khan
Bahawalnagar
Mianwali
Rahimyar Kahn
Kotli
Tando Adam
Lakki Marwat
Khairpur
Kohat
Shikarpur
Nawabshah
Sukkur
Jacobabad
Thatta
Rawlakot
Mirpurkhas
Karak
Abbottabad
Dadu
Bahawalpur
Larkana
Bannu
Umarkot
Khyber
Mingora
Muzaffarabad
Shangla
Bajaur
Dir
Dera Bugti
Kurram
Sibi
Loralai
Gwadar
Ormara
Quetta
Lasbela
Pishin
Kharan
Mastung
Turbat
Kech
Khuzdar
Awaran
Panjgur
Chaman
Zhob
Chagai
Kalat
Cities

857

Figure 12: Ranking of extremely polluted to polluted cities in Pakistan according to OMI NO_2 TVCDs (molecules/cm^2) from 2004 to 2019. (a) polluted cities based on mean NO_2, (b) pixel counts, (c) polluted months based on mean NO_2, and (d) polluted years based on mean NO_2.

5.3.2 Characterization of extremely polluted cities using SO_2 data

Power plants, oil and gas refineries, and metal smelters are the major sources of anthropogenic SO_2 (Dahiya and Myllyvirta 2019). In Figure 13a, extremely polluted to polluted cities are ranked based on OMI-derived SO_2 vertical column density and the top 10 polluted cities are Lahore (10.6×10^{15} molecules/cm^2), Mirpur (10.5×10^{15} molecules/cm^2), Gujranwala (10.3×10^{15} molecules/cm^2), Rawalpindi (10.3×10^{15} molecules/cm^2), Islamabad (10.3×10^{15} molecules/cm^2), Sialkot (10.3×10^{15} molecules/cm^2), Gujrat (10.3×10^{15} molecules/cm^2), Faisalabad (10.3×10^{15} molecules/cm^2), Bhimber (10.2×10^{15} molecules/cm^2), and Jhelum (10.2×10^{15} molecules/cm^2). According to the global SO_2 emission hotspot database (Dahiya and Myllyvirta 2019), five oil power plants near Lahore are the main sources of high SO_2 emissions over Lahore. The lower number (1080–2520) of successful SO_2 retrievals (Figure 13b) as compared to NO_2 retrievals (Figure 12b) is attributed to the high noise level in the OMI-retrieved SO_2 data. Only the relatively strong SO_2 signal over point sources (e.g., power plants, metal smelters) can be detected. (Fioletov et al. 2011; Li et al. 2017; Li et al. 2020). The temporal variation of the monthly mean SO_2 VCDs (Figure 13C) have a pattern similar to that of $PM_{2.5}$ and NO_2 TVCD, with high values in the winter and low in the summer. For the top polluted cities, the high SO_2 observed during November, December, and January may be attributed to the power plants and brick kilns (Dahiya and Myllyvirta 2019; Rahman et al. 2000). Brick kilns are considered as major sources of SO_2

879 resulting in extremely poor air quality. This is clearly observed over Punjab (Adrees et al. 2016;
880 Colbeck et al. 2010; Pervaiz et al. 2021; Ur Rehman et al. 2019). Therefore, every year during late
881 autumn and winter, the government of Pakistan bans these kilns to control pollution levels. The
882 SO_2 accumulates in the BL during the stable atmospheric conditions and shallow BLH at this time
883 of year, in response to the low solar irradiation resulting in little surface heating and turbulence
884 mixing. Unlike NO_2, the contribution of SO_2 to poor air quality in Pakistani cities varies from year
885 to year, as shown in Figure 13d. The SO_2 VCD is higher in 2004, 2008, and 2011 than in other
886 years. The investigation of the year-to-year variability requires a separate study.

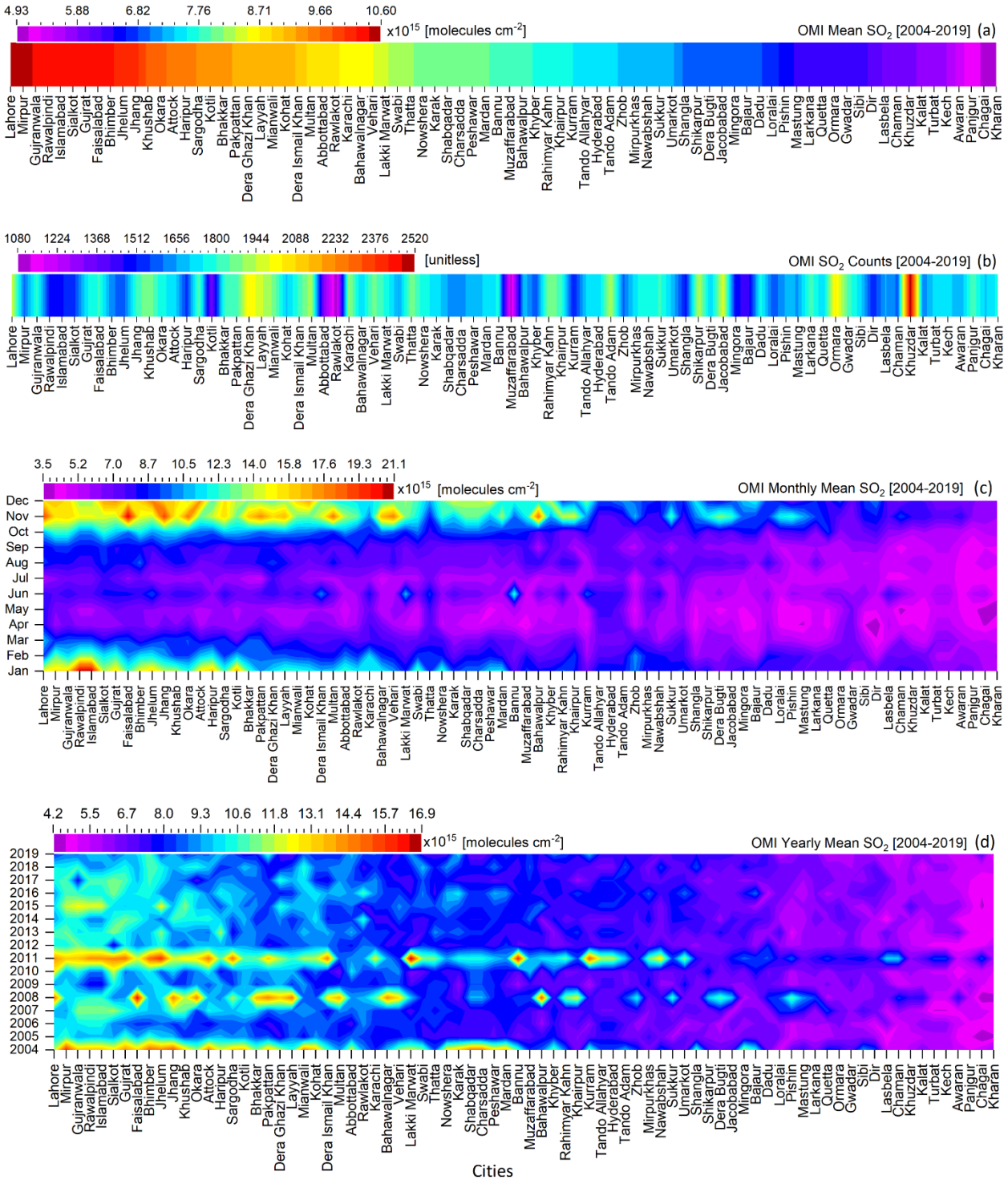
4.93 5.88 6.82 7.76 8.71 9.66 10.60
x10^15 [molecules cm^-2]
OMI Mean SO2 [2004-2019] (a)
1080 1224 1368 1512 1656 1800 1944 2088 2232 2376 2520
[unitless]
OMI SO2 Counts [2004-2019] (b)
3.5 5.2 7.0 8.7 10.5 12.3 14.0 15.8 17.6 19.3 21.1
x10^15 [molecules cm^-2]
OMI Monthly Mean SO2 [2004-2019] (c)
Dec
Nov
Oct
Sep
Aug
Jul
Jun
May
Apr
Mar
Feb
Jan
4.2 5.5 6.7 8.0 9.3 10.6 11.8 13.1 14.4 15.7 16.9
x10^15 [molecules cm^-2]
OMI Yearly Mean SO2 [2004-2019] (d)
2019
2018
2017
2016
2015
2014
2013
2012
2011
2010
2009
2008
2007
2006
2005
2004
Lahore Mirpur Gujranwala Rawalpindi Islamabad Sialkot Gujrat Faisalabad Bhimber Jhelum Jhang Khushab Okara Attock Haripur Sargodha Kotli Bhakkar Pakpattan Dera Ghazi Khan Layyah Mianwali Kohat Dera Ismail Khan Multan Abbottabad Rawlakot Karachi Bahawalnagar Vehari Lakki Marwat Swabi Thatta Nowshera Karak Shabqadar Charsadda Peshawar Mardan Bannu Muzaffarabad Bahawalpur Khyber Rahimyar Kahn Khairpur Kurram Tando Allahyar Hyderabad Tando Adam Zhob Mirpurkhas Nawabshah Sukkur Umarkot Shangla Shikarpur Dera Bugti Jacobabad Mingora Bajaur Dadu Loralai Pishin Mastung Larkana Quetta Ormara Gwadar Sibi Dir Lasbela Chaman Khuzdar Kalat Turbat Kech Awaran Panjgur Chagai Kharan
Cities

887

Figure 13: Ranking of high to low polluted cities in Pakistan according to OMI SO_2 VCDs (molecules/cm^2) from 2004 to 2019. (a) polluted cities based on mean SO_2, (b) pixel counts, (c) polluted months based on mean SO_2, and (d) polluted years based on mean SO_2.

5.4 Spatial distributions of aerosols and trace gases

The purpose of this section is to link the spatial distributions of aerosols and trace gases with each other as well as with population density, nighttime lights, land cover types (cropland and urban areas), and presumed vegetation fire activities. Here, the PM_x data are interpolated using cubic convolution (Keys 1981) from 0.75° grid size to 0.125° grid size to better show the smooth spatial distributions over different administrative units. The spatial distributions of the multi-year averaged concentrations of aerosols (AOD, PM_x) and trace gases (VCDs) (Figure 14) show that Punjab is the most polluted region of Pakistan, followed by Sindh. It is significant that other environmental data including population density (Figure 14g), VIIRS nighttime lights (Figure 14h), cropland (Figure 14i), and vegetation fires (Figure 14j) show similar spatial patterns. It is obvious that vegetation fires would have the same spatial pattern as cropland, but not obvious that population density and nighttime lights would have the same pattern. As nighttime lights and vegetation fires represent human activities, having the same spatial patterns suggests that the majority of human settlements including urban, suburban and, industrial regions, are inter-mixed with cropland. Interestingly, these coincident spatial distributions (population, nighttime lights, land cover, and fires) correspond to the higher ranges of pollutants i.e., AOD > 0.4, PM_1 > 20 μg/m^3, $PM_{2.5}$ > 40 μg/m^3, PM_{10} > 60 μg/m^3, NO_2 > 1.0×10^{15} molecules/cm^2, and SO_2 > 6.5×10^{15} molecules/cm^2. These results suggested that the primary (directly emitted) and the secondary

909 (gas-to-particles formation) aerosol emissions and trace gases are mainly from local
910 anthropogenic sources such as power plants, oil and gas refineries, vehicular emissions, crop
911 residue burning, and industrial activities including construction, manufacturing of cement,
912 ceramic, and bricks, and metals smelting. These anthropogenic sources are mainly responsible
913 for NO_2, SO_2, and PM_x (Adrees et al. 2016; Shah et al. 2012; Ur Rehman et al. 2019). Among these
914 anthropogenic sources, brick kilns industries are considered a major source. Small-scale
915 traditional brick kilns, located in rural and suburban areas, produce large amounts of gaseous
916 pollutants (NO_2, SO_2, O_3, and CO) and PM_x due to the usage of low-quality fuels including coal,
917 oil, wood, rice straw, rice husk, rubber tires, bagasse, and corncobs (Adrees et al. 2016; Ishaq et
918 al. 2010). Besides this, the combustion of agricultural biomass and crop residue burning are also
919 contributing to deteriorating rural and urban air quality (Irfan et al. 2015; Irfan et al. 2014). Irfan
920 et al. (2015) reported that Punjab produced more aerosol pollutants than Sindh from crop
921 residue burning and among the crop residues, wheat straw is the main contributor of NO_x, SO_2,
922 CO_2, and CO. Pakistan's 23.6 million vehicles emitted 58% of the country's total NO_2 emission and
923 34% is emitted by power plants and industries (Amnesty International 2019; Government of
924 Pakistan 2019; UNDP 2019). Another important source of aerosol pollutants, missed by previous
925 studies, is the burning of solid waste and street garbage which is a common practice in Pakistan,
926 even in major urban cities such as Islamabad, Lahore, Rawalpindi, Faisalabad, Gujranwala, Okara,
927 etc. To support this statement, some illustrations with references are provided in the
928 supplementary data (Figure S2). Figures 14a to 14d show that deserts (see Figure 1 for locations)
929 are another source of increasing AOD and PM_x levels in Pakistan. Although local anthropogenic
930 activities are the mains source of aerosol pollutants and severe air quality problems in Pakistan,

931 transboundary transport of aerosols may also influence Pakistan's air quality. Contributions of
932 transboundary transport are investigated in section 5.7, using PSCF analyses, integrated with
933 HYSPLIT backward trajectory analysis and ground-based $PM_{2.5}$ measurements.

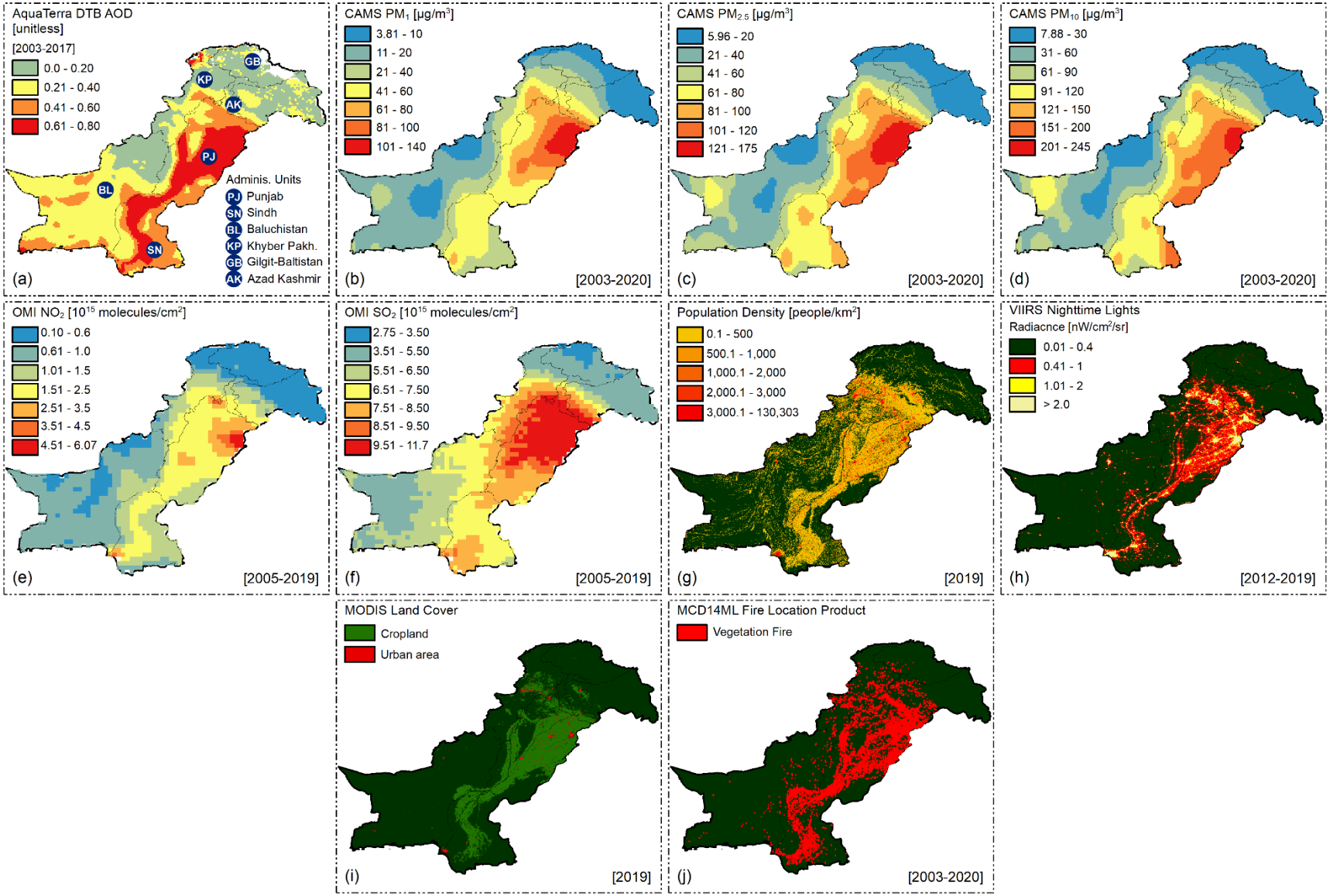
AquaTerra DTB AOD
[unitless]
[2003-2017]
0.0 - 0.20
0.21 - 0.40
0.41 - 0.60
0.61 - 0.80
Adminis. Units
PJ Punjab
SN Sindh
BL Baluchistan
KP Khyber Pakh.
GB Gilgit-Baltistan
AK Azad Kashmir
(a)
CAMS PM1 [μg/m3]
3.81 - 10
11 - 20
21 - 40
41 - 60
61 - 80
81 - 100
101 - 140
(b) [2003-2020]
CAMS PM2.5 [μg/m3]
5.96 - 20
21 - 40
41 - 60
61 - 80
81 - 100
101 - 120
121 - 175
(c) [2003-2020]
CAMS PM10 [μg/m3]
7.88 - 30
31 - 60
61 - 90
91 - 120
121 - 150
151 - 200
201 - 245
(d) [2003-2020]
OMI NO2 [10^15 molecules/cm2]
0.10 - 0.6
0.61 - 1.0
1.01 - 1.5
1.51 - 2.5
2.51 - 3.5
3.51 - 4.5
4.51 - 6.07
(e) [2005-2019]
OMI SO2 [10^15 molecules/cm2]
2.75 - 3.50
3.51 - 5.50
5.51 - 6.50
6.51 - 7.50
7.51 - 8.50
8.51 - 9.50
9.51 - 11.7
(f) [2005-2019]
Population Density [people/km2]
0.1 - 500
500.1 - 1,000
1,000.1 - 2,000
2,000.1 - 3,000
3,000.1 - 130,303
(g) [2019]
VIIRS Nighttime Lights
Radiacnce [nW/cm2/sr]
0.01 - 0.4
0.41 - 1
1.01 - 2
> 2.0
(h) [2012-2019]
MODIS Land Cover
Cropland
Urban area
(i) [2019]
MCD14ML Fire Location Product
Vegetation Fire
(j) [2003-2020]

934

Figure 14: Spatial distributions of yearly mean (a) AOD averaged over the years 2003–2017 (b) PM_1 [2003–2020] (c) $PM_{2.5}$ [2003–2020], (d) PM_{10} [2003–2020], (e) NO_2 [2005–2019], (f) SO_2 [2005–2019], (g) Population density [2019], (h) VIIRS Nighttime Lights [2012–2019], (i) Land cover types [2019], and (j) Presumed vegetation fire data [2003–2020].

5.5 Relationship of PM_x with AOD, NO_2, and SO_2

AOD provides valuable information about the aerosol loading in the atmospheric column, while the PM_x represents the aerosol concentrations near the ground. This section assesses how well satellite-based AOD describes PM_1, $PM_{2.5}$, and PM_{10} by examining the monthly correlation between AOD and PM_x. We have also examined the monthly correlation between PM_x and SO_2 and NO_2 to understand the common sources that originated mainly from a combustion process. The relationships between AOD and PMx vary spatially and temporally and are influenced by several factors such as meteorological variables including boundary layer height and relative humidity, and the vertical distribution of aerosol layer (Li et al. 2016; Mhawish et al. 2021). The linear correlation between AOD and PMx shows a higher correlation coefficient from October to January (see Figure 15a) when the atmosphere is stably stratified and the boundary layer is shallow. This suggests that the AOD and PMx variability are well agreed during the stable atmospheric conditions (from Oct to Jan) and AOD can explain > 65% in the PMx variability. On the other hand, during April and May when the atmosphere is unstable and the boundary layer deeper, the correlation between AOD and PM_x was smaller ($r < 0.4$). In the rainy season (July to August), the correlation coefficient between AOD and PM_{10} was found higher than $PM_{2.5}$ and PM_1 which may be due to the larger contribution of coarse dust particles to the total aerosol loading

than $PM_{2.5}$ and PM_1. The high relative humidity in the summer season enhanced the AOD retrieval due to the hygroscopic growth of aerosol particles. On the other hand, the wash-out of PM_x due to precipitation, deeper boundary layer, and strong convection during rainy months leads to a reduction in the ground-level PM_x concentrations, while the AOD retrieval remains high under cloud-free conditions during the inactive rain phase (Mhawish et al. 2021). The results suggested that using satellite-based AOD to infer the ground-level PMx variability is limited to specific meteorological conditions such as stable atmospheric conditions and dry seasons. On the other hand, the weak linear relationship between AOD and ground-level PMx concentrations found during unstable conditions in spring and summer and more influenced by meteorological variables and atmospheric mixing height.

Tropospheric NO_2 and SO_2 are precursors for the formation of secondary aerosols which are produced by anthropogenic activities such as fossil fuel burning and power plants. The strong correlation coefficient between PM_x vs. SO_2 and NO_2 in the spring months suggests that photochemical reactions can contribute to the formation of PM_x. The strong correlation in winter suggests that both trace gases NO_2 and SO_2 originated from the same emission sources of PM_x, mainly domestic heating, industrial activities, and vehicular emissions. While the lower correlation in the summer monsoon may be attributed to the higher contribution of natural sources of PM_x and the deeper boundary layer that enhance the dispersion of air pollutants.

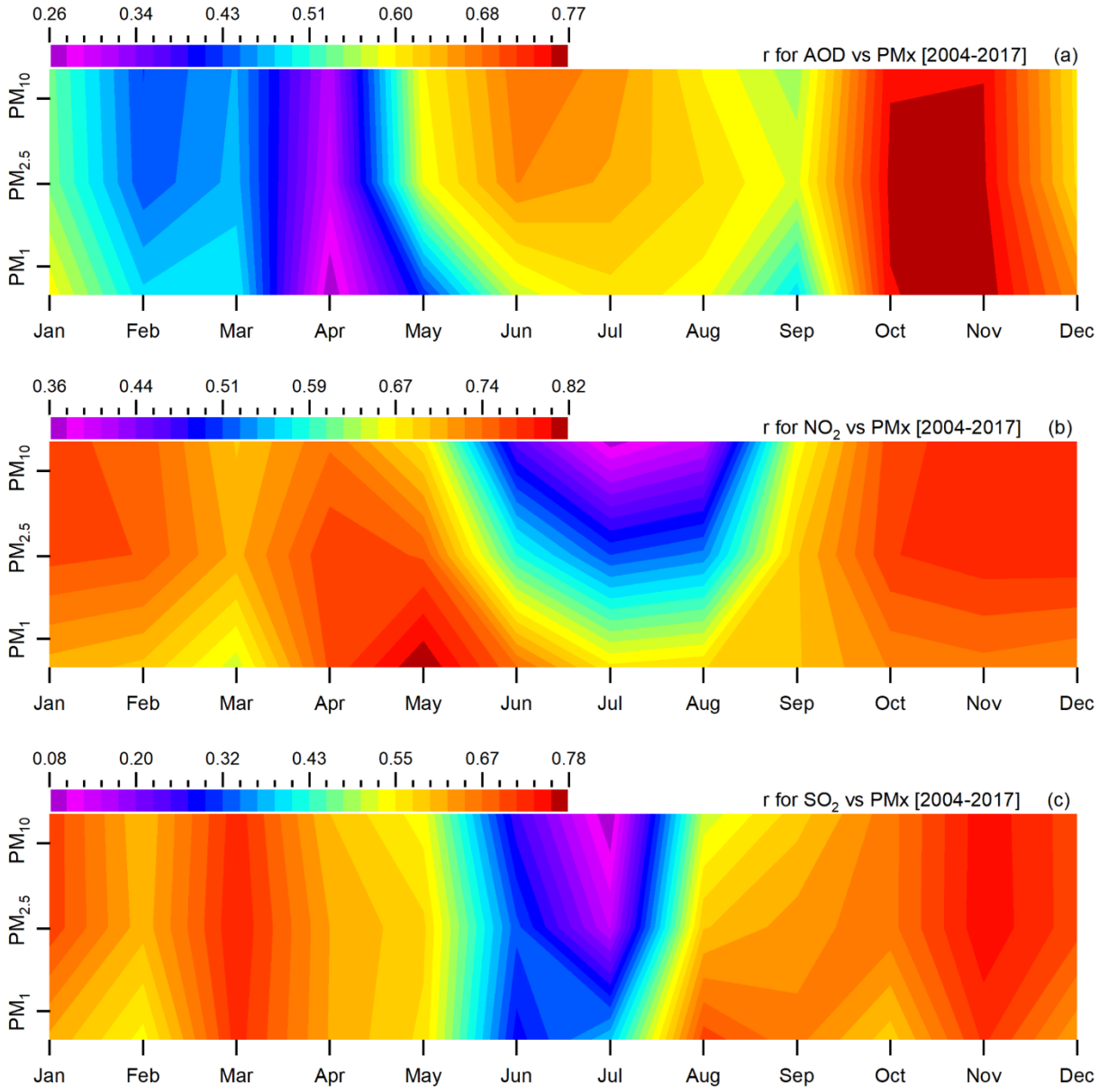

Figure 15: Relationship from PMx with (a) AOD, (b) NO_2, and (c) SO_2 from 2004-2017.

5.6 Trends of aerosol and trace gas concentrations

This section presents the annual trends in the six parameters used to assess the air quality in each city of Pakistan. The annual trends were calculated after removing the seasonality from the monthly mean time series data which also accounted for temporal autocorrelation. Figure 16

shows the magnitude of the trends as Theil-Sen's slope over each individual city, for the periods indicated at the top of each Figure. A significant positive trend in PM_x was found over most cities, particularly in Punjab, Khyber Pakhtunkhwa, and the Islamabad Capital Territory. The PM_x trends found over cities in Punjab range from +0.35 to +1.10 $\mu g/m^3\ yr^{-1}$, +0.42 to +1.52 $\mu g/m^3\ yr^{-1}$ and +0.57 to +2.20 $\mu g/m^3\ yr^{-1}$ for PM_1, $PM_{2.5}$ and PM_{10}, respectively. Correspondingly, the AOD trend in Punjab cities was positive, with the strongest increase over Lahore (0.008 yr^{-1}). Over cities in Khyber Pakhtunkhwa and Azad Kashmir, the AOD trend was also positive, but smaller than in Punjab. The positive trends in PMx and AOD, particularly over cities in Punjab, may be due to increasing aerosol emissions and/or secondary aerosol formation. Anthropogenic activities and biomass burning are considered major sources of ultrafine and fine particles (PM_1 and $PM_{2.5}$) over the region (Alam et al. 2015; Stone et al. 2010). Anthropogenic activities also result in the production of NO_2 and SO_2 and ~91%, and ~88% of the cities the trends in the NO_2 and SO_2, respectively, are positive. This increase in trace gas concentrations would be a further source of increased particulate pollution, as trace gases facilitate secondary aerosol formation via gas-to-particle conversion reactions (Seinfeld and Pandis 1998).

In terms of monthly trends, the common feature is that the statistically significant positive trends of PM_x were largest during the cold months (November to February), particularly over major Punjab cities (Lahore, Faisalabad, and Gujranwala) and Islamabad (Figure S3). In contrast, during the summer months, the trends over many cities are negative. The overall positive annual trends indicate that the increase of the PMx concentrations in the winter is stronger than the decrease in the summer. The reasons for these opposing trends are beyond the scope of the current study and require further, more detailed investigation.

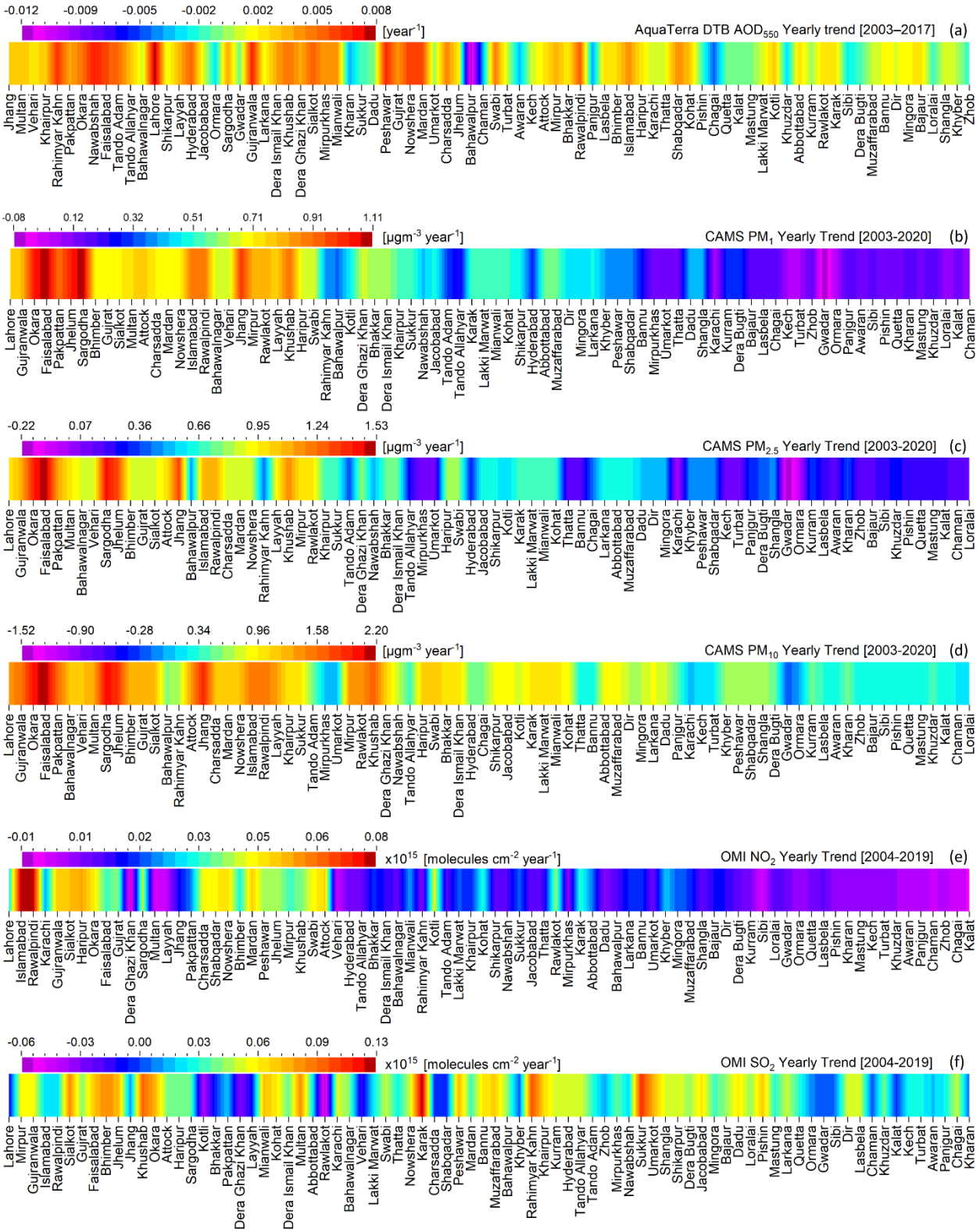

Figure 16: Annual mean trend in aerosols and trace gas concentrations for (a) AOD, (b) PM_1, (c) $PM_{2.5}$, (d) PM_{10}, (e) NO_2, and (f) SO_2. The trends were calculated over different periods of time,

which are indicated on top of each figure on the right-hand side, together with the type of species.

5.7 Potential Source Contribution Function (PSCF) Analysis

PSCF analysis was used to identify the potential source areas for $PM_{2.5}$ at four receptor cities: Peshawar, Islamabad, Lahore, and Karachi, for the period from March 2020 to February 2021. 72 hours HYSPLIT backward trajectories were computed for each receptor site, arriving every 6 hours at the height of 500 m above ground level (AGL). The results were grouped by season as shown in Figure 17. The results show strong differences between cities and seasons. Starting with Peshawar, in spring there are some local sources regions around the city, within a few hundreds of km, but also strong contributions from the WNW (West-NorthWest) in Afghanistan and from the SE in India. In the summer, the source regions are mostly located in Pakistan, but with a contribution from sources to the SE (SouthEast), in India. In contrast, in the autumn the contributions from India are very small but those from Afghanistan, both to the NW (NorthWest) and W (West) are relatively large. Whereas, in the winter source regions in NW and SE directions (Afghanistan and India, respectively) are stronger than in other seasons. In Islamabad, not far from Peshawar, the situation is quite different. In the spring, the source regions have a rather low PSCF, and are distributed over specific directions to the W (West) into Afghanistan and toward the SE in India, with few local sources. In the summer, the source regions are similar to those in Peshawar, but with low PSCF except for the source regions in Afghanistan which seem to contribute most to the air pollution in Islamabad in the summer, but still with moderate PSCF. In the autumn sources to the W and N dominate with stronger contributions from Afghanistan than from the local sources. In the winter, the source regions redistributed over a much larger area than in other seasons, with strong contributions from both local sources and Afghanistan, as well as some contributions from India. The situation in Lahore is remarkably different, with the strongest contributions from sources inside Pakistan (PJ and KP), some contributions from

sources to the SE in India, during all seasons, and in the spring a strong contribution from sources in Afghanistan. The situation in Karachi is again different, both as regards source regions and seasonal behaviour. The strongest contributions come from local sources within a few hundreds of km in Pakistan, except in the summer when all source regions are weak contributors (PSCF <0.2) and almost all located over the ocean. In the spring, source regions to the NW, reaching far into Afghanistan, contribute to the PM2.5 in Karachi. Oceanic sources also contribute some to the PM2.5 in other seasons

In summary, the values of PSCF indicate the regional transport of aerosol from source regions in Afghanistan and India (see Figure 1 for locations). Karachi is influenced by fine dust particles from the Cholistan and Thar deserts (see Figure 1 for locations). Figure 17 shows that the $PM_{2.5}$ in Lahore, the top polluted city of Pakistan, is mainly influenced by source areas in Pakistan, during all seasons. This suggests that increases in local anthropogenic activities play an important role in the worsening of Lahore's air quality. Overall, the higher values of PSCF > 0.6 identify potential source areas which are located both inside and outside of Pakistan, which indicates that the air quality in Pakistan is not only influenced by local sources but also influenced by transport from regional sources areas.

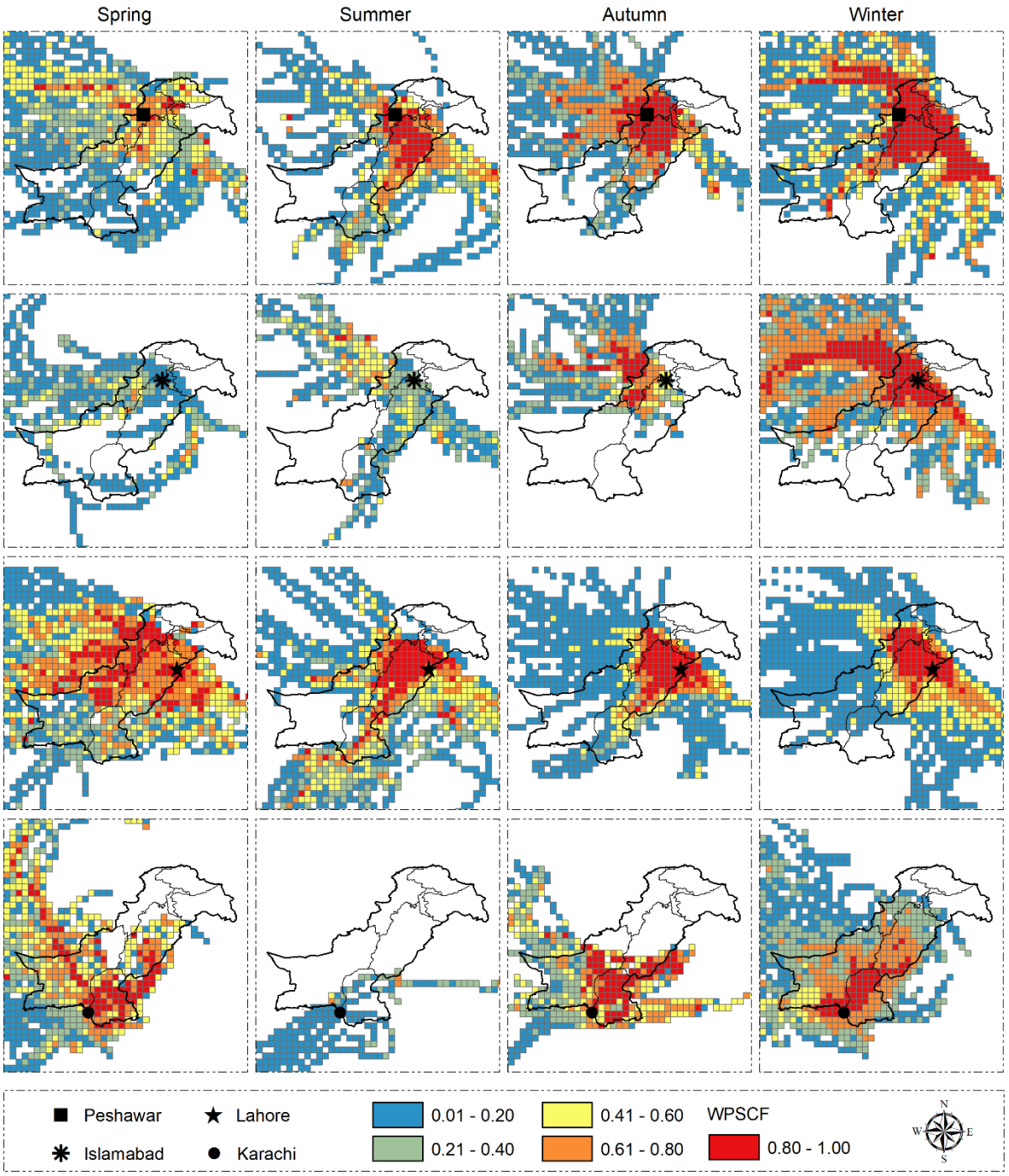

Figure 17: Potential source contribution function plots for $PM_{2.5}$ at seasonal scales from March 2020 to February 2021 for four receptor cities namely, Peshawar, Islamabad, Lahore, and Karachi (see legend for identification).

6. Conclusions

In this study, long-term (2003–2020) remote sensing, ground-based, and model simulation datasets were combined to provide the most comprehensive and extensive evaluation ever, of air quality conditions over Pakistan. Long-term spatio-temporal distributions of aerosol pollutants and trace gases, recent long-term trends at the city level, ranking of cities in terms of air pollution levels into three categories (extremely polluted, highly polluted, polluted cities), and the potential sources of air pollution across Pakistan were reported.

The highest AOD was observed in the summer months (June to August), mainly attributed to the hygroscopic growth of aerosol particles during the humid summer season. High AOD levels were also observed during cold months (October to January), mainly over biomass burning affected regions such as Punjab. For PMx and trace gases, the highest values were observed during cold months from October to February, when the atmosphere is stably stratified and the boundary layer is shallow, and emissions from anthropogenic activities and biomass burning are higher than in other seasons.

The CAMS $PM_{2.5}$ data are in better agreement with ground-based $PM_{2.5}$ concentrations than MERRA-2 reanalysis $PM_{2.5}$ data and were therefore used to rank the cities in terms of concentrations of particulate matter (PMx). The 18 years average of the $PM_{2.5}$ concentrations for the 80 cities of Pakistan show that a total of 21 cities fall within the category of extremely polluted cities ($PM_{2.5} > 92.84$) (namely Punjab: 17, Khyber Pakhtunkhwa: 3, Azad Kashmir: 1), 40 cities fall within the category of highly polluted cities ($45.69 < PM_{2.5} < 92.84$) (namely 6 in Punjab, 14 in Sindh, 3 in Balochistan, 13 in Khyber Pakhtunkhwa and 4 in Azad Kashmir); 19 cities fall within

the category of polluted cities ($PM_{2.5}$ < 45.69) (16 in Balochistan and 3 in Khyber Pakhtunkhwa). No single city in Pakistan falls within the $PM_{2.5}$ standards defined by Pak-NEQS and WHO, and the values of PM_1 and $PM_{2.5}$ for the top 10 cities are 5.6 (8.4) to 9.0 (13.5) times and 7.2 (10.8) to 11.4 (17.1) times larger than the Pak-NEQS (WHO AQG). The map of annual average $PM_{2.5}$ shows that people in the whole country are exposed to high $PM_{2.5}$ concentrations for many years, with the annual mean concentrations for all cities exceeding the Pak-NEQS (<15 μg/m3), and 68, 73, and 80 cities exceeding the WHO Interim Target-1 (<35 μg/m3), Target-2 (<25 μg/m3), and Target-3 (<15 μg/m3), respectively. In terms of pollution sources, the study indicates that biomass (crop residue) burning activities may not be the main source of severe air quality conditions in Pakistan: the highest PMx concentrations were observed in December and January when also the NO_2 TVCD and SO_2 VCD, used as proxies for NO_2 and SO_2 concentrations, were highest. The emissions of these trace gases are known to be associated with anthropogenic activities including transport, industrial activities, and power generation. Interestingly, higher levels of AOD, PM_1, $PM_{2.5}$, PM_{10}, NO_2, SO_2, population density, nighttime lights, and vegetation fire activities showed the same spatial pattern as cropland: most of the major cities, as well as rural areas in Pakistan, are surrounded by cropland and transport of pollutants generated from anthropogenic activities mix with aerosol and trace gases generated from agricultural activities, biomass burning and natural aerosols such as dust, to produce a rather smooth mixture of the metrics reported in this study. These findings suggest that Pakistan's extreme air pollution problems are strongly influenced by anthropogenic activities within Pakistan. This is also confirmed by the PSCF (> 0.6) analysis based on HYSPLIT air parcel back trajectories and ground-

based $PM_{2.5}$ concentrations. In addition, meteorological factors have a strong influence on the occurrence of pollution episodes.

Significant positive trends in the concentrations of AOD, PM_1, $PM_{2.5}$, PM_{10}, NO_2, and SO_2 were observed from November to February, particularly over Lahore, Islamabad, Gujranwala, and Faisalabad.

The final remark of this study is that all cities in Pakistan have been exposed to long-term PMx, NO_2, and SO_2 concentrations throughout the last two decades. The pollution levels in these cities imply extremely poor air quality conditions, mainly due to local anthropogenic activities, which severely threaten human life. This comprehensive study, based on long-term multi-source information on aerosols and trace gases may be considered a baseline study by the Ministry of Climate Change, Pakistan, and other policymakers, to mitigate air pollution problems in Pakistan.

CRediT authorship contribution statement

Muhammad Bilal: Conceptualization, Data curation, Methodology, Formal analysis, Investigation, Validation, Visualization, Writing - original draft. **Janet E. Nichol:** Supervision, Investigation, Writing - review & editing. **Zhongfeng Qiu:** Supervision, Investigation, Writing - review & editing. **Alaa Mhawish:** Data curation, Writing - review & editing. **Majid Nazeer:** Data curation, Writing - review & editing. **Md. Arfan Ali:** Data curation, Writing - review & editing. **Gerrit de Leeuw:** Supervision, Writing - review & editing. **Robert C. Levy:** Writing - review & editing. **Yu Wang:** Data curation**. Yang Chen:** Data curation. **Lunche Wang:** Data curation. **Yuan**

Shi: Writing - review & editing. **Max P. Bleiweiss:** Supervision, Investigation, **Luqman Atique:** Visualization. **Usman Mazhar:** Visualization.

Declaration of competing interest

The authors declare that they have no known competing financial interests or personal relationships that could have appeared to influence the work reported in this paper.

Acknowledgment

The authors would like to acknowledge NASA's Level-1 and Atmosphere Archive and Distribution System (LAADS) Distributed Active Archive Center (DAAC) (https://ladsweb.modaps.eosdis.nasa.gov/) for MODIS data, the Copernicus Atmosphere Monitoring Service (CAMS) for air quality data (PM_1, $PM_{2.5}$, and PM_{10}), the Goddard Earth Science DISC (https://daac.gsfc.nasa.gov/) for OMI data, Principal Investigators of Lahore AERONET site, and the NOAA Air Resources Laboratory (ARL) for the provision of the HYSPLIT air parcel back trajectories (https://www.ready.noaa.gov) used in this publication. The authors are grateful to Mr. Abid Omar, founder of Pakistan Air Quality Initiative (PAQI), and gratefully acknowledge the U.S. Department of State for providing the open access ground-based $PM_{2.5}$ data. The authors also acknowledge the use of data from NASA's Fire Information for Resource Management System (FIRMS) (https://earthdata.nasa.gov/firms), part of NASA's Earth Observing System Data and Information System (EOSDIS). The authors are thankful to Mr. Pravash Tiwari for helping in PSCF analysis and Dr. Devin White (Oak Ridge National Laboratory) for MODIS Conversion Tool Kit (MCTK).

Funding

This work was supported by the National Key Research and Development Program of China (2016YFC1400901), the Special Project of Jiangsu Distinguished Professor (R2018T22), the National Natural Science Foundation of China (41976165), Jiangsu Technology Project of Nature Resources (KJXM2019042), and the Startup Foundation for Introduction Talent of NUIST (2017r107). Additional support came from the New Mexico State University College of Agriculture Consumer and Environmental Sciences' Agricultural Experiment Station.

References

Adrees, M., Ibrahim, M., Shah, A.M., Abbas, F., Saleem, F., Rizwan, M., Hina, S., Jabeen, F., & Ali, S. (2016). Gaseous pollutants from brick kiln industry decreased the growth, photosynthesis, and yield of wheat (Triticum aestivum L.). *Environ Monit Assess, 188*, 267

Alam, K., Rahman, N., Khan, H.U., Haq, B.S., & Rahman, S. (2015). Particulate Matter and Its Source Apportionment in Peshawar, Northern Pakistan. *Aerosol and Air Quality Research, 15*, 634-647

Ali, M., Tariq, S., Mahmood, K., Daud, A., Batool, A., & Zia ul, H. (2013). A study of aerosol properties over Lahore (Pakistan) by using AERONET data. *Asia-Pacific Journal of Atmospheric Sciences, 50*, 153-162

Ali, M.A., & Assiri, M. (2019). Analysis of AOD from MODIS-Merged DT–DB Products Over the Arabian Peninsula. *Earth Systems and Environment, 3*, 625-636

Amnesty International (2019). Pakistan: Hazardous air puts lives at risk. In

Ashraf, N., Mushtaq, M., Sultana, B., Iqbal, M., Ullah, I., & Shahid, S.A. (2013). Preliminary monitoring of tropospheric air quality of Lahore City in Pakistan. *Int. J. Chem. Biochem. Sci., 3*, 19-28

Begum, A.B., Kim, E., Jeong, C.-H., Lee, D.-W., & Hopke, P.K. (2005). Evaluation of the potential source contribution function using the 2002 Quebec forest fire episode. *Atmospheric Environment, 39*, 3719-3724

Bilal, M., Nazeer, M., Nichol, J.E., Bleiweiss, M.P., Qiu, Z., Jäkel, E., Campbell, J.R., Atique, L., Huang, X., & Lolli, S. (2019a). A Simplified and Robust Surface Reflectance Estimation Method (SREM) for Use over Diverse Land Surfaces Using Multi-Sensor Data. *Remote Sensing, 11*

Bilal, M., Nazeer, M., Nichol, J.E., Qiu, Z., Wang, L., Bleiweiss, M.P., Shen, X., Campbell, J.R., & Lolli, S. (2019b). Evaluation of Terra-MODIS C6 and C6.1 Aerosol Products against Beijing, XiangHe, and Xinglong AERONET Sites in China during 2004-2014. *Remote Sensing, 11*, 486

Bilal, M., Nazeer, M., Qiu, Z., Ding, X., & Wei, J. (2018a). Global Validation of MODIS C6 and C6.1 Merged Aerosol Products over Diverse Vegetated Surfaces. *Remote Sensing, 10*

Bilal, M., & Nichol, J. (2017). Evaluation of the NDVI-Based Pixel Selection Criteria of the MODIS C6 Dark Target and Deep Blue Combined Aerosol Product. *IEEE Journal of Selected Topics in Applied Earth Observations and Remote Sensing, 10*, 3448 - 3453

Bilal, M., Nichol, J., & Wang, L. (2017). New customized methods for improvement of the MODIS C6 Dark Target and Deep Blue merged aerosol product. *Remote Sensing of Environment, 197*, 115–124

Bilal, M., Nichol, J.E., Bleiweiss, M.P., & Dubois, D. (2013). A Simplified high resolution MODIS Aerosol Retrieval Algorithm (SARA) for use over mixed surfaces. *Remote Sensing of Environment, 136*, 135-145

Bilal, M., Nichol, J.E., & Chan, P.W. (2014). Validation and accuracy assessment of a Simplified Aerosol Retrieval Algorithm (SARA) over Beijing under low and high aerosol loadings and dust storms. *Remote Sensing of Environment, 153*, 50-60

Bilal, M., Nichol, J.E., & Nazeer, M. (2016). Validation of Aqua-MODIS C051 and C006 Operational Aerosol Products Using AERONET Measurements Over Pakistan. *IEEE Journal of Selected Topics in Applied Earth Observations and Remote Sensing, 9*, 2074-2080

Bilal, M., Nichol, J.E., Nazeer, M., Shi, Y., Wang, L., Kumar, K.R., Ho, H.C., Mazhar, U., Bleiweiss, M.P., Qiu, Z., Khedher, K.M., & Lolli, S. (2019c). Characteristics of Fine Particulate Matter (PM2.5) over Urban, Suburban, and Rural Areas of Hong Kong. *Atmosphere, 10*

Bilal, M., Qiu, Z., Campbell, J.R., Spak, S., Shen, X., & Nazeer, M. (2018b). A New MODIS C6 Dark Target and Deep Blue Merged Aerosol Product on a 3 km Spatial Grid. *Remote Sensing, 10*, 463

Buchard, V., da Silva, A.M., Randles, C.A., Colarco, P., Ferrare, R., Hair, J., Hostetler, C., Tackett, J., & Winker, D. (2016). Evaluation of the surface PM2.5 in Version 1 of the NASA MERRA Aerosol Reanalysis over the United States. *Atmospheric Environment, 125*, 100-111

Buchard, V., Randles, C.A., da Silva, A.M., Darmenov, A., Colarco, P.R., Govindaraju, R., Ferrare, R., Hair, J., Beyersdorf, A.J., Ziemba, L.D., & Yu, H. (2017). The MERRA-2 Aerosol Reanalysis, 1980 Onward. Part II: Evaluation and Case Studies. *J Clim, 30*, 6851-6872

Carn, S.A., Fioletov, V.E., McLinden, C.A., Li, C., & Krotkov, N.A. (2017). A decade of global volcanic SO2 emissions measured from space. *Sci Rep, 7*, 44095

Che, H., Yang, L., Liu, C., Xia, X., Wang, Y., Wang, H., Wang, H., Lu, X., & Zhang, X. (2019). Long-term validation of MODIS C6 and C6.1 Dark Target aerosol products over China using CARSNET and AERONET. *Chemosphere, 236*, 124268

Chen, G., Li, S., Zhang, Y., Zhang, W., Li, D., Wei, X., He, Y., Bell, M.L., Williams, G., Marks, G.B., Jalaludin, B., Abramson, M.J., & Guo, Y. (2017). Effects of ambient PM 1 air pollution on daily emergency hospital visits in China: an epidemiological study. *The Lancet Planetary Health, 1*, e221-e229

Cheng, M.M., Jiang, H., & Guo, Z. (2012). Evaluation of long-term tropospheric NO2 columns and the effect of different ecosystem in Yangtze River Delta. *Procedia Environmental Sciences, 13*, 1045-1056

Chin, M., Ginoux, P., Kinne, S., Torres, O., Holben, B.N., Duncan, B.N., Martin, R.V., Logan, J.A., Higurashi, A., & Nakajima, T. (2002). Tropospheric Aerosol Optical Thickness from the GOCART Model and Comparisons with Satellite and Sun Photometer Measurements. *Journal of the Atmospheric Sciences, 59*, 461-483

Colarco, P., da Silva, A., Chin, M., & Diehl, T. (2010). Online simulations of global aerosol distributions in the NASA GEOS-4 model and comparisons to satellite and ground-based aerosol optical depth. *Journal of Geophysical Research, 115*

Colbeck, I., Nasir, Z.A., & Ali, Z. (2010). The state of ambient air quality in Pakistan--a review. *Environ Sci Pollut Res Int, 17*, 49-63

Cuevas, E., Camino, C., Benedetti, A., Basart, S., Terradellas, E., Baldasano, J.M., Morcrette, J.J., Marticorena, B., Goloub, P., Mortier, A., Berjón, A., Hernández, Y., Gil-Ojeda, M., & Schulz, M. (2015). The MACC-II 2007–2008 reanalysis: atmospheric dust evaluation and characterization over northern Africa and the Middle East. *Atmospheric Chemistry and Physics, 15*, 3991-4024

Dahiya, S., & Myllyvirta, L. (2019). Global SO2 emission hotspot database: Ranking the world's worst sources of SO2 pollution. In K. Ford, N. Sivalingam, S. Ayech, & A. Jacobsen (Eds.)

de Leeuw, G., Sogacheva, L., Rodriguez, E., Kourtidis, K., Georgoulias, A.K., Alexandri, G., Amiridis, V., Proestakis, E., Marinou, E., Xue, Y., & van der A, R. (2018). Two decades of satellite observations of AOD over mainland China using ATSR-2, AATSR and MODIS/Terra: data set evaluation and large-scale patterns. *Atmospheric Chemistry and Physics, 18*, 1573-1592

Dickerson, R.R., Kondragunta, S., Stenchikov, G., Civerolo, K.L., Doddridge, B.G., & Holben, B.N. (1997). The impact of aerosols on solar ultraviolet radiation and photochemical smog. *Science, 278*, 827-830

Ding, A.J., Huang, X., Nie, W., Sun, J.N., Kerminen, V.M., Petaja, T., Su, H., Cheng, Y.F., Yang, X.Q., Wang, M.H., Chi, X.G., Wang, J.P., Virkkula, A., Guo, W.D., Yuan, J., Wang, S.Y., Zhang, R.J., Wu, Y.F., Song, Y., Zhu, T., Zilitinkevich, S., Kulmala, M., & Fu, C.B. (2016). Enhanced haze pollution by black carbon in megacities in China. *Geophysical Research Letters, 43*, 2873-2879

Eck, T.F., Holben, B.N., Reid, J.S., Dubovik, O., Smirnov, A., O'Neill, N.T., Slutsker, I., & Kinne, S. (1999). Wavelength dependence of the optical depth of biomass burning, urban, and desert dust aerosols. *Journal of Geophysical Research: Atmospheres, 104*, 31333-31349

Elvidge, C.D., Zhizhin, M., Ghosh, T., Hsu, F.-C., & Taneja, J. (2021). Annual Time Series of Global VIIRS Nighttime Lights Derived from Monthly Averages: 2012 to 2019. *Remote Sensing, 13*

Fan, A., Chen, W., Liang, L., Sun, W., Lin, Y., Che, H., & Zhao, X. (2017). Evaluation and Comparison of Long-Term MODIS C5.1 and C6 Products against AERONET Observations over China. *Remote Sensing, 9*, 1269

Filonchyk, M., Yan, H., Zhang, Z., Yang, S., Li, W., & Li, Y. (2019). Combined use of satellite and surface observations to study aerosol optical depth in different regions of China. *Sci Rep, 9*, 6174

Fioletov, V.E., McLinden, C.A., Krotkov, N., Moran, M.D., & Yang, K. (2011). Estimation of SO2emissions using OMI retrievals. *Geophysical Research Letters, 38*, n/a-n/a

Fleming, Z.L., Monks, P.S., & Manning, A.J. (2012). Review: Untangling the influence of air-mass history in interpreting observed atmospheric composition. *Atmospheric Research, 104-105*, 1-39

Flemming, J., Benedetti, A., Inness, A., Engelen, R.J., Jones, L., Huijnen, V., Remy, S., Parrington, M., Suttie, M., Bozzo, A., Peuch, V.-H., Akritidis, D., & Katragkou, E. (2017). The CAMS interim Reanalysis of Carbon Monoxide, Ozone and Aerosol for 2003–2015. *Atmospheric Chemistry and Physics, 17*, 1945-1983

Flemming, J., Huijnen, V., Arteta, J., Bechtold, P., Beljaars, A., Blechschmidt, A.M., Diamantakis, M., Engelen, R.J., Gaudel, A., Inness, A., Jones, L., Josse, B., Katragkou, E., Marecal, V., Peuch, V.H.,

Richter, A., Schultz, M.G., Stein, O., & Tsikerdekis, A. (2015). Tropospheric chemistry in the Integrated Forecasting System of ECMWF. *Geoscientific Model Development, 8*, 975-1003

Giles, D.M., Sinyuk, A., Sorokin, M.G., Schafer, J.S., Smirnov, A., Slutsker, I., Eck, T.F., Holben, B.N., Lewis, J.R., Campbell, J.R., Welton, E.J., Korkin, S.V., & Lyapustin, A.I. (2019). Advancements in the Aerosol Robotic Network (AERONET) Version 3 database – automated near-real-time quality control algorithm with improved cloud screening for Sun photometer aerosol optical depth (AOD) measurements. *Atmospheric Measurement Techniques, 12*, 169-209

Government of Pakistan, F.D. (2019). Pakistan Economic Survey 2018-19. In

Granier, C., Bessagnet, B., Bond, T., D'Angiola, A., Denier van der Gon, H., Frost, G.J., Heil, A., Kaiser, J.W., Kinne, S., Klimont, Z., Kloster, S., Lamarque, J.-F., Liousse, C., Masui, T., Meleux, F., Mieville, A., Ohara, T., Raut, J.-C., Riahi, K., Schultz, M.G., Smith, S.J., Thompson, A., van Aardenne, J., van der Werf, G.R., & van Vuuren, D.P. (2011). Evolution of anthropogenic and biomass burning emissions of air pollutants at global and regional scales during the 1980–2010 period. *Climatic Change, 109*, 163-190

Gupta, P., Khan, M.N., da Silva, A., & Patadia, F. (2013). MODIS aerosol optical depth observations over urban areas in Pakistan: quantity and quality of the data for air quality monitoring. *Atmospheric Pollution Research, 4*, 43-52

Hamed, K.H., & Ramachandra Rao, A. (1998). A modified Mann-Kendall trend test for autocorrelated data. *Journal of Hydrology, 204*, 182-196

Harper, W.V. (2016). Reduced Major Axis Regression. *Wiley StatsRef: Statistics Reference Online* (pp. 1-6)

He, L., Lin, A., Chen, X., Zhou, H., Zhou, Z., & He, P. (2019). Assessment of MERRA-2 Surface PM2.5 over the Yangtze River Basin: Ground-based Verification, Spatiotemporal Distribution and Meteorological Dependence. *Remote Sensing, 11*

He, L., Wang, L., Lin, A., Zhang, M., Bilal, M., & Wei, J. (2018). Performance of the NPP-VIIRS and aqua-MODIS Aerosol Optical Depth Products over the Yangtze River Basin. *Remote Sensing, 10*, 117

Health Effects Institute (2019). State of Global Air 2019: A Special Report On Global Exposure to Air Pollution and Its Disease Burden. In. Boston, MA

Holben, B.N., Eck, T.F., Slutsker, I., Tanré, D., Buis, J.P., Setzer, A., Vermote, E., Reagan, J.A., Kaufman, Y.J., Nakajima, T., Lavenu, F., Jankowiak, I., & Smirnov, A. (1998). AERONET—A Federated Instrument Network and Data Archive for Aerosol Characterization. *Remote Sensing of Environment, 66*, 1-16

Holben, N., Tanr, D., Smirnov, A., Eck, T.F., Slutsker, I., Newcomb, W.W., Schafer, J.S., Chatenet, B., Lavenu, F., Kaufman, J., Castle, J.V., Setzer, A., Markham, B., Clark, D., Halthore, R., Karneli, A., Neill, N.T.O.,

Pietras, C., Pinker, T., Voss, K., & Zibordi, G. (2001). An emerging ground-based aerosol climatology : Aerosol optical depth from AERONET. *Journal of Geophysical Research: Atmospheres, 106*, 12067-12097

Hsu, N.C., Jeong, M.-J., Bettenhausen, C., Sayer, A.M., Hansell, R., Seftor, C.S., Huang, J., & Tsay, S.-C. (2013). Enhanced Deep Blue aerosol retrieval algorithm: The second generation. *Journal of Geophysical Research: Atmospheres, 118*, 9296-9315

Inness, A., Ades, M., Agustí-Panareda, A., Barré, J., Benedictow, A., Blechschmidt, A.-M., Dominguez, J.J., Engelen, R., Eskes, H., Flemming, J., Huijnen, V., Jones, L., Kipling, Z., Massart, S., Parrington, M., Peuch, V.-H., Razinger, M., Remy, S., Schulz, M., & Suttie, M. (2019). The CAMS reanalysis of atmospheric composition. *Atmospheric Chemistry and Physics, 19*, 3515-3556

Irfan, M., Riaz, M., Arif, M.S., Shahzad, S.M., Hussain, S., Akhtar, M.J., van den Berg, L., & Abbas, F. (2015). Spatial distribution of pollutant emissions from crop residue burning in the Punjab and Sindh provinces of Pakistan: uncertainties and challenges. *Environ Sci Pollut Res Int, 22*, 16475-16491

Irfan, M., Riaz, M., Arif, M.S., Shahzad, S.M., Saleem, F., Rahman, N.-u., van den Berg, L., & Abbas, F. (2014). Estimation and characterization of gaseous pollutant emissions from agricultural crop residue combustion in industrial and household sectors of Pakistan. *Atmospheric Environment, 84*, 189-197

Ishaq, M., Khan, M.A., Jan, F.A., & Ahmad, I. (2010). Heavy metals in brick kiln located area using atomic absorption spectrophotometer: a case study from the city of Peshawar, Pakistan. *Environ Monit Assess, 166*, 409-420

Islam, M.N., Ali, M.A., & Islam, M.M. (2019). Spatiotemporal Investigations of Aerosol Optical Properties Over Bangladesh for the Period 2002–2016. *Earth Systems and Environment, 3*, 563-573

Jacob, D.J., & Winner, D.A. (2009). Effect of climate change on air quality. *Atmospheric Environment, 43*, 51-63

Jain, S., Sharma, S.K., Vijayan, N., & Mandal, T.K. (2020). Seasonal characteristics of aerosols (PM2.5 and PM10) and their source apportionment using PMF: A four year study over Delhi, India. *Environ Pollut, 262*, 114337

Janssens-Maenhout, G., Pagliari, V., Guizzardi, D., & Muntean, M. (2013). Global emission inventories in the Emission Database for Global Atmospheric Research (EDGAR) – Manual (I), Gridding: EDGAR emissions distribution on global gridmaps. In. Luxembourg: Publications Office of the European Union

Jethva, H., Torres, O., Field, R.D., Lyapustin, A., Gautam, R., & Kayetha, V. (2019). Connecting Crop Productivity, Residue Fires, and Air Quality over Northern India. *Sci Rep, 9*, 16594

Kendall, M., & Gibbons, J.D. (1990). *Rank Correlation Methods*. (5th Edition ed.). London: Edward Arnold

Keys, R. (1981). Cubic convolution interpolation for digital image processing. *IEEE Transactions on Acoustics, Speech, and Signal Processing, 29*, 1153-1160

Khanum, F., Chaudhry, M.N., & Kumar, P. (2017). Characterization of five-year observation data of fine particulate matter in the metropolitan area of Lahore. *Air Qual Atmos Health, 10*, 725-736

Khokhar, M.F., Mehdi, H., Abbas, Z., & Javed, Z. (2016). Temporal Assessment of NO2 Pollution Levels in Urban Centers of Pakistan by Employing Ground-Based and Satellite Observations. *Aerosol and Air Quality Research, 16*, 1854-1867

Khokhar, M.F., Yasmin, N., Fatima, N., Beirle, S., & Wagner, T. (2015). Detection of Trends and Seasonal Variation in Tropospheric Nitrogen Dioxide over Pakistan. *Aerosol and Air Quality Research, 15*, 2508-2524

Krotkov, N.A., Lamsal, L.N., Celarier, E.A., Swartz, W.H., Marchenko, S.V., Bucsela, E.J., Chan, K.L., Wenig, M., & Zara, M. (2017). The version 3 OMI NO₂ standard product. *Atmospheric Measurement Techniques, 10*, 3133-3149

Krotkov, N.A., McLinden, C.A., Li, C., Lamsal, L.N., Celarier, E.A., Marchenko, S.V., Swartz, W.H., Bucsela, E.J., Joiner, J., Duncan, B.N., Boersma, K.F., Veefkind, J.P., Levelt, P.F., Fioletov, V.E., Dickerson, R.R., He, H., Lu, Z., & Streets, D.G. (2016). Aura OMI observations of regional SO2 and NO2 pollution changes from 2005 to 2015. *Atmospheric Chemistry and Physics, 16*, 4605-4629

Kulmala, M., Dada, L., Daellenbach, K.R., Yan, C., Stolzenburg, D., Kontkanen, J., Ezhova, E., Hakala, S., Tuovinen, S., Kokkonen, T.V., Kurppa, M., Cai, R., Zhou, Y., Yin, R., Baalbaki, R., Chan, T., Chu, B., Deng, C., Fu, Y., Ge, M., He, H., Heikkinen, L., Junninen, H., Liu, Y., Lu, Y., Nie, W., Rusanen, A., Vakkari, V., Wang, Y., Yang, G., Yao, L., Zheng, J., Kujansuu, J., Kangasluoma, J., Petaja, T., Paasonen, P., Jarvi, L., Worsnop, D., Ding, A., Liu, Y., Wang, L., Jiang, J., Bianchi, F., & Kerminen, V.M. (2020). Is reducing new particle formation a plausible solution to mitigate particulate air pollution in Beijing and other Chinese megacities? *Faraday Discuss*

Latza, U., Gerdes, S., & Baur, X. (2009). Effects of nitrogen dioxide on human health: systematic review of experimental and epidemiological studies conducted between 2002 and 2006. *Int J Hyg Environ Health, 212*, 271-287

Le Blond, J.S., Woskie, S., Horwell, C.J., & Williamson, B.J. (2017). Particulate matter produced during commercial sugarcane harvesting and processing: A respiratory health hazard? *Atmospheric Environment, 149*, 34-46

Lee, D.S., Köhler, I., Grobler, E., Rohrer, F., Sausen, R., Gallardo-Klenner, L., Olivier, J.G.J., Dentener, F.J., & Bouwman, A.F. (1997). Estimations of global no, emissions and their uncertainties. *Atmospheric Environment, 31*, 1735-1749

Levy, R.C., Mattoo, S., Munchak, L.A., Remer, L.A., Sayer, A.M., Patadia, F., & Hsu, N.C. (2013). The Collection 6 MODIS aerosol products over land and ocean. *Atmospheric Measurement Techniques, 6*, 2989-3034

Levy, R.C., Remer, L.a., Kleidman, R.G., Mattoo, S., Ichoku, C., Kahn, R., & Eck, T.F. (2010). Global evaluation of the Collection 5 MODIS dark-target aerosol products over land. *Atmospheric Chemistry and Physics, 10*, 10399-10420

Li, C., Krotkov, N.A., Carn, S., Zhang, Y., Spurr, R.J.D., & Joiner, J. (2017). New-generation NASA Aura Ozone Monitoring Instrument (OMI) volcanic SO₂ dataset: algorithm description, initial results, and continuation with the Suomi-NPP Ozone Mapping and Profiler Suite (OMPS). *Atmospheric Measurement Techniques, 10*, 445-458

Li, C., Krotkov, N.A., Leonard, P.J.T., Carn, S., Joiner, J., Spurr, R.J.D., & Vasilkov, A. (2020). Version 2 Ozone Monitoring Instrument SO₂ product (OMSO2 V2): new anthropogenic SO₂ vertical column density dataset. *Atmospheric Measurement Techniques, 13*, 6175-6191

Li, L., & Wang, Y. (2014). What drives the aerosol distribution in Guangdong--the most developed province in Southern China? *Sci Rep, 4*, 5972

Li, L., Wu, J., Ghosh, J.K., & Ritz, B. (2013). Estimating Spatiotemporal Variability of Ambient Air Pollutant Concentrations with A Hierarchical Model. *Atmos Environ (1994), 71*, 54-63

Li, Z.Q., Zhang, Y., Shao, J., Li, B.S., Hong, J., Liu, D., Li, D.H., Wei, P., Li, W., Li, L., Zhang, F.X., Guo, J., Deng, Q., Wang, B.X., Cui, C.L., Zhang, W.C., Wang, Z.Z., Lv, Y., Xu, H., Chen, X.F., Li, L., & Qie, L.L. (2016). Remote sensing of atmospheric particulate mass of dry PM2.5 near the ground: Method validation using ground-based measurements. *Remote Sensing of Environment, 173*, 59-68

Liu, L., Breitner, S., Schneider, A., Cyrys, J., Bruske, I., Franck, U., Schlink, U., Marian Leitte, A., Herbarth, O., Wiedensohler, A., Wehner, B., Pan, X., Wichmann, H.E., & Peters, A. (2013). Size-fractioned particulate air pollution and cardiovascular emergency room visits in Beijing, China. *Environ Res, 121*, 52-63

Livingston, J.M., Redemann, J., Shinozuka, Y., Johnson, R., Russell, P.B., Zhang, Q., Mattoo, S., Remer, L., Levy, R., Munchak, L., & Ramachandran, S. (2014). Comparison of MODIS 3 km and 10 km resolution aerosol optical depth retrievals over land with airborne sunphotometer measurements during ARCTAS summer 2008. *Atmospheric Chemistry and Physics, 14*, 2015-2038

Mann, H.B. (1945). Nonparametric Tests Against Trend. *Econometrica, 13*

Mannucci, P.M., & Franchini, M. (2017). Health Effects of Ambient Air Pollution in Developing Countries. *Int J Environ Res Public Health, 14*

Mehta, M., Singh, R., Singh, A., Singh, N., & Anshumali (2016). Recent global aerosol optical depth variations and trends - A comparative study using MODIS and MISR level 3 datasets. *Remote Sensing of Environment, 181*, 137-150

Mei, L., Zhao, C., de Leeuw, G., Che, H., Che, Y., Rozanov, V., Vountas, M., & Burrows, J.P. (2019). Understanding MODIS dark-target collection 5 and 6 aerosol data over China: Effect of surface type, aerosol loading and aerosol absorption. *Atmospheric Research, 228*, 161-175

Meng, X., Ma, Y., Chen, R., Zhou, Z., Chen, B., & Kan, H. (2013). Size-fractionated particle number concentrations and daily mortality in a Chinese city. *Environ Health Perspect, 121*, 1174-1178

Mhawish, A., Banerjee, T., Broday, D.M., Misra, A., & Tripathi, S.N. (2017). Evaluation of MODIS Collection 6 aerosol retrieval algorithms over Indo-Gangetic Plain: Implications of aerosols types and mass loading. *Remote Sensing of Environment, 201*, 297-313

Mhawish, A., Banerjee, T., Sorek-Hamer, M., Bilal, M., Lyapustin, A.I., Chatfield, R., & Broday, D.M. (2020). Estimation of High-Resolution PM2.5 over the Indo-Gangetic Plain by Fusion of Satellite Data, Meteorology, and Land Use Variables. *Environmental science & technology, 54*, 7891-7900

Mhawish, A., Banerjee, T., Sorek-Hamer, M., Lyapustin, A., Broday, D.M., & Chatfield, R. (2019). Comparison and evaluation of MODIS Multi-angle Implementation of Atmospheric Correction (MAIAC) aerosol product over South Asia. *Remote Sensing of Environment, 224*, 12-28

Mhawish, A., Sorek-Hamer, M., Chatfield, R., Banerjee, T., Bilal, M., Kumar, M., Sarangi, C., Franklin, M., Chau, K., Garay, M., & Kalashnikova, O. (2021). Aerosol Characteristics from Earth Observation Systems: A Comprehensive Investigation over South Asia (2000-2019). *Remote Sensing of Environment, (in press)*

Miao, Y., Li, J., Miao, S., Che, H., Wang, Y., Zhang, X., Zhu, R., & Liu, S. (2019). Interaction Between Planetary Boundary Layer and PM2.5 Pollution in Megacities in China: a Review. *Current Pollution Reports, 5*, 261-271

Miao, Y., & Liu, S. (2019). Linkages between aerosol pollution and planetary boundary layer structure in China. *Sci Total Environ, 650*, 288-296

Miao, Y., Liu, S., Guo, J., Huang, S., Yan, Y., & Lou, M. (2018). Unraveling the relationships between boundary layer height and PM2.5 pollution in China based on four-year radiosonde measurements. *Environ Pollut, 243*, 1186-1195

More, S., Kumar, P.P., Gupta, P., Devara, P., & Aher, G. (2013). Comparison of Aerosol Products Retrieved from AERONET, MICROTOPS and MODIS over a Tropical Urban City, Pune, India. *Aerosol and Air Quality Research, 13*, 107-121

Navinya, C.D., Vinoj, V., & Pandey, S.K. (2020). Evaluation of PM2.5 Surface Concentrations Simulated by NASA's MERRA Version 2 Aerosol Reanalysis over India and its Relation to the Air Quality Index. *Aerosol and Air Quality Research, 20*, 1329-1339

Nichol, J., & Bilal, M. (2016). Validation of MODIS 3 km Resolution Aerosol Optical Depth Retrievals Over Asia. *Remote Sensing, 8*, 328

Nichol, J.E., Bilal, M., Ali, M.A., & Qiu, Z. (2020). Air Pollution Scenario over China during COVID-19. *Remote Sensing, 12*

Olivier, J.G.J., Bouwman, A.F., Van der Hoek, K.W., & Berdowski, J.J.M. (1998). Global air emission inventories for anthropogenic sources of NOx, NH3 and N2O in 1990. *Environmental Pollution, 102*, 135-148

PAQI (2018). LahoreSmog, Just how bad is it? In: Pakistan Air Quality Initiative

Pervaiz, S., Akram, M.A.N., Khan, F.Z., Javid, K., & Zahid, Y. (2021). Brick Sector and Air Quality: An Integrated Assessment towards 2020 Challenge of Environment Development. *Environment and Natural Resources Journal, 19*, 153-164

Pope, C.A., Burnett, R.T., Thun, M.J., Calle, E.E., Krewski, D., Ito, K., & Thurston, G.D. (2002). Lung cancer, cardiopulmonary mortality, and long-term exposure to fine particulate air pollution. *JAMA : the journal of the American Medical Association, 287*, 1132-1141

Provencal, S., Buchard, V., da Silva, A.M., Leduc, R., Barrette, N., Elhacham, E., & Wang, S.H. (2017). Evaluation of PM2.5 surface concentration simulated by Version 1 of the NASA's MERRA Aerosol Reanalysis over Israel and Taiwan. *Aerosol Air Qual Res, 17*, 253-261

Purohit, P., Munir, T., & Rafaj, P. (2013). Scenario analysis of strategies to control air pollution in Pakistan. *Journal of Integrative Environmental Sciences, 10*, 77-91

Qu, Y., Han, Y., Wu, Y., Gao, P., & Wang, T. (2017). Study of PBLH and Its Correlation with Particulate Matter from One-Year Observation over Nanjing, Southeast China. *Remote Sensing, 9*

Rahman, U., Awan, M.A., Hassan, S.T., & Khattak, M.M. (2000). Mosses as Indicators of Atmospheric Pollution of Trace Metals (Cd, Cu, Pb, Mn and Zn) in the Vicinity of Coal-Fired Brick Kilns in North-Eastern Suburbs of Islamabad, Pakistan. *Journal of Radioanalytical and Nuclear Chemistry, 246*, 331-336

Randles, C.A., Da Silva, A.M., Buchard, V., Colarco, P.R., Darmenov, A., Govindaraju, R., Smirnov, A., Holben, B., Ferrare, R., Hair, J., Shinozuka, Y., & Flynn, C.J. (2017). The MERRA-2 Aerosol Reanalysis, 1980 - onward, Part I: System Description and Data Assimilation Evaluation. *J Clim, 30*, 6823-6850

Remer, L.A., Mattoo, S., Levy, R.C., & Munchak, L.A. (2013). MODIS 3 km aerosol product: algorithm and global perspective. *Atmospheric Measurement Techniques, 6*, 1829-1844

Rémy, S., Kipling, Z., Flemming, J., Boucher, O., Nabat, P., Michou, M., Bozzo, A., Ades, M., Huijnen, V., Benedetti, A., Engelen, R., Peuch, V.-H., & Morcrette, J.-J. (2019). Description and evaluation of the tropospheric aerosol scheme in the European Centre for Medium-Range Weather Forecasts (ECMWF) Integrated Forecasting System (IFS-AER, cycle 45R1). *Geoscientific Model Development, 12*, 4627-4659

Richter, A., & Burrows, J.P. (2002). Tropospheric NO2 from GOME measurements. *Advances in Space Research, 29*, 1673-1683

Rose, A.N., McKee, J.J., Sims, K.M., Bright, E.A., Reith, A.E., & Urban, M.L. (2020). LandScan 2019. In. Oak Ridge, TN: Oak Ridge National Laboratory

Salmi, T., Määttä, A., Anttila, P., Ruoho-Airola, T., Amnell, T., & Maatta, A. (2002). *Detecting Trends of Annual Values of Atmospheric Pollutants by the Mann-Kendall Test and Sen's Solpe Estimates the Excel Template Application MAKESENS*. Helsinki: Finnish Meteorological Institute, Air Quality Research

Sayer, A.M., Hsu, N.C., Bettenhausen, C., & Jeong, M.-J. (2013). Validation and uncertainty estimates for MODIS Collection 6 “Deep Blue” aerosol data. *Journal of Geophysical Research: Atmospheres, 118*, 7864-7872

Sayer, A.M., Munchak, L.A., Hsu, N.C., Levy, R.C., Bettenhausen, C., & Jeong, M.J. (2014). MODIS Collection 6 aerosol products: Comparison between Aqua's e-Deep Blue, Dark Target, and “merged” data sets, and usage recommendations. *Journal of Geophysical Research: Atmospheres, 119*, 13965-13989

Sayer, A.M., USA, N.G.S.F.C.G.M., USA, U.S.R.A.G.E.S.T.a.R.G.G.M., Hsu, N.C., USA, N.G.S.F.C.G.M., Bettenhausen, C., USA, N.G.S.F.C.G.M., Science Systems and Applications, I.L.M.U., Jeong, M.J., Korea, G.W.N.U.G.C., Meister, G., & USA, N.G.S.F.C.G.M. (2015). Effect of MODIS Terra radiometric

calibration improvements on Collection 6 Deep Blue aerosol products: Validation and Terra/Aqua consistency. *Journal of Geophysical Research: Atmospheres, 120*, 12157-12174

Seinfeld, J.H., & Pandis, S.N. (1998). *Atmospheric Chemistry and Physics, from Air Pollution to climate Change*. New York: John Wiley and Sons

Sen, P.K. (1968). Estimates of the Regression Coefficient Based on Kendall's Tau. *Journal of the American Statistical Association, 63*, 1379-1389

Shah, M.H., Shaheen, N., & Nazir, R. (2012). Assessment of the trace elements level in urban atmospheric particulate matter and source apportionment in Islamabad, Pakistan. *Atmospheric Pollution Research, 3*, 39-45

Shen, X., Bilal, M., Qiu, Z., Sun, D., Wang, S., & Zhu, W. (2018). Validation of MODIS C6 Dark Target Aerosol Products at 3 km and 10 km Spatial Resolutions Over the China Seas and the Eastern Indian Ocean. *Remote Sensing, 10*

Shi, Y., Bilal, M., Ho, H.C., & Omar, A. (2020). Urbanization and regional air pollution across South Asian developing countries – A nationwide land use regression for ambient PM2.5 assessment in Pakistan. *Environmental Pollution, 266*

Shi, Y., Zhang, J., Reid, J.S., Hyer, E.J., & Hsu, N.C. (2013). Critical evaluation of the MODIS Deep Blue aerosol optical depth product for data assimilation over North Africa. *Atmospheric Measurement Techniques, 6*, 949-969

Singh, N., Mhawish, A., Deboudt, K., Singh, R.S., & Banerjee, T. (2017). Organic aerosols over Indo-Gangetic Plain: Sources, distributions and climatic implications. *Atmospheric Environment, 157*, 59-74

Smirnov, A., Holben, B.N., Eck, T.F., Dubovik, O., & Slutsker, I. (2000). Cloud-Screening and Quality Control Algorithms for the AERONET Database. *Remote Sensing of Environment, 73*, 337-349

Sogacheva, L., de Leeuw, G., Rodriguez, E., Kolmonen, P., Georgoulias, A.K., Alexandri, G., Kourtidis, K., Proestakis, E., Marinou, E., Amiridis, V., Xue, Y., & van der A, R.J. (2018). Spatial and seasonal variations of aerosols over China from two decades of multi-satellite observations – Part 1: ATSR (1995–2011) and MODIS C6.1 (2000–2017). *Atmospheric Chemistry and Physics, 18*, 11389-11407

Song, Z., Fu, D., Zhang, X., Wu, Y., Xia, X., He, J., Han, X., Zhang, R., & Che, H. (2018). Diurnal and seasonal variability of PM2.5 and AOD in North China plain: Comparison of MERRA-2 products and ground measurements. *Atmospheric Environment, 191*, 70-78

Stein, A.F., Draxler, R.R., Rolph, G.D., Stunder, B.J.B., Cohen, M.D., & Ngan, F. (2015). NOAA's HYSPLIT Atmospheric Transport and Dispersion Modeling System. *Bulletin of the American Meteorological Society, 96*, 2059-2077

Stone, E., Schauer, J., Quraishi, T.A., & Mahmood, A. (2010). Chemical characterization and source apportionment of fine and coarse particulate matter in Lahore, Pakistan. *Atmospheric Environment, 44*, 1062-1070

Sun, T., Che, H., Qi, B., Wang, Y., Dong, Y., Xia, X., Wang, H., Gui, K., Zheng, Y., Zhao, H., Ma, Q., Du, R., & Zhang, X. (2019). Characterization of vertical distribution and radiative forcing of ambient aerosol over the Yangtze River Delta during 2013-2015. *Sci Total Environ, 650*, 1846-1857

Tabinda, A.B., Ali, H., Yasar, A., Rasheed, R., Mahmood, A., & Iqbal, A. (2019). Comparative Assessment of Ambient Air Quality of Major Cities of Pakistan. *Mapan, 35*, 25-32

Tariq, S., & Ali, M. (2015). Spatio–temporal distribution of absorbing aerosols over Pakistan retrieved from OMI onboard Aura satellite. *Atmospheric Pollution Research, 6*, 254-266

Tariq, S., ul-Haq, Z., & Ali, M. (2015). Analysis of optical and physical properties of aerosols during crop residue burning event of October 2010 over Lahore, Pakistan. *Atmospheric Pollution Research, 6*, 969-978

Tariq, S., Zia, u.-H., & Ali, M. (2016). Satellite and ground-based remote sensing of aerosols during intense haze event of October 2013 over lahore, Pakistan. *Asia-Pacific Journal of Atmospheric Sciences, 52*, 25-33

Theil, H. (1992). A Rank-Invariant Method of Linear and Polynomial Regression Analysis. *Henri Theil's Contributions to Economics and Econometrics* (pp. 345-381)

Tong, Y., Feng, L., Sun, K., & Tang, J. (2020). Assessment of the Representativeness of MODIS Aerosol Optical Depth Products at Different Temporal Scales Using Global AERONET Measurements. *Remote Sensing, 12*

Torres, O., Ahn, C., & Chen, Z. (2013). Improvements to the OMI near-UV aerosol algorithm using A-train CALIOP and AIRS observations. *Atmospheric Measurement Techniques, 6*, 3257-3270

Torres, O., Tanskanen, A., Veihelmann, B., Ahn, C., Braak, R., Bhartia, P.K., Veefkind, P., & Levelt, P. (2007). Aerosols and surface UV products from Ozone Monitoring Instrument observations: An overview. *Journal of Geophysical Research, 112*, D24S47

Ukhov, A., Mostamandi, S., da Silva, A., Flemming, J., Alshehri, Y., Shevchenko, I., & Stenchikov, G. (2020). Assessment of natural and anthropogenic aerosol air pollution in the Middle East using MERRA-2, CAMS data assimilation products, and high-resolution WRF-Chem model simulations. *Atmospheric Chemistry and Physics, 20*, 9281-9310

ul-Haq, Z., Tariq, S., & Ali, M. (2017). Spatiotemporal assessment of CO2 emissions and its satellite remote sensing over Pakistan and neighboring regions. *Journal of Atmospheric and Solar-Terrestrial Physics, 152-153*, 11-19

ul–Haq, Z., Tariq, S., Ali, M., Mahmood, K., Batool, S.A., & Rana, A.D. (2014). A study of tropospheric NO2 variability over Pakistan using OMI data. *Atmospheric Pollution Research, 5*, 709-720

Ul_Haq, Z., Tariq, S., Rana, A.D., Ali, M., Mahmood, K., & Shahid, P. (2015). Satellite remote sensing of total ozone column (TOC) over Pakistan and neighbouring regions. *International Journal of Remote Sensing, 36*, 1038-1054

UNDP (2019). Sustainable Urbanization. In: Development Advocate Pakistan

Ur Rehman, S.A., Cai, Y., Siyal, Z.A., Mirjat, N.H., Fazal, R., & Kashif, S.U.R. (2019). Cleaner and Sustainable Energy Production in Pakistan: Lessons Learnt from the Pak-TIMES Model. *Energies, 13*

Veefkind, J.P., de Haan, J.F., Brinksma, E.J., Kroon, M., & Levelt, P.F. (2006). Total ozone from the Ozone Monitoring Instrument (OMI) using the DOAS technique. *IEEE Transactions on Geoscience and Remote Sensing, 44*, 1239 –1244

Wang, H., Lu, K., Chen, X., Zhu, Q., Wu, Z., Wu, Y., & Sun, K. (2018). Fast particulate nitrate formation via N2O5 uptake aloft in winter in Beijing. *Atmospheric Chemistry and Physics, 18*, 10483-10495

Wang, Q., Sun, L., Wei, J., Yang, Y., Li, R., Liu, Q., & Chen, L. (2017). Validation and Accuracy Analysis of Global MODIS Aerosol Products over Land. *Atmosphere, 8*, 155

Wang, Y., Yuan, Q., Li, T., Shen, H., Zheng, L., & Zhang, L. (2019). Evaluation and comparison of MODIS Collection 6.1 aerosol optical depth against AERONET over regions in China with multifarious underlying surfaces. *Atmospheric Environment, 200*, 280-301

Wang, Y.Q., Zhang, X.Y., & Draxler, R.R. (2009). TrajStat: GIS-based software that uses various trajectory statistical analysis methods to identify potential sources from long-term air pollution measurement data. *Environmental Modelling & Software, 24*, 938-939

Wang, Y.Q., Zhang, X.Y., Sun, J.Y., Zhang, X.C., Che, H.Z., & Li, Y. (2015). Spatial and temporal variations of the concentrations of PM10, PM2.5 and PM1 in China. *Atmospheric Chemistry and Physics, 15*, 13585-13598

WHO (2018a). 9 out of 10 people worldwide breathe polluted air, but more countries are taking action. In. Geneva

WHO (2018b). WHO Global Ambient Air Quality Database (update 2018). In. Geneva

Xiao, Q., Zhang, H., Choi, M., Li, S., Kondragunta, S., Kim, J., Holben, B., Levy, R.C., & Liu, Y. (2016). Evaluation of VIIRS, GOCI, and MODIS Collection 6 AOD retrievals against ground sunphotometer observations over East Asia. *Atmospheric Chemistry and Physics, 16*, 1255-1269

Xie, Y., Zhang, Y., Xiong, X., Qu, J.J., & Che, H. (2011). Validation of MODIS aerosol optical depth product over China using CARSNET measurements. *Atmospheric Environment, 45*, 5970-5978

Zhang, M., Su, B., Bilal, M., Atique, L., Usman, M., Qiu, Z., Ali, M.A., & Han, G. (2020). An Investigation of Vertically Distributed Aerosol Optical Properties over Pakistan Using CALIPSO Satellite Data. *Remote Sensing, 12*

Zhang, R., Sun, X., Shi, A., Huang, Y., Yan, J., Nie, T., Yan, X., & Li, X. (2018). Secondary inorganic aerosols formation during haze episodes at an urban site in Beijing, China. *Atmospheric Environment, 177*, 275-282